AD-A137 508 MODIFIED BETATRON ACCELERATOR STUDIES(U) MISSION RESEARCH CORP ALBUQUERQUE NM T P HUGHES ET AL. DEC 83 AMRC-R-524 N00014-81-C-0647 1/2

UNCLASSIFIED F/G 20/7 NL

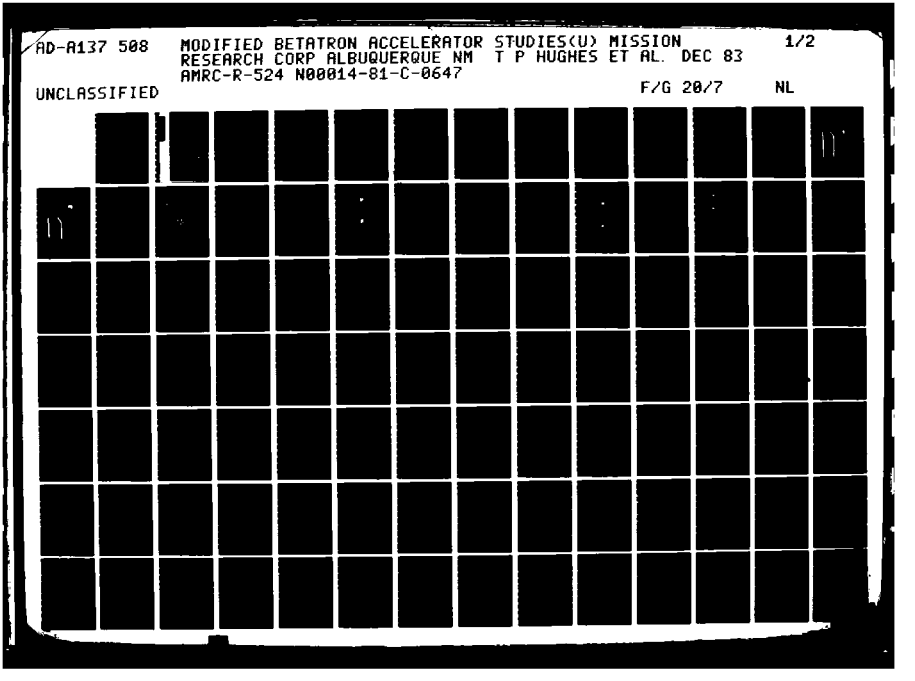

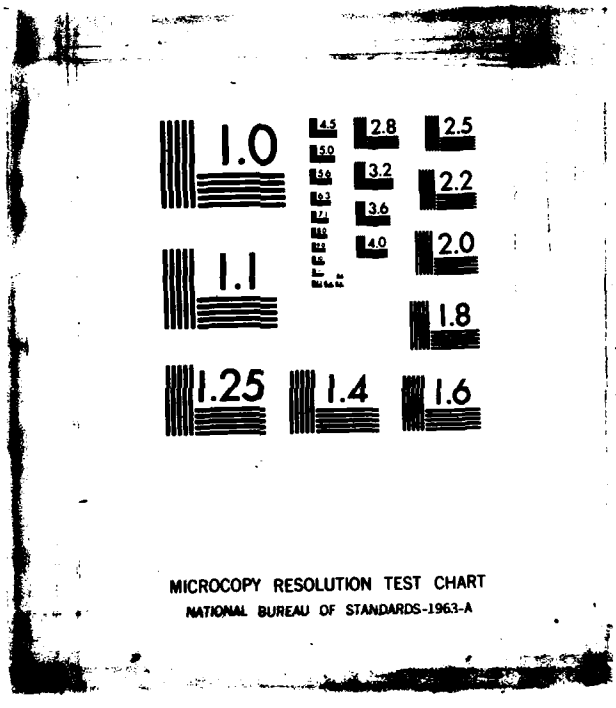
1.0
1.1
1.25
1.4
1.6
2.8
3.2
3.6
4.0
2.5
2.2
2.0
1.8
MICROCOPY RESOLUTION TEST CHART
NATIONAL BUREAU OF STANDARDS-1963-A

AMRC-R-524
Copy 23

FINAL REPORT: MODIFIED BETATRON ACCELERATOR STUDIES

T. P. Hughes
B. B. Godfrey
M. M. Campbell

December 1983

Prepared for: Office of Naval Research
Physical Sciences Division
800 North Quincy Street
Arlington, Virginia 22217

Under Contract: N00014-81-C-0647

Prepared by: MISSION RESEARCH CORPORATION
1720 Randolph Road, S.E.
Albuquerque, New Mexico 87106

UNCLASSIFIED

SECURITY CLASSIFICATION OF THIS PAGE (When Data Entered)

REPORT DOCUMENTATION PAGE

READ INSTRUCTIONS BEFORE COMPLETING FORM

1. REPORT NUMBER	2. GOVT ACCESSION NO. AD-A137508
3. RECIPIENT'S CATALOG NUMBER	
4. TITLE (and Subtitle) FINAL REPORT: MODIFIED BETATRON ACCELERATOR STUDIES	5. TYPE OF REPORT & PERIOD COVERED FINAL 1 Sept 81-31 Oct 83
6. PERFORMING ORG. REPORT NUMBER AMRC-R-524	
7. AUTHOR(s) T. P. Hughes, B. B. Godfrey, M. M. Campbell	8. CONTRACT OR GRANT NUMBER(s) N00014-81-C-0647
9. PERFORMING ORGANIZATION NAME AND ADDRESS MISSION RESEARCH CORPORATION 1720 Randolph Road, S.E. Albuquerque, New Mexico 87106	10. PROGRAM ELEMENT PROJECT, TASK AREA & WORK UNIT NUMBERS
11. CONTROLLING OFFICE NAME AND ADDRESS OFFICE OF NAVAL RESEARCH 800 North Quincy Street Arlington, Virginia 22217	12. REPORT DATE December 1983
	13. NUMBER OF PAGES 144
14. MONITORING AGENCY NAME & ADDRESS(if different from Controlling Office)	15. SECURITY CLASS (of this report) Unclassified
	15a. DECLASSIFICATION DOWNGRADING SCHEDULE

16. DISTRIBUTION STATEMENT (of this Report)

Approved for Public Release - Distribution Unlimited

17. DISTRIBUTION STATEMENT (of the abstract entered in Block 20, if different from Report)

18. SUPPLEMENTARY NOTES

19. KEY WORDS (Continue on reverse side if necessary and identify by block number)

Modified Betatron
Recirculating Accelerator
Negative Mass Instability
Resistive Wall Instability
Beam Breakup Instability
Image Displacement Instability

two dimensional

20. ABSTRACT (Continue on reverse side if necessary and identify by block number)

Results of an extensive study of the modified betatron accelerators are reported. The topics are beam injection, equilibrium and stability. Three-dimensional particle simulations of injections were performed. The results show good agreement with theory. Various types of equilibria were studied using 2-D simulations. Results are compared to the calculations of Finn and Manheimer. Beam stability is investigated using a combination of analytic and numerical techniques. Growth rates of the negative mass, resistive wall, beam breakup, and image displacement instabilities are calculated. A new theory of the

DD FORM 1 JAN 73 1473 EDITION OF 1 NOV 65 IS OBSOLETE

SECURITY CLASSIFICATION OF THIS PAGE (When Data Entered)

negative mass instability, keeping toroidal corrections to Maxwell's equations, is derived. Good agreement between theory and simulations is obtained. The negative mass instability is shown to be the dominant instability. Simulations show that it can disrupt the beam in a time of order one microsecond. Stabilization may require a beam of large minor radius. Work on the other instabilities show that measures can be taken to make their effect negligible.

TABLE OF CONTENTS

LIST OF ILLUSTRATIONS

LIST OF ILLUSTRATIONS (Continued)

LIST OF TABLES

I. Introduction

The possibility of using betatrons to accelerate high current electron beams to high energy has generated renewed interest in these devices. If successful, they will provide a source of high power beams which is much more compact and economical than linear machines. In order to overcome the space charge repulsion which limits current in the conventional betatron,[1] a toroidal magnetic field is added. This combination, shown in Fig. 1, is the Modified Betatron Accelerator (MBA). Successful operation of the modified betatron requires (a) the ability to inject a high current (~10 kA) of low energy (~2 MeV) electrons onto a cyclotron orbit in the presence of a strong (1-5 kG) toroidal magnetic field; (b) a stable beam equilibrium for the duration of the acceleration period, typically thousands of revolutions; and (c) extraction of the beam, which has been accelerated to high energy (~50 MeV), preferably in a time equal to one rotation period. If instabilities are present, their cumulative effect must be small enough such that macroscopic disruption of the beam is minimal.

During the period of our contract with the Office of Naval Research (ONR) (1 Sept 81 - 31 Oct 83), we concentrated primarily on requirement (b), with some work being done on (a). This choice was made after consideration of what was of most relevance to the overall modified betatron program and consideration of where we could make the greatest contributions. The existence of a stable, or at any rate confined, state for the beam over many circulation periods is the minimal requirement for the MBA. In addition, this subject can be addressed with confidence using a combination of analytical and numerical techniques which serve as a check on each other. For the issue of injection, one must rely on three-dimensional numerical simulations alone. A number of such simulations were performed under this contract, but their expense was such that a detailed study of injection was not feasible with the computing resources available. Concerning the issue of beam extraction, it was felt that it would be premature to start work

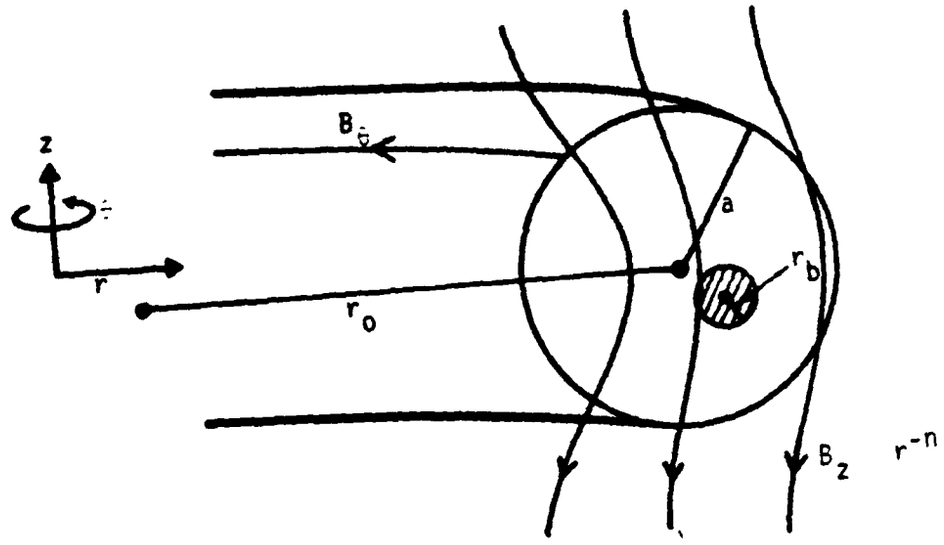

Figure 1. Illustration of modified betatron concept. The major radius of the torus is r_o, the minor radius is a and the beam is r_b. The external magnetic fields consist of a focusing mirror field B_z and a toroidal field B_θ.

on this subject, given the uncertainty relating to requirements (a) and (b). Also, there are several uses for the modified betatron which would not necessarily require extraction of the beam, e.g., microwave and free-electron laser applications.

This report describes in detail the work we have done. In Chapter II we give the results obtained from one-turn injection simulations of the scheme in which the diode is placed inside the torus. In Chapter III we describe investigations into different types of beam equilibria and how these equilibria are affected by the addition of a spread in energy or increased transverse emittance to the beam. In Chapter IV the results of extensive analytic and numerical investigations into beam stability are presented. The main emphasis here is on the negative mass instability, but we have also done calculations on resistive wall and beam breakup instabilities. The latter occurs in devices in which the beam passes through acceleration gaps. In the modified betatron, injection and extraction ports, and slots to enhance magnetic flux diffusion into the torus can give rise to the same type of instability. Chapter V gives our main conclusions.

II. Beam Injection

Injection of a high current beam into the modified betatron is complicated by the presence of the toroidal magnetic field. The simplest way to overcome the problem is to place the diode inside the torus, and inject along the toroidal field lines.[2] An alternative scheme is to have the diode outside the torus and to inject along temporarily open field lines.[3] We have looked only at the first scheme.

In the modified betatron the equilibrium radial position of the beam centroid, r_c, is determined by equating the centrifugal force to the opposing force from the self and applied field, i.e., $\gamma V_\theta^2/r_c = E_r^{self} + V_\theta (B_z^{ext} + B_z^{self})$, where γ is the beam energy and V_θ is the toroidal velocity. (We are using units in which m = c = 1.) As shown by Kapetanakos et al.[2] there is a convenient cancellation of the space-charge depression of the injection energy γ_i by the toroidal correction to the self magnetic field B_z^{self}. As a result, the equilibrium radius is given simply by $r_c = \gamma_i \beta / B_z^{ext}$, where $\beta = (1-1/\gamma^2)^{1/2}$. This result was confirmed by a three-dimensional PIC simulation using IVORY.[4] In this study, a pulse was injected into a torus of major radius r_0 = 1 m. The coordinate system used was cylindrical, r, θ, z, where the z-axis coincided with the major axis of the torus, and θ was the toroidal angle (Fig. 1). Two cases were studied, one in which injection took place at $r = r_0$, $z = 0$, $\theta = 0$ (centered-injection case) and one ion in which injection was at $r = r_0 + 4$ cm, $z = 0$, $\theta = 0$ (offset-injection case). The injected pulse had a radius of 2 cm and had a trapezoidal time profile of current I and energy γ. Over the first 5 ns, the current rose from I=0 to 10 kA, and energy went from $\gamma = 2$ to 5. This was followed by a 10 ns "body" in which I = 10 kA, $\gamma = 5$ and finally by a 5 ns tail which was the mirror image of the head. These values for γ are the space-charge depressed values. The injection energy γ_i was larger: $\gamma_i = 7$ in the body of the pulse. The applied B_θ and B_z fields were modeled by the required curl-free forms.[5] The values of B_z and the external field index n were chosen to ensure that the main body of the beam followed a stable orbit which did not

intersect the wall. The results of a centered-injection case in which the beam was initially cold are shown in Fig. 2. In this simulation, we chose $n = 0.25$, B_z $(r = r_0) = 114$ kG and B_θ $(r = r_0) = 3$ kG. When combined with the value of γ_i, this yields a predicted equilibrium radius of 100 cm. The body of the pulse in fact propagated quiescently through the first turn (which is as far as the simulation ran) at exactly this radius. Figure 2 shows that the head of the pulse is drifted into the upper wall at $z = 8.9$ cm. This is due to the fact that in the head (and tail) we did not have radial force balance because of the lower value of γ. As a result, there was a net radial force F_r on the particles causing an $F_r \times B_\theta$ drift in the z-direction. The resulting deposition of energy on the wall may create plasma leading to vacuum degradation and possibly an ion resonance instability of the beam.[6] However, serious damage to the wall is not expected, since the point where the beam contacts the wall moves along with $v \approx c$. The area of contact is about $r_0 \Delta\theta \, \Delta r = 30 \times 4.5$ cm^2.

In the offset injection case the centroid of the beam was injected at $r = 104$ cm and the applied vertical field was 112 G. The injection energy γ_i was the same as before, so that the theoretically predicted equilibrium radius is $r_c = 105$ cm. As seen in Fig. 3, the body of the pulse propagated around the torus at about this radius. We conclude that a large radial offset in the injection does not adversely affect beam propagation or beam quality.

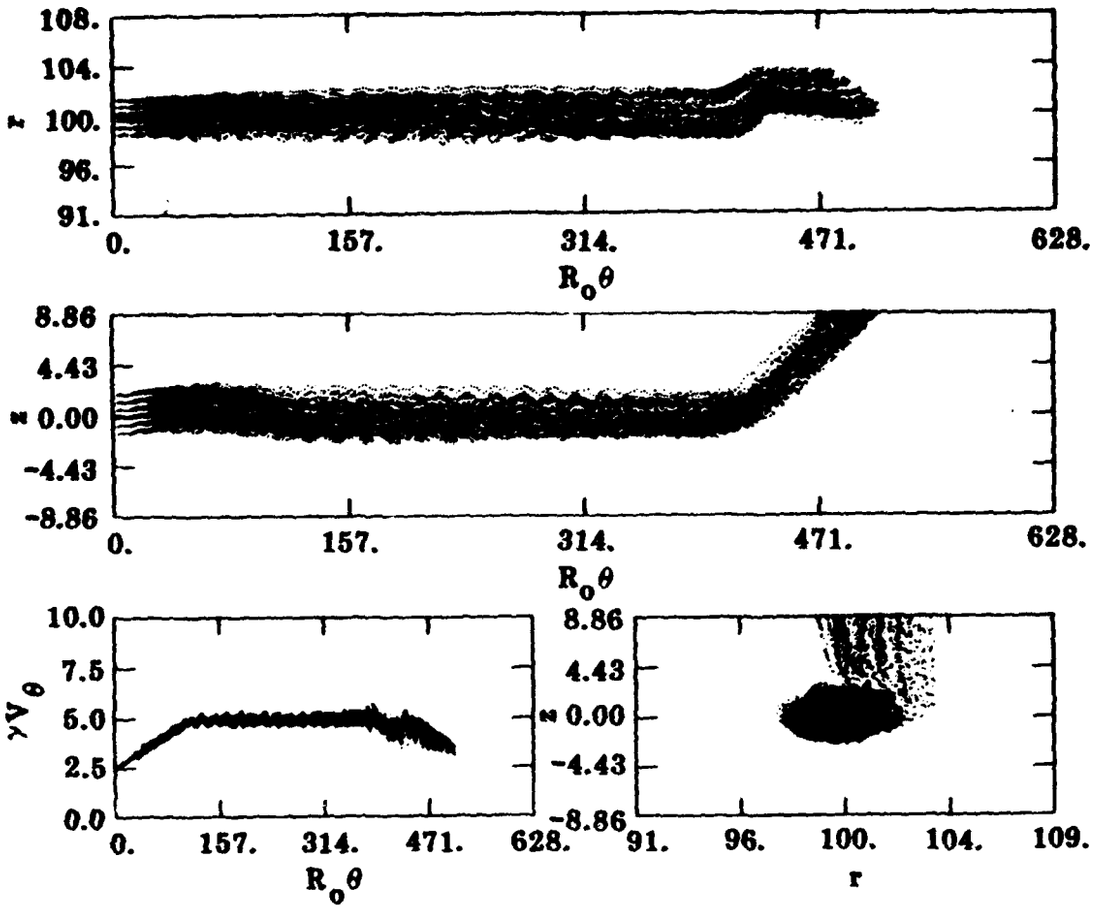

Figure 2. Phase space plots of a 20 ns beam pulse being injected at $\theta = 0$, $r = r_0 = 100$ cm, $z = 0$ into a betatron. This plot was made 19 ns after the beginning of injection. While the plots are rectangular, the simulations was done in r-θ cylindrical geometry. Lengths are in centimeters; V_0 is normalized to c.

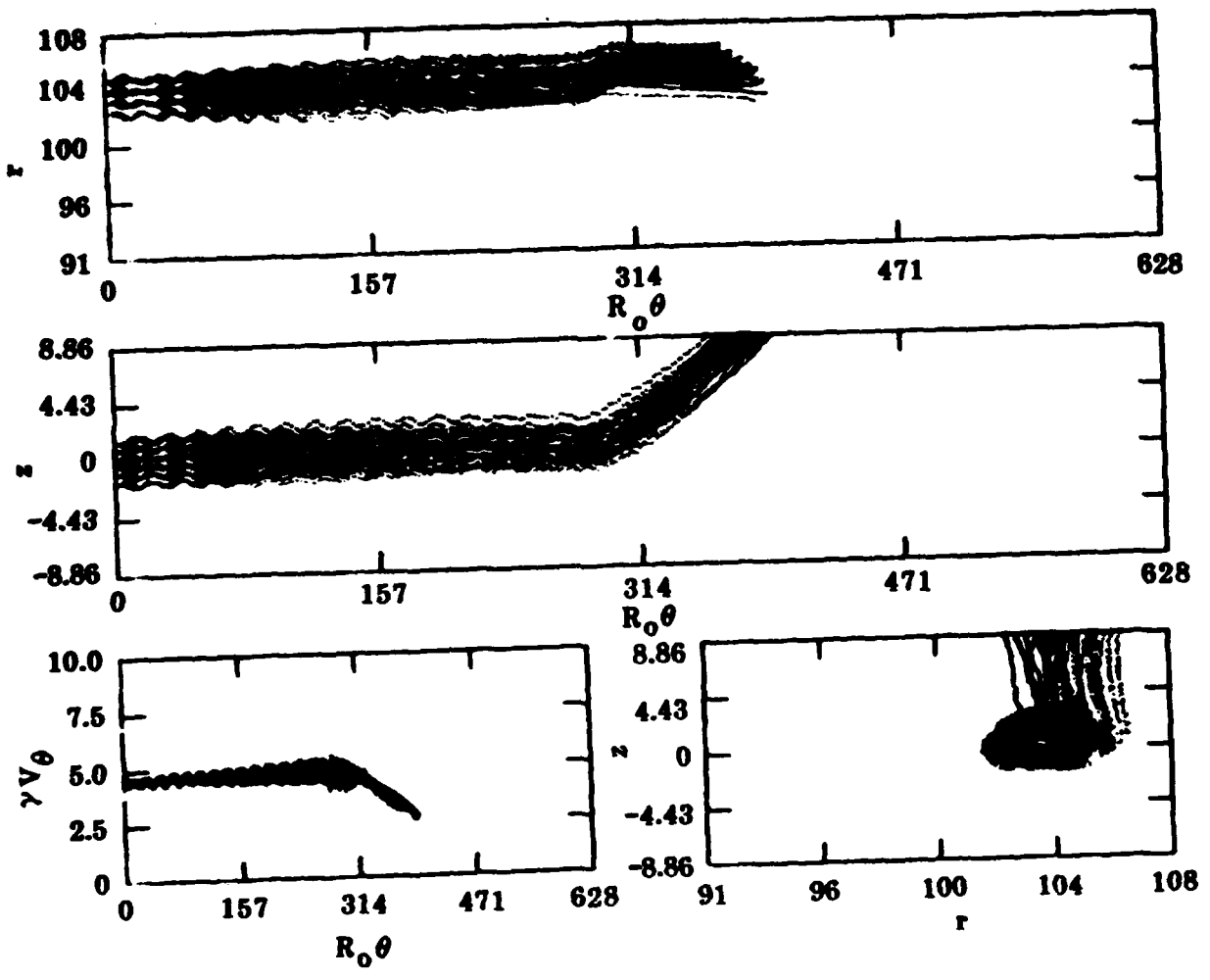

Figure 3. Phase space plots of a 20 ns beam pulse injected at $\theta = 0$, $r = 104$ cm, $z = 0$. The plot was made 15 ns after the beginning of injection.

III. Beam Equilibrium

During a hypothetical 1 millisecond acceleration time in a 1 m radius betatron, the beam circulates about 48,000 times. It is therefore essential to have accessible self-consistent equilibria for the beam. In analytic and numerical work, such equilibria form the starting point for the study of beam stability. The most detailed and exact calculations of beam equilibria to date have been carried out by Finn and Manheimer,[7] using a cold-fluid model of the beam. Their results show that self-consistent equilibria do in fact exist in the parameter regime of the proposed NRL experiment (10 kA, 2 kG toroidal field, $\gamma \gtrsim 3$). These equilibria are analogous to the slow mode of rotation of a cylindrical laminar beam in an axial guide field. In order to test the sensitivity of their equilibria to the cold-fluid assumption, we used Finn's code EQUIL3[8] to initialize IVORY for $\gamma_i = 14$, $I = 10$ kA, $B_\theta = 1$ kG. In IVORY, numerical noise due to discrete particle effects causes deviations from the perfect laminarity assumed in EQUIL3. The drift surfaces obtained from EQUIL3 are shown in Fig. 4. The fact that these surfaces are closed in the region where the beam indicates that an equilibrium exists. In the simulation, we propagated the beam for twenty revolutions around the torus during which time the beam rotated twice about its own axis. No drifting off center was observed, and the beam minor radius remained constant. We conclude that the EQUIL3 equilibria are not significantly affected by the addition of small amounts of temperature.

The methods of Finn and Manheimer break down as the transition from diamagnetic to paramagnetic rotation of the beam about its own axis is approached. The transition occurs at the energy at which the self forces of the beam are equal to the weak focusing force due to the external field index. For a uniform density beam with Budker's parameter ν and beam radius r_b, the transition occurs at

$$\gamma_T = (4\nu\, r_o^2/r_b^2)^{1/3} \qquad (1)$$

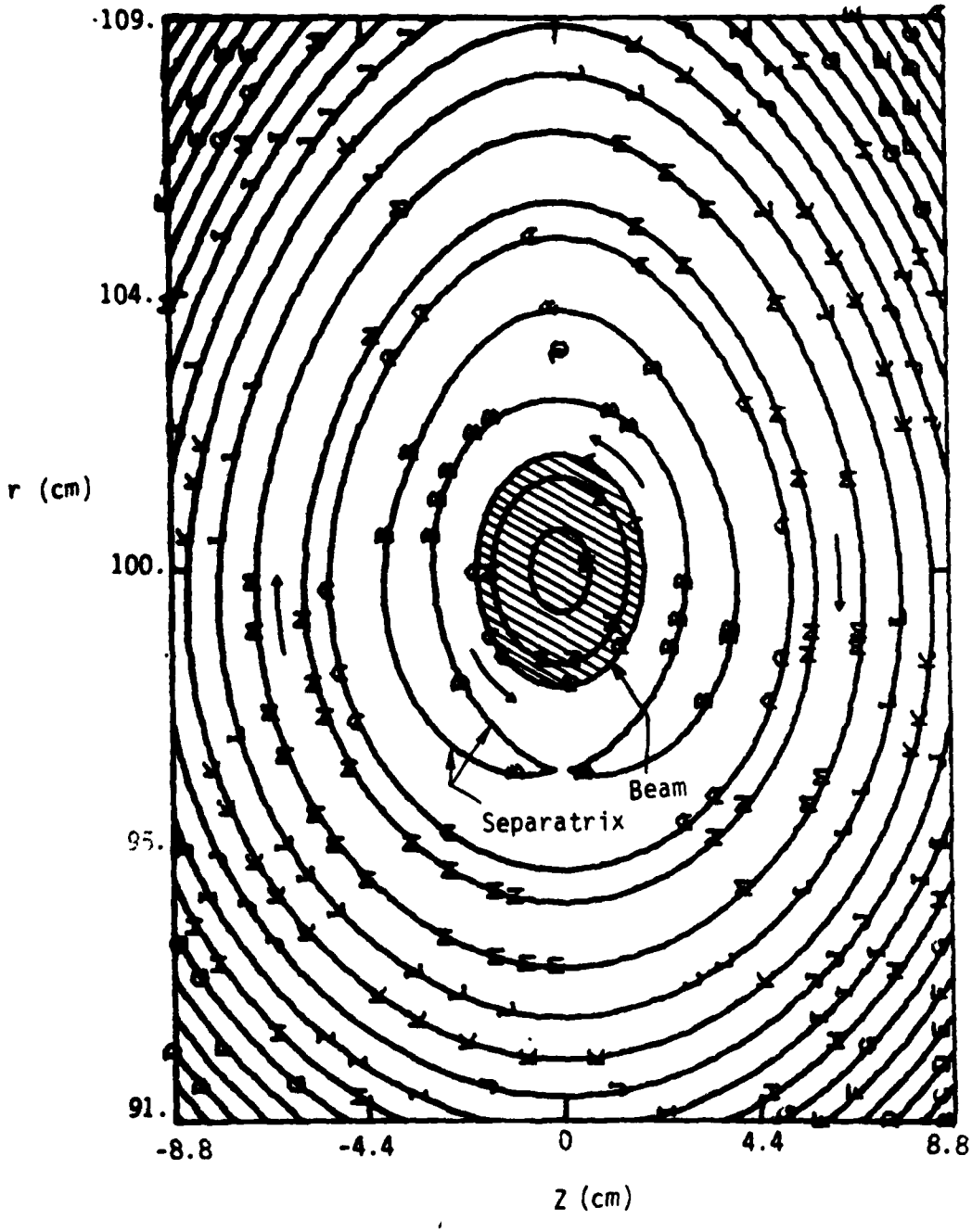

Figure 4. Drift surfaces obtained from EQUIL3. Inside the separatrix, the drift is diamagnetic (anti-clockwise here). Outside, it is paramagnetic (clockwise).

For the parameters we have adhered to in all our simulations, namely r_b = 2 cm, r_0 = 1 m, I = 10 kA, we have γ_T = 18. Above this energy, the toroidal field is not needed for equilibrium. However, for reasons related to beam stability, orbital resonances etc., the toroidal field will in practice probably be maintained throughout the acceleration of the beam. No detailed cold-fluid calculations of beam equilibria along the lines of Ref. 7 have been carried out for $\gamma > \gamma_T$. In our simulations we have found that by using the same numerical presciption as for $\gamma < \gamma_T$ we can find satisfactory equilibria above transition.

Since betatron equilibria analogous to the slow rotation mode in cold cylindrical beams have been found, it is natural to ask whether other cylindrical beam equilibria carry over to the betatron. We have looked at both a "fast mode" and a Kapchinsky-Vladimirsky (K-V) distribution, but neither appears to a modified betatron equilibrium, at least in the regime we examined. In the "fast mode" the beam is again laminar, but rotates at approximately the cyclotron frequency $\Omega\theta/\gamma = eB_\theta/mc\gamma$, where B_θ is the toroidal magnetic field. When initialized in this manner at B_θ = 1 kG, γ = 12, the beam slowly expanded in minor radius, and 1/3 of the particles were lost to the wall after 14 turns.

If a beam from a non-immersed cathode is propagated into a region with an axial magnetic field, then a K-V distribution can result. The beam rotates at half the cyclotron frequency, $\Omega_\theta/2\gamma$, and transverse emittance supplies the additional radial force needed for equilibrium. With B_θ = 1 kG and γ = 12, a beam with a K-V distribution expanded and lost over half of its particles in 15 turns. At γ = 20 the behavior was similar. When the toroidal field was turned off at γ = 20 ($> \gamma_T$), however, the K-V distribution showed no significant increase in minor radius. At present we do not have physical explanations for these observations.

An issue of particular importance with regard to beam stability is the amount of energy spread and transverse emittance the equilibrium can tolerate.[9] Lacking self-consistent models to initialize our simulations, we

decided simply to add these effects to the slow-mode equilibrium and see how the beam evolved. Taking the equilibrium at $\gamma = 12$, $B_\theta = 1$ kG, we added a small random component $\Delta\gamma$ to the energy of each particle, drawing from a Gaussian of the form $e^{-\Delta\gamma^2/2\gamma_{th}^2}$, where the γ_{th} is the width. We find that the beam develops spiral arms, made up of particles" evaporating" from the beam, as shown in Fig. 5. These particles can end up on the wall. If γ_{th} is large enough, the whole beam eventually disappears in this manner. This behavior can be understood using results from EQUIL3. Fo the equilibrium shown in Fig. 4, one can compute the drift-surfaces of test-particles with energies different from the equilibrium value. For $\Delta\gamma = \pm 0.1$ (less than 1% deviation from $\gamma = 12$) there are closed diamagnetic drift-surfaces only for particles less than 1 cm from the beam center, as shown in Fig. 6. For $\Delta\gamma = \pm 0.2$, the diamagnetic region is still smaller, as shown in Fig. 7. Particles outside this region are on paramagnetic surfaces, which are distorted near the beam and give the spiraling effect. Particles with energy greater than the equilibrium value form one arm and those with less energy form the other (see Fig. 7). The arms do not rotate. As current is lost from the beam through these arms, the diamagnetic region shrinks. (In the low current limit all equilibria are paramagnetic.) Thus, one can have an "instability" in which all of the beam eventually migrates to paramagnetic surfaces, which may intersect the wall. Choosing $\gamma_{th} = 0.5$, $B_\theta = 1$ kG, we find that 2/3 of the particles are lost to the wall after about four circulations. The remaining particles rotate in the paramagnetic direction, and the energy spread is greatly reduced. For $\gamma_{th} = 0.1$ (Fig. 5), less than 10% of the particles are lost through the "arms", and the remaining beam is cold. The ability of the beam to sustain a temperature spread improves as one gets further below the transition energy. For $\gamma = 4$, for example, Ref. 7 estimates that a low density tail with $\Delta\gamma/\gamma \sim 50\%$ can be confined in the beam.

The effect of increasing the transverse emittance of the beam, leaving everything else fixed, is what one would expect: the beam is mismatched and expands and contracts with an average radius larger than the initial

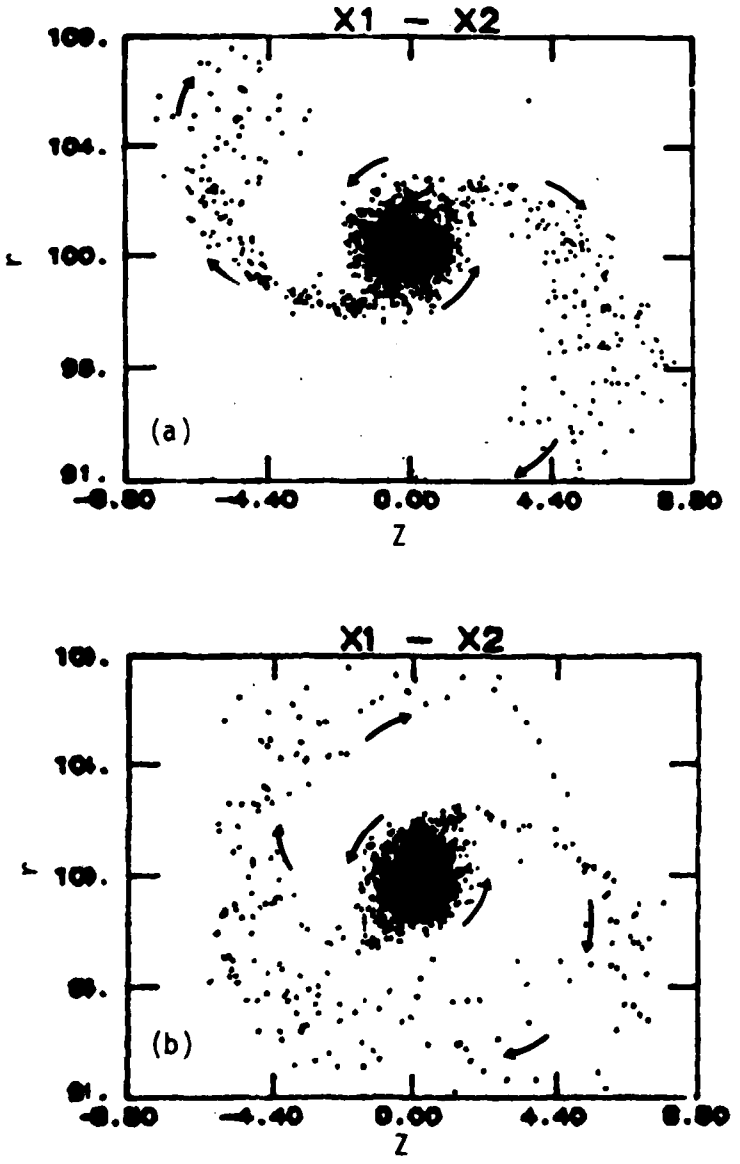

Figure 5. Plots of minor cross-section of beam with 1% energy spread after (a) 4 and (b) 8 turns around torus. Arrows show direction of motion.

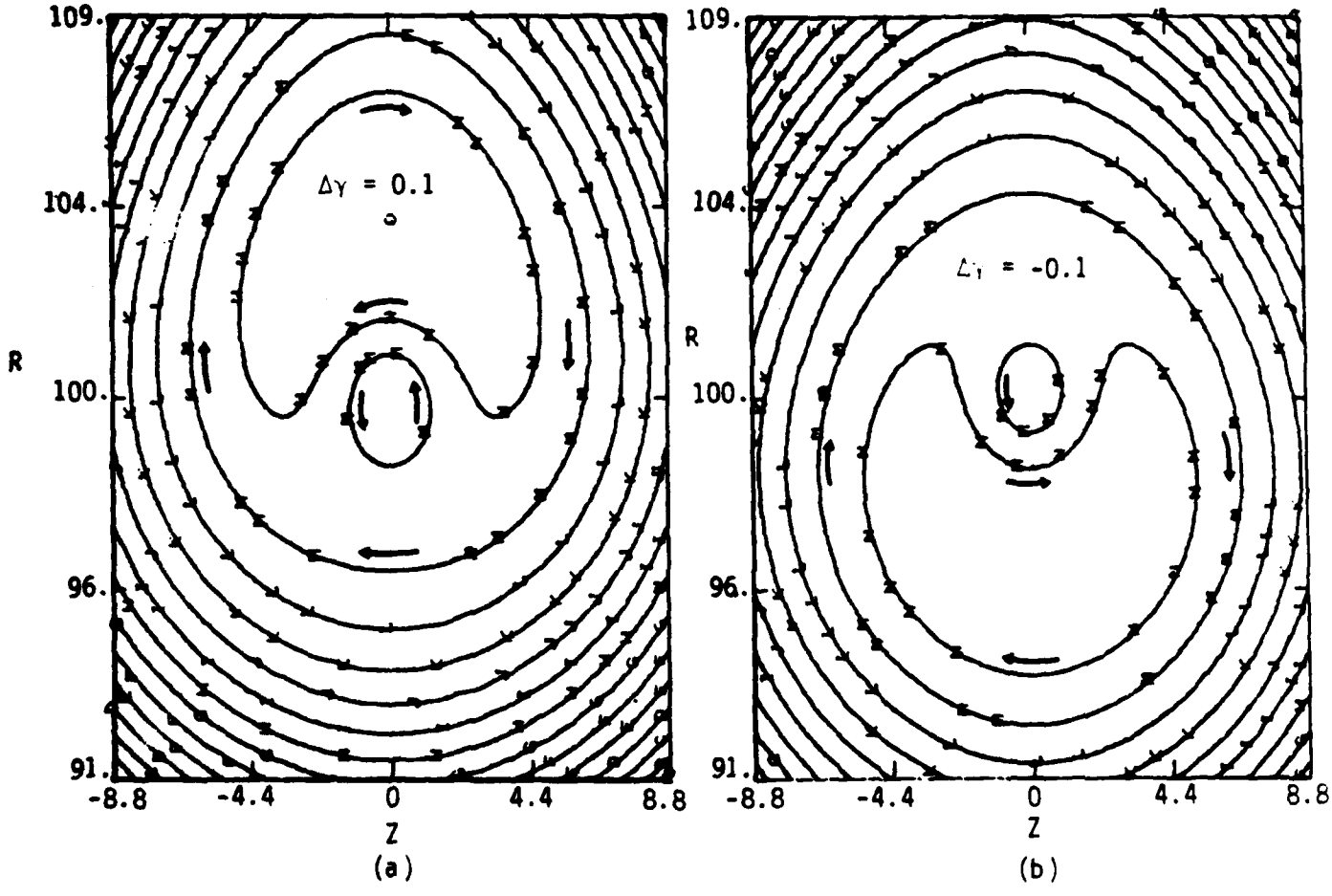

Figure 6. Drift surfaces of test particles with energy mismatch $\Delta\gamma = \pm 0.1$.

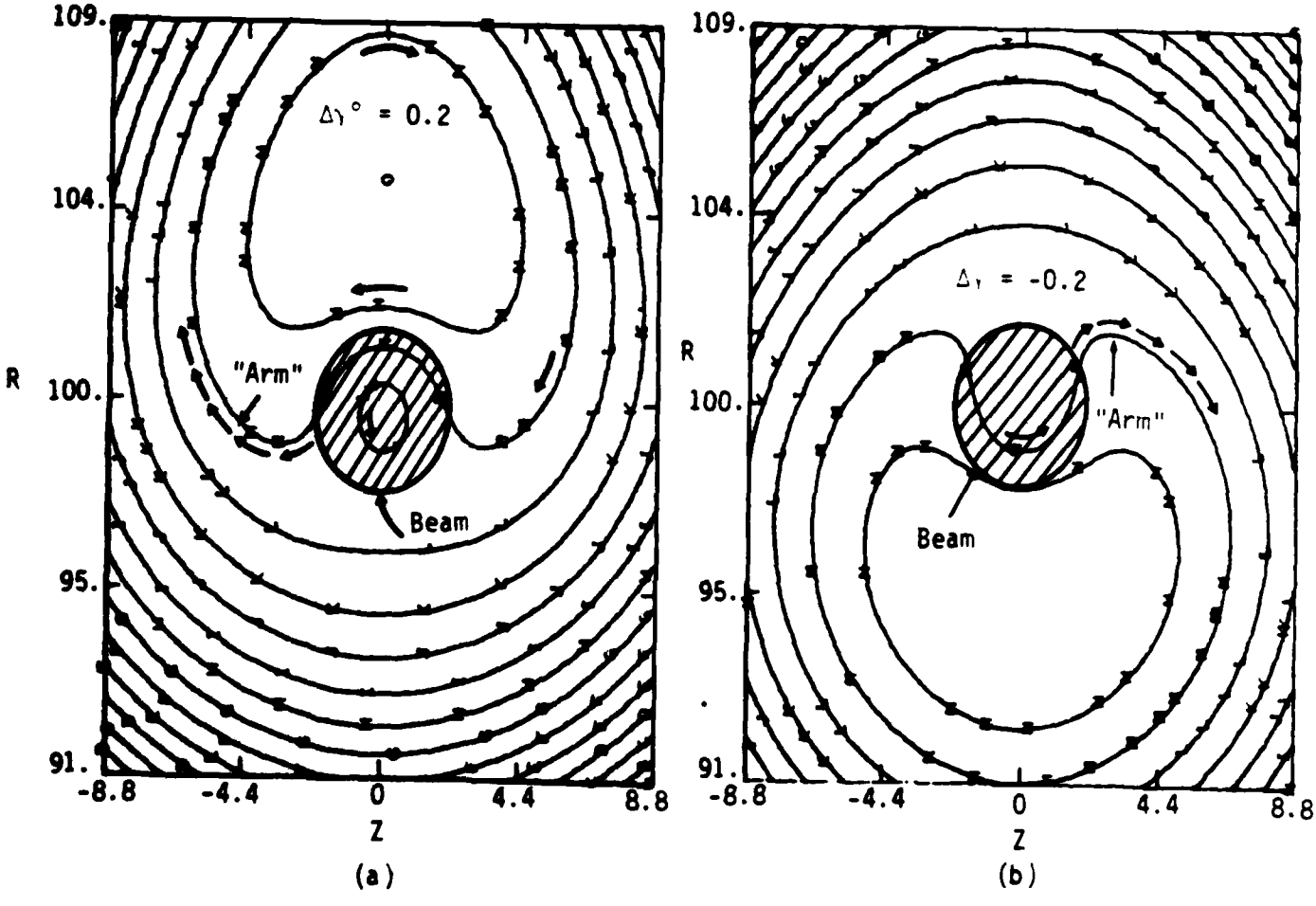

Figure 7. Drift surfaces of test particles with energy mismatch $\Delta\gamma = \pm 0.2$. Arrows indicate how spiral arms arise.

2 cm. Emittance was introduced by giving the particles random perpendicular momenta $P_\perp$ drawn from the distribution $e^{-p_\perp^2/2p_{th}^2}$ where p_{th} is the width. A picture of a beam with $\gamma = 12$, $B_\theta = 1$ kG, $p_{th}/m = 0.28$ is shown in Fig. 8. The beam expands and contracts between radii of 3 and 2 cm. The addition of emittance creates an energy spread, and the formation of spiral arms is observed during the evolution of the beam. These are not very pronounced, however, since the energy spread is small. For a case with $p_{th}/m = 0.4$, the only difference noted was that the maximum beam radius was about 4 cm. No particle loss was observed in these simulations. One would expect that one could obtain a matched state in the presence of increased emittance by making the beam rotate faster about its own axis. Recent work by Grossmann, Finn, and Manheimer[10] confirms this.

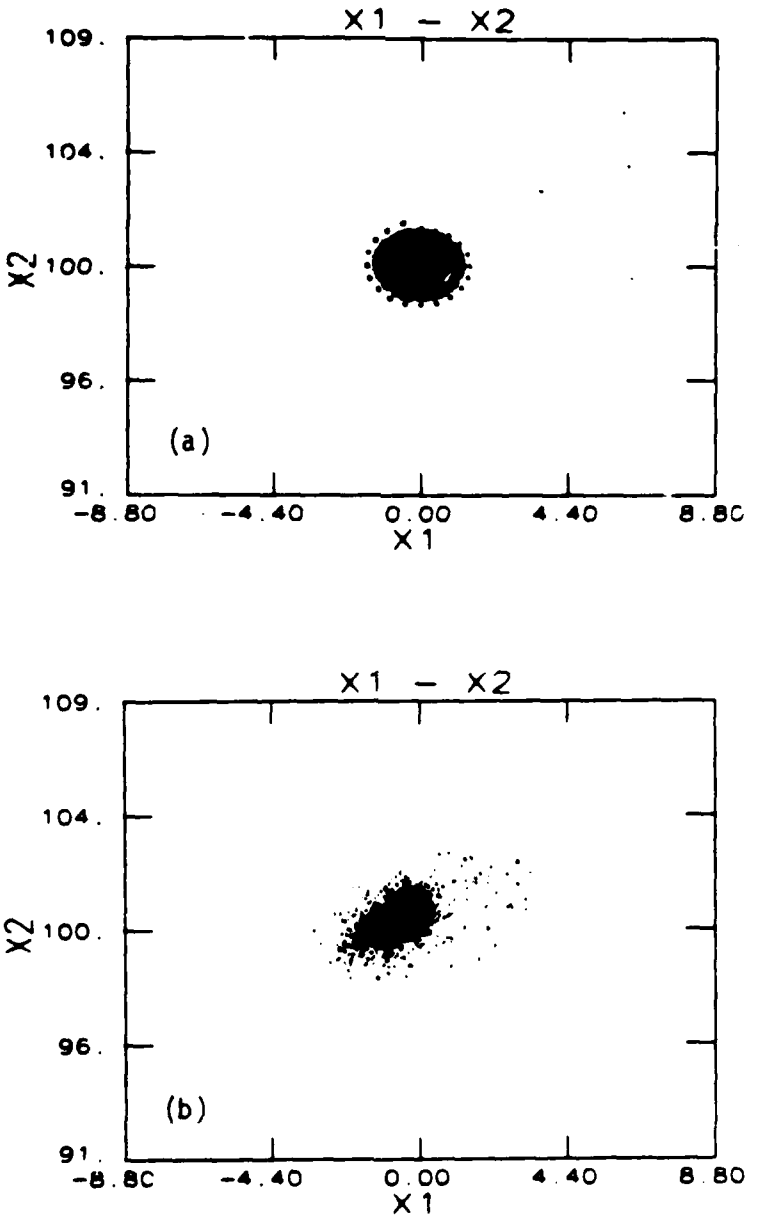

Figure 8. Plots of minor cross-section of beam with increased transverse emittance (a) initially (b) after 3 turns.

IV. Beam Stability

The circulating electron ring in the modified betatron possesses a number of modes of oscillation which can be driven unstable through interactions with each other, with a resistive wall, with gaps in the wall of the device, etc. These instabilities have received a good deal of attention in connection with synchrotron accelerators and storage rings (low current, high energy).[11] It appears, however, that for the high-current regime we are concerned with, some of these instabilities are qualitatively different from what is found at low current. The self-fields and toroidal magnetic field play important roles.

The main emphasis in our work has been on the negative mass instability, since it appears to have the largest growth rate. In addition, it is the instability most readily amenable to analytic and numerical treatment. Our main tool in this study has been the 3-D PIC simulation code IVORY. In conjunction with running simulations, we have reanalyzed the theory of the negative mass instability. The numerical and analytic approaches provide a check on each other. For the resistive wall and beam breakup instabilities, we have performed only analytic and semi-analytic studies owing to the difficulty of performing numerical PIC simulations.

Since there is a considerable amount of algebra associated with derivations for the above instabilities, we have relegated the derivations to the appendices. Only the relevant physical results will be described here.

A. Description of Negative Mass Instability

The conventional negative mass instability causes a toroidal beam to bunch in the toroidal direction.[12] Experimentally, it was found to limit the intensity of the beam by creating a spread in energy, which caused the beam to spread out.[12] In our simulations of the high current betatron, however, very little toroidal bunching is observed. The mode we see is a primarily transverse, almost rigid kinking of the beam, as in Fig. 9.

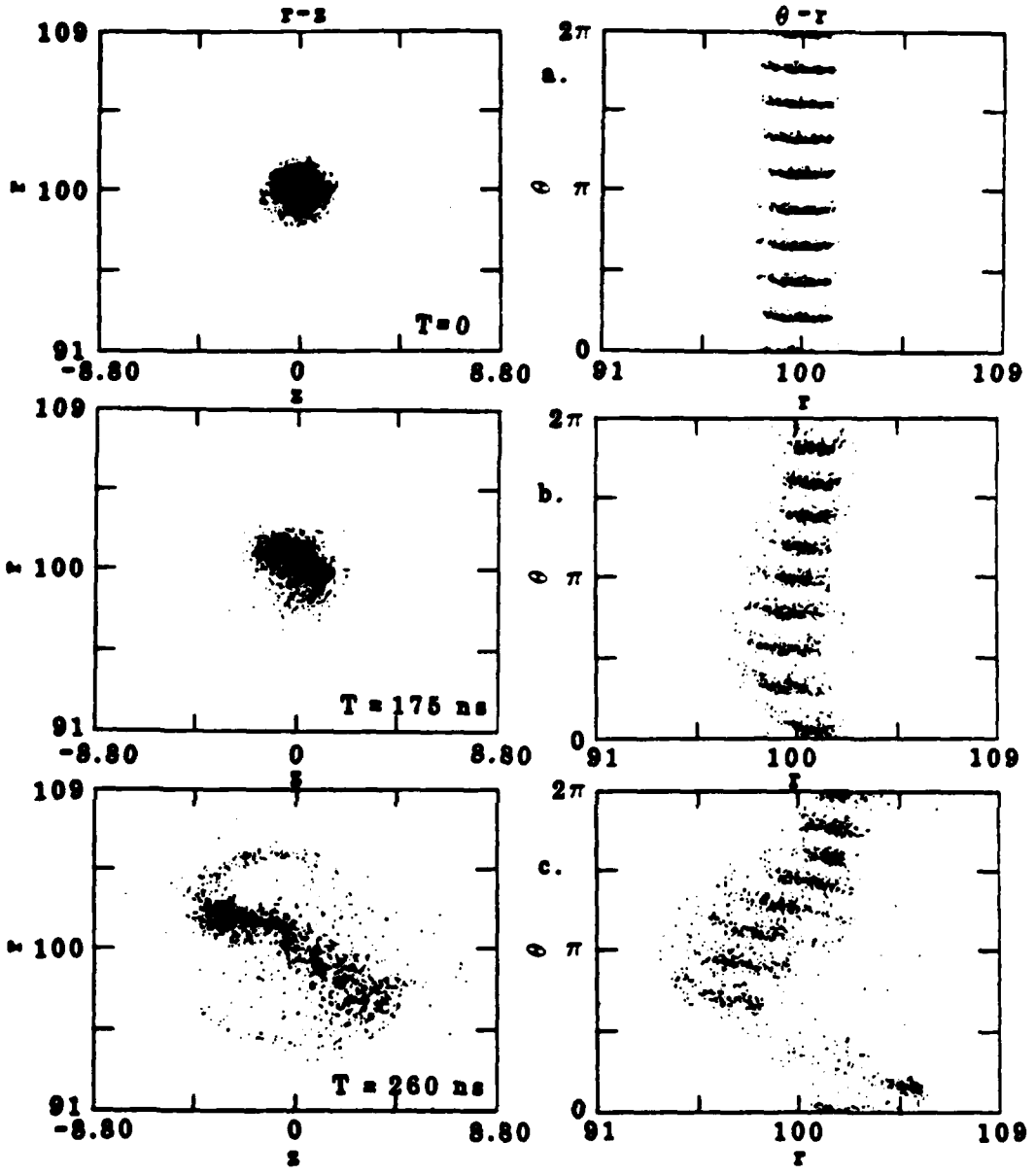

Figure 9. Illustration of transverse kinking effect of negative mass instability. Shown are plots (r vs. z and θ vs. r) of the beam at successive times during the development of the $\ell = 1$ negative mass instability. In the r-z plot, particles at all θ-positions are plotted. Dimensions are in cm.

Some description of our simulation scheme is necessary in order to understand this figure. For stability simulations, IVORY uses a spatial grid to resolve the minor cross-section of the beam. The toroidal dependence of the fields is treated by a sum of Fourier modes. In most of our simulations to date, just three mode numbers are resolved, namely $0,\pm\ell$ where ℓ is an integer. Thus, only a section of $2\pi/\ell$ radians of the torus needs to be modeled. The other ℓ-1 sections are identical. The particles are pushed in a three-dimensional, nonlinear manner. For the sake of economy in computing, just nine groups of particles are used to resolve the wavelength we are simulating. Initially, these groups are identical and equally spaced (Fig. 9a), so that only equilibrium fields are produced. We then initiate the instability by giving the particles a small-amplitude (less than 1% of the beam radius) sinusoidal displacement from their equilibrium position. The instability then commences to grow at a well-defined linear growth rate, with a real frequency approximately equal to $\ell\Omega_z/\gamma$ where Ω_z is the cyclotron frequency associated with the vertical field B_z. The perturbed fields generally grow about four decades in energy during the linear growth regime. As their energy becomes comparable to the equilibrium field energy the effect of the instability on the ring becomes visible, as seen in Fig. 9b. Since the phase velocity of the unstable wave is almost equal to the particle circulation velocity, the sideways displacement of each particle increases monotonically in time. Particles moving to larger radius take longer to go around the torus, and so slip back relative to those at the equilibrium radius. Conversely, particles moving to smaller radii advance relative to those at the equilibrium radius. As a result, the beam eventually breaks in the toroidal direction, as shown in Fig. 9c. Soon after this, the beam strikes the wall and about 2/3 of the current is lost. The remainder continues to circulate for some time as a diffuse cloud. For our typical parameters (10 kA, 6 MeV) and choosing ℓ=1, this whole process takes about 20 circulation periods, or 0.4 μsec, to occur.

B. Linear Growth Rates of Negative Mass Instability: Theory and Simulations

The simulations we performed of the negative mass instability showed substantially different growth rates from those predicted by existing theories.[5,13] These theories neglected the toroidal corrections to Maxwell's equations without rigorous justification. By including these effects to first order in the parameter $\varepsilon = a/r_0$ = (minor radius/major radius), we obtain good agreement with simulations over a wide range of parameters. The details of this calculation are in Appendix A. A comparison between the theory and IVORY simulations for different ℓ-numbers is shown in Fig. 10. Here the beam parameters are $\gamma = 12$, $I = 10$ kA, $B_\theta = 1$ kG. The agreement is rather good even up to $\ell = 20$, where the long wavelength approximation $\ell/r_0 \ll 1/a$, used in the theory, is starting to break down. The growth rate scales approximately as $\ell^{1/2}$. It is noticeable that the agreement for $\ell = 1$ is poorer than for $\ell = 2$ to 8. We suspect that some second order toroidal terms dropped from the theory may be responsible. A derivation keeping these terms is planned (see Appendix A).

The variation of growth rate Γ with γ for $\ell = 1$ is shown in Fig. 11. This figure contains results for both $B_\theta = 1$ and 0 kG. At $B_\theta = 1$ kG, the theory predicts a sharp cutoff at about $\gamma = 21$. Due to numerical noise in IVORY, it is not possible to see zero growth rate. One can only put an upper bound on Γ. At $\gamma = 25$, Γ was reduced by a factor of four from the value at $\gamma = 20$. For $B_\theta = 0$ no equilibrium is possible for $\gamma < 18$ as we saw in Chapter III. The theory predicts that for $\gamma > 12$, there is no negative mass instability. A simulation for $\gamma = 20$ tends to confirm this: we find $\Gamma/c < 2\times10^{-5}$ cm^{-1}.

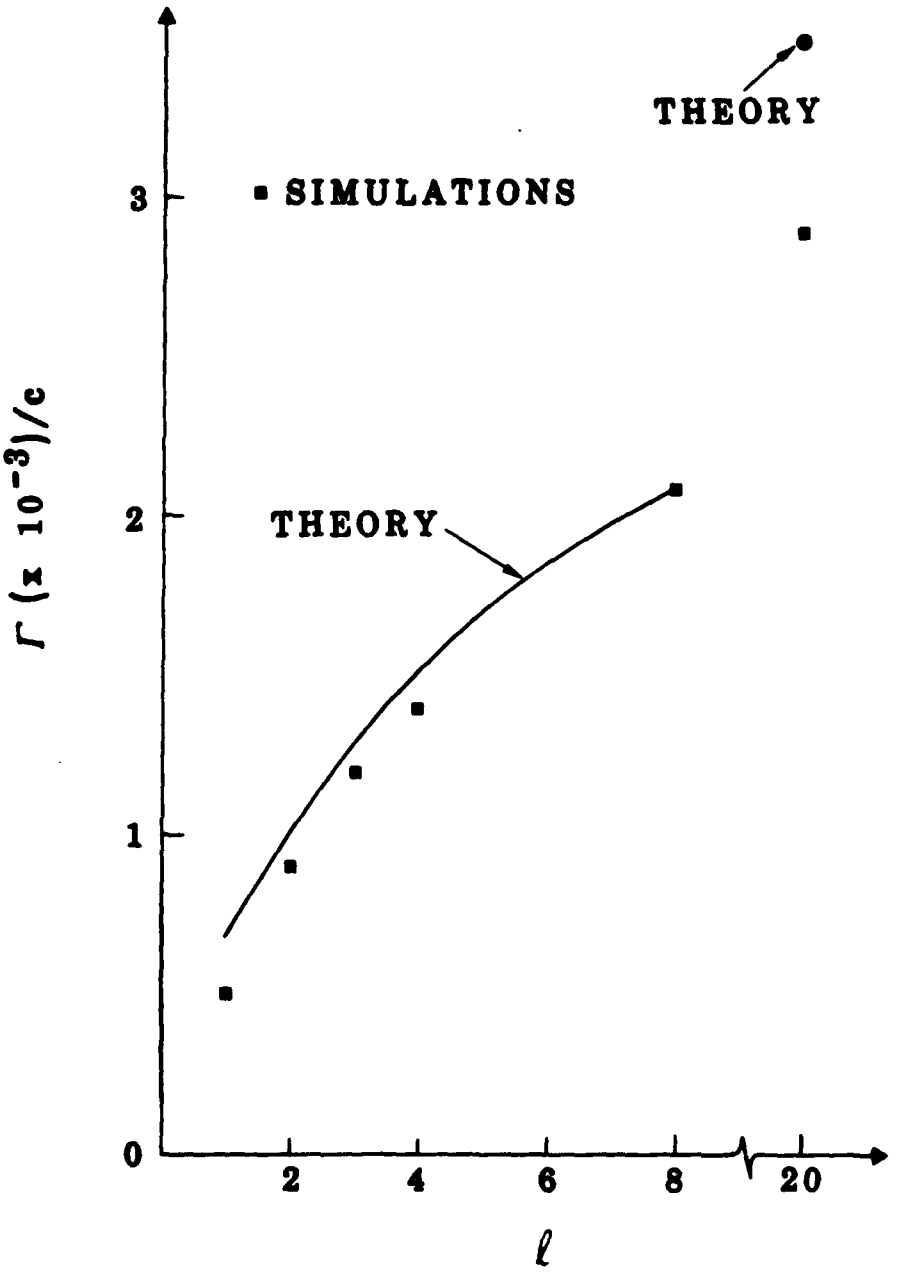

Figure 10. Growth rate of negative mass instability: comparison between theory and simulations for different mode numbers ℓ.

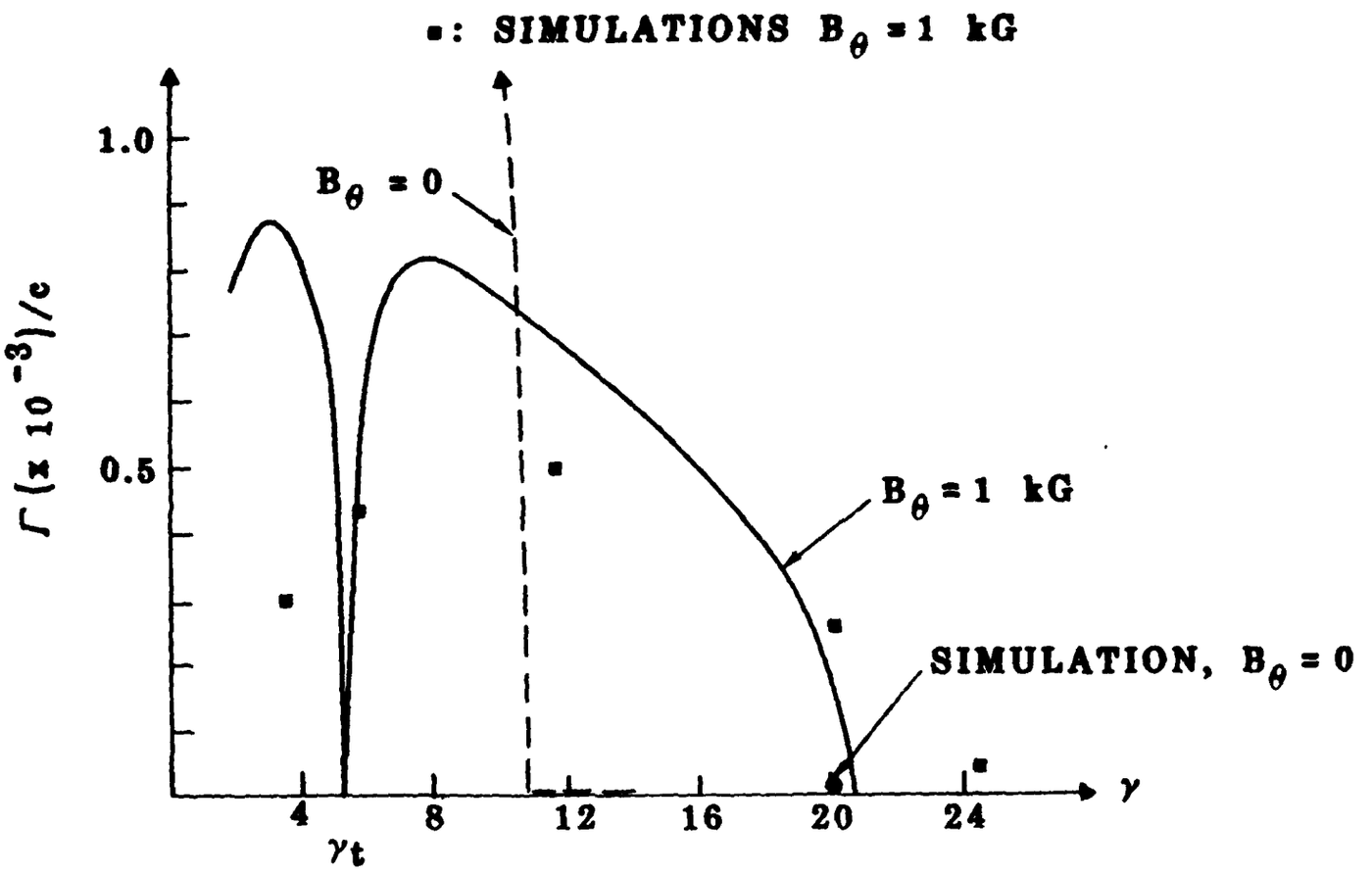

Figure 11. Growth rate of ℓ = 1 negative mass instability vs. γ: comparison between theory and simulations. Data for B_θ = 1 kG and B_θ = 0 are shown.

C. Effects of Transverse Emittance and Energy Spread on Negative Mass Instability

The growth rates computed for the negative mass instability in the last section are very large in practical terms. It has been suggested[5,9] that Landau damping due to a spread in toroidal rotation frequencies can contribute significantly to the stabilization of these modes. Since the beams we are concerned with have $V_\theta \approx c$, a spread in rotation frequencies can come only from a spread Δr in the radii of the particle orbits. If the particles were tied to the field-lines, then the toroidal frequency spread $\Delta\Omega$ would be

$$\frac{\Delta\Omega}{\Omega} = \frac{\Delta r}{r_o} \qquad (2)$$

For the general case, in which particles are not tied to the field lines, Eq. (2) gives an upper bound on the toroidal frequency spread to first order in $\Delta r/r_o$. "Betatron" oscillations of the particles across field lines can add corrections of order $(\Delta r/r_o)^2$ to Eq. (2). For the Finn-Manheimer equilibria, we have computed $\Delta\Omega/\Omega$ by direct measurement of particle rotation frequencies in our simulations. One would expect to achieve the maximum value of $\Delta\Omega/\Omega$ at the transition energy ($\gamma_T = 18$), since poloidal rotation ceases and the particles follow the toroidal field lines. Equation (2) then predicts $\Delta\Omega/\Omega \approx 4\times10^{-2}$, since the beam diameter is 4 cm and $r_o = 100$ cm. At $\gamma = 20$ and $\gamma = 12$ we measured $\Delta\Omega/\Omega = 3\times10^{-2}$ and $\Delta\Omega/\Omega = 6\times10^{-3}$ respectively. The deviations from Eq. (2) are due to poloidal rotation.

To estimate the stabilizing effect of the frequency spread, we did some simulations in which the spread was zero. This was accomplished by replacing the particle beam with a ring made up of rigid disks. We find that for $\gamma = 12$, the growth rates obtained are not significantly different from those of the particle equilibrium, as shown in Fig. 12. For $\ell = 4$, the equations of Ref. 9 would predict a 10% reduction in the growth rate due to the frequency spread which is not inconsistent with our results.

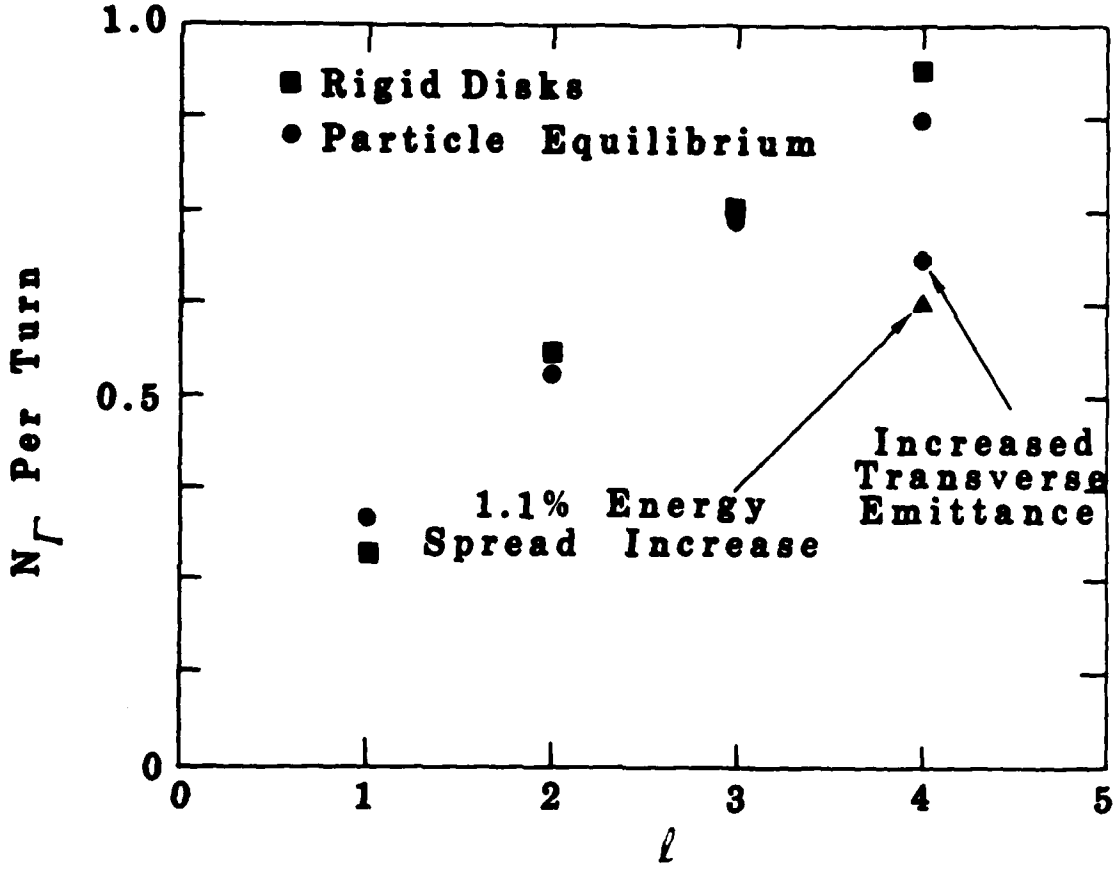

Figure 12. Comparison of growth rates for a rigid beam model with growth rates for self-consistent particle equilibrium, as a function of toroidal mode-number. Also shown are reduced growth rates for a beam with enhanced energy spread or enhanced transverse emittance.

A key question is whether the beam equilibria we are simulating can be modified to obtain substantial reductions in growth rate. In Chapter III, we looked at two ways of increasing the spread in frequencies; viz., by introducing an energy spread on the beam, and by increasing the transverse emittance. The result of having a 1% energy spread is to decrease the growth rate by 30%, as shown in Fig. 12. We saw in Chapter III however, that further increases in energy spread lead to serious loss of confinement. By increasing the transverse emittance from 30 mrad-cm to 90 mrad-cm, the growth rate dropped by somewhat less than 30% (Fig. 12). Again, larger decreases can be obtained only at the expense of beam quality.

D. Resistive Wall Instability

The resistive wall instability is driven by the phase lag between the electric and magnetic response of the wall image to perturbations of the beam. In this section, we summarize the results on this instability obtained in Appendices B and C. There, we find that any slow mode on the beam is driven unstable by a resistive wall. There are two transverse slow modes with frequencies given by $\omega \approx \ell\Omega_z/\gamma - \Omega_{\theta z}/\gamma$ for the cyclotron mode and $\omega \approx \ell\Omega_z/\gamma - \omega_B$ for the "E×B" or "space-charge" mode. Here ω_B is the slow transverse bounce frequency of the beam.

For the slow cyclotron mode, the growth rate peaks at $\omega \approx 0$, which occurs for $\ell \approx \Omega_\theta/\Omega_z$. Since Ω_z and γ increase during beam acceleration, this constraint is satisfied only for a limited time period Δt which corresponds to a band width

$$\Delta\omega \approx \frac{\Omega_\theta}{\gamma^2} \frac{d\gamma}{dt} \Delta t$$

Setting $\Delta\omega$ equal to the growth rate Γ, we obtain the expression for the number of e-foldings as the beam goes through the resonance:

$$\Gamma\Delta t = \frac{\Gamma^2}{\ell(\Omega_z/\gamma)} \frac{\gamma}{d\gamma/dt} \tag{4}$$

Equation (3) is maximized late in the acceleration cycle, when γ is large and the resonant value ℓ is small.

After passing through $\omega \approx 0$, the instability transitions to a lower growth rate regime which persists for the remainder of the acceleration cycle. In this regime the number of e-foldings is given by

$$(\Gamma\Delta t)_{eff} = \int \Gamma dt \tag{5}$$

where the integration is from the time when $\omega \gtrsim 0$ to the end of the acceleration.

For the slow space-charge mode there is no $\omega = 0$ resonance, because $0 < \omega_B/(\Omega_z/\gamma) < 1$. Thus, one has only the regime of adiabatic growth corresponding to Eq. (5). This regime covers the entire acceleration cycle.

Besides the transverse slow modes, there is also a longitudinal slow space-charge mode which is resistive-wall unstable. There is no resonance associated with this mode.

We illustrate the relative importance of the various forms of the resistive wall instability for the typical modified betatron parameters shown in Table 1. A stainless steel wall with normalized conductivity $4\pi\sigma = 5.24\times10^6$ cm^{-1} is assumed. For the cyclotron mode with $\omega = 0$, we find

TABLE 1. TYPICAL MODIFIED BETATRON PARAMETERS USED IN EVALUATING RESISTIVE WALL INSTABILITY GROWTH RATES

Toroidal Magnetic Field	B_θ	2.5 kg
Vertical Magnetic Field (Initial)	B_z	115 g
Toroid Major Radius	R_o	100 cm
Toroid Minor Radius	R	10 cm
Beam Radius	a	1 cm
Beam Current	ν	0.59
Beam Energy	γ	7-100
Acceleration Time	τ	$3 \cdot 10^7$ cm

a growth rate $\Gamma = 4\times10^{-5}$ cm^{-1}. Equation (4) is maximized for $\gamma \approx 70$, for which $\ell = 1$. Total growth is $\Gamma\Delta t = 3.6$ near $\omega = 0$. The contribution from Eq. (5) is much larger, however, giving $(\Gamma\Delta t)_{eff} = 51$.

The growth rate of the transverse space-charge mode is comparable to the cyclotron mode, but growth occurs over the whole acceleration cycle, giving $(\Gamma\Delta t)_{eff} = 150$.

The preceding analysis ignores any thermal spread of beam energy, which would tend to damp the instabilities. In Appendix C, we show that for a spread of a few percent in the initial beam energy, damping should be significant. We saw in Chapter III however, that attempting to stabilize the instability in this way can seriously disrupt the beam if it is near the transition energy.

Successful operation of the modified betatron requires cutting the growth $(\Gamma\Delta t)_{eff}$ to about unity. Employing more highly conducting cavity walls (e.g., copper) can reduce growth by a factor of six. Reducing the acceleration time by an order of magnitude would then effectively eliminate these instabilities. Alternatively, a spread of a few percent in the electron energy may be sufficient to damp out the modes.

E. Beam Breakup and Image Displacement Instabilities

Our work on the beam breakup and image displacement instabilities was motivated mainly by the proposed racetrack induction accelerator.[14] This device, sketched in Fig. 13, is a recirculating accelerator like the modified betatron. However, it uses accelerating gaps instead of a betatron field to increase the beam energy. In a linear device the beam breakup instability arises from a resonant coupling between beam transverse oscillations and m=1 (m = azimuthal mode number) electromagnetic cavity modes localized to the acceleration gaps. This coupling can result in large lateral displacements of the beam.[15] The instability is not due to the accelerating function of the gap. Any discontinuity in the wall can have a

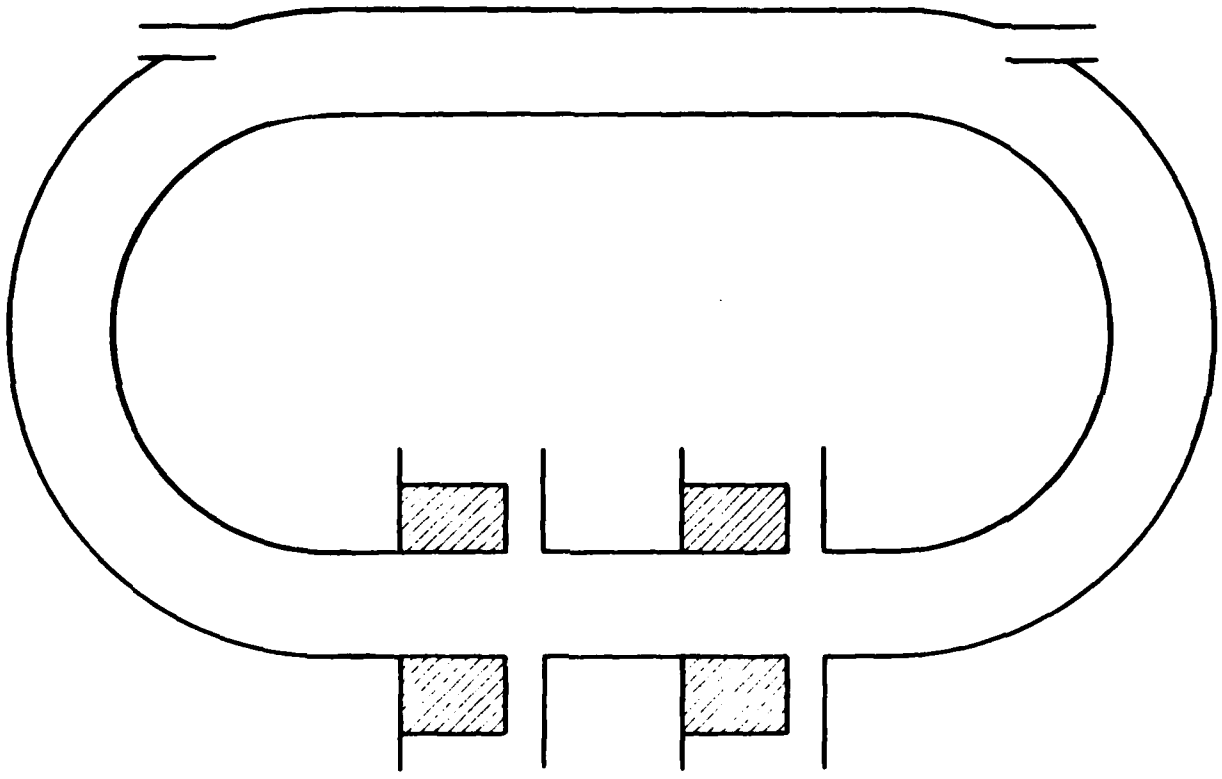

Figure 13. Simplified representation of cyclic induction accelerator racetrack drift tube, acceleration gaps, and injection and extraction ports.

similar effect. Thus, beam injection and extraction ports in the racetrack or modified betatron accelerators could excite beam breakup. Recirculating devices differ from linear devices in that (1) the beam keeps passing the same gaps and (2) there could be a resonant interaction between the beam-breakup and negative mass instabilities. As we saw in Section D, there are two transverse slow modes and one longitudinal slow mode on the beam. These have negative energy and so can couple unstably to the gaps. Coupling to the longitudinal mode occurs only due to toroidal curvature. To model the effect of the gaps, we used a gap response function defined by

$$F = -\frac{Z_\perp}{Q}\ \frac{\omega_o^{\,3}\ \nu}{\omega^2 + i\omega_o\omega/Q - \omega_o^{\,2}} \qquad (6)$$

where $Z_\perp$ is the transverse impedance of the gap, Q is the quality factor and ω_o is the gap resonant frequency. Details of the calculations are given in Appendices D and E.

In Appendix D toroidal terms are dropped so that the beam behaves as if it were in a straight but periodic system. In this way we can study the effect of passing by the same gaps repeatedly. The parameters we studied are given in Table 2. The acceleration gap parameters are those of a linear induction accelerator developed by the National Bureau of Standards. We find a beam breakup growth rate $\Gamma = 1.3\times10^{-3}$ cm^{-1}, yielding 30 e-foldings during the acceleration. This amplification can be cut by reducing Q. If a value of Q = 6 can be attained, then only 5.5 e-foldings occur.

In order to do more exact calculations taking account of beam acceleration and transients, we used the code BALTIC.[16] Table 3 summarizes thirteen runs, varying N (the number of gaps), Q, ω_o, and γ, but keeping $NZ_\perp/Q$ fixed. Cases 1-4 show the effect of changing the gap resonant frequency ω_o. The interaction is greatest when ω_o is an integral multiple of the beam circulation frequency Ω_z/γ, e.g., when $\omega_o = 0.17757 = 13\ \Omega_z/\gamma$. Cases 5 and 6 show the effect of dropping γ. Case 7 shows that by decreasing Q from 60 to 10, the growth rate drops significantly.

TABLE 2. NOMINAL RACETRACK INDUCTION ACCELERATOR PARAMETERS

Path Lengths	L = 460 cm	
Drifttube Radius	R = 7 cm	
Beam Radius	a = 1 cm	
Guide Field	B_z = 2 kg	(ω_c = 1.173 cm^{-1})
Beam Current	I = 1 kA	(ν = 0.0588)
Beam Energy	U = 0.4 - 40 MeV	(γ = 1.5 - 80)
Number of Revolutions	50	
Number of Gaps	N = 4	
Acceleration per Gap	ΔU = 0.2 MeV	($\Delta\gamma$ = 0.4)
Gap Resonant Frequency	880 MHz	
Mode Quality Factor	Q = 60	
Gap Transverse Impedance	15 ohms	($Z_\perp/Q$ = 0.5)
Gap Width	ℓ = 5 cm	

TABLE 3. SUMMARY OF BEAM BREAKUP INSTABILITY CALCULATIONS WITH BALTIC

Case	N	Q	ω_o (cm^{-1})	γ	Γ (10^{-4} cm^{-1})
1	1	60	0.18	80	8.3
2	1	60	0.1732	80	3.3
3	1	60	0.17757	80	8.9
4	1	60	0.1787	80	8.8
5	1	60	0.18	60	10.0
6	1	60	0.17757	60	12.3
7	1	10	0.18	80	3.4
8	2	60	0.18	80	9.6
9	2	60	0.18	1.5	12.0
10	4	60	0.18	1.5-80	9.8
11	4	10	0.18	1.5-80	2.6
12	4	6	0.18	1.5-80	1.2
13	4	6	0.17757	1.5-80	1.6

Cases 8 and 9 treat two evenly spaced gaps, showing that the growth rates are about the same as for a single gap ($NZ_\perp/Q$ is fixed). In cases 10-13 there are 4 gaps spaced 30 cm apart, and the beam is accelerated. The average growth rate is shown. From these we see that with Q = 6 growth of the beam breakup instability is negligible (< 3 e-foldings occur).

The image displacement instability arises due to the interruption of the beam image current at a discontinuity in the drift-tube wall. It is the long wavelength limit of the beam-breakup instability. For our parameters, we compute a peak growth of 9×10^{-5} cm^{-1}, and this occurs only over a narrow range of parameters. Its effect is therefore negligible. No evidence of coherent growth of this instability was seen in the BALTIC runs.

In Appendix E, the effect of the accelerating gaps is put into the full toroidal dispersion relation. In that way, the interaction between the beam breakup and negative mass instabilities can be investigated. The strongest interaction would be expected when the gap resonant frequency matched a harmonic of the beam circulation frequency. For r_o = 70 cm, this occurs for ℓ = 13. The main result of this work is that the coupling between the two instabilities is weak. No strong hybridization occurs. Figure 14 shows that the negative mass instability is dominant and its growth rate is insensitive to the presence of the gaps (Q = 6 is assumed).

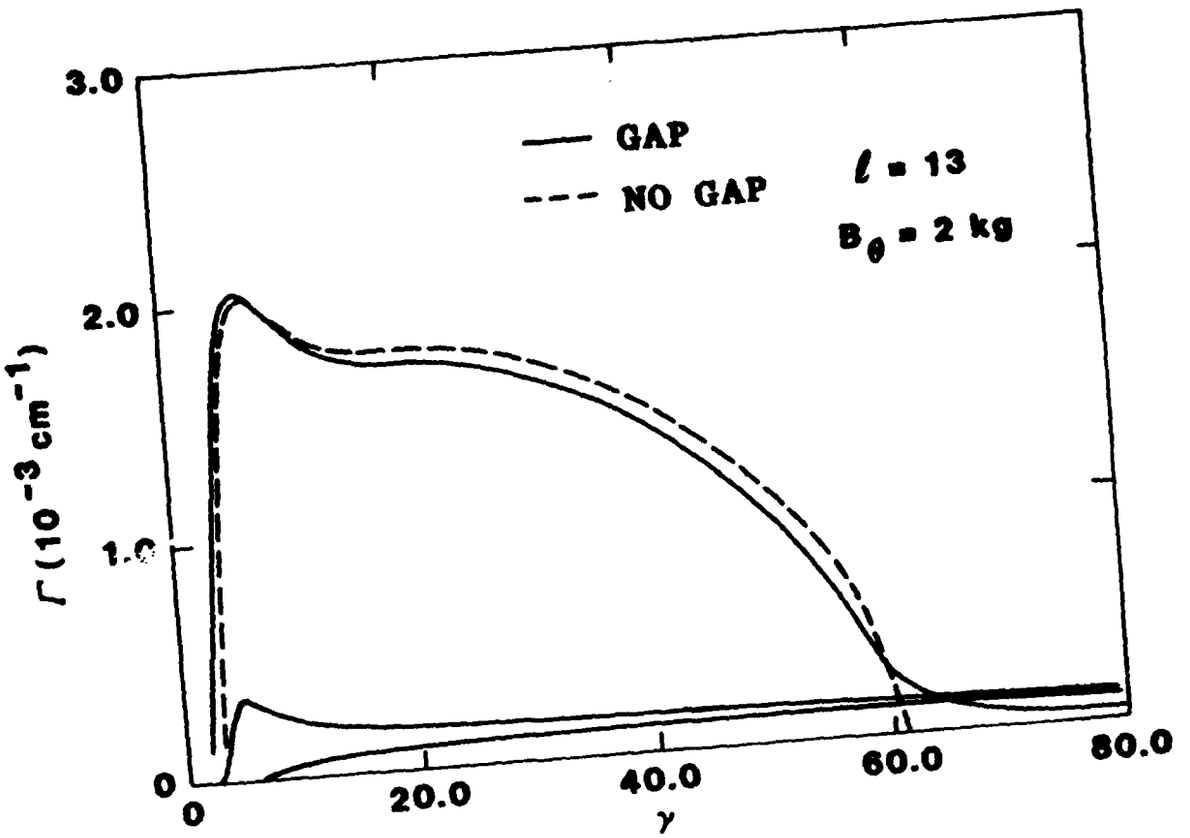

Figure 14. Combined negative mass and beam breakup instability growth rates (solid curves) for ℓ = 13 and B_θ = 2 kG. Growth of the negative mass instability alone (dashed curve) is included for comparison.

V. Conclusions

Our work on the modified betatron accelerator has dealt with a range of topics involving beam injection, equilibrium and stability. For the problem of injection, we performed the first detailed particle simulations of firing a beam into a torus. These showed that the body of the injected pulse propagates in a well-behaved manner around the torus at the theoretically predicted radius. The head and tail of the pulse, which are unmatched, drift rapidly in the vertical direction, striking the wall. No serious wall damage is expected to result.

On the subject of beam equilibrium, we attempted to find in the betatron the counterparts of beam equilibria found in linear devices. Following the work of Manheimer and Finn, we sucessfully simulated the slow rotation mode of the beam. We found that this type of equilibrium was relatively insensitive to the addition of small amounts of transverse temperature. For the fast mode of rotation and for a Kapchinsky-Vladimirsky distribution, no equilibrium could be found for the parameters we chose. We emphasize that our search for these alternative equilibria was not exhaustive.

The addition of an energy spread or of increased transverse emittance to the beam is commonly advocated in order to improve beam stability. We investigated the effect these changes have on the slow-mode equilibrium. We found that unless the beam energy is far removed from the diamagnetic-paramagnetic transition energy, the tolerance of the beam for an energy spread is very limited. The beam tends to develop spiral arms, along which the mismatched particles escape. Significant loss of particles can result. The development of the arms is explained using the Finn-Manheimer model. By adding transverse emittance to the beam, large oscillations of the minor beam radius could be produced. No significant loss of confinement resulted.

The bulk of our work concerned beam stability, and the negative mass instability in particular. Analytic and numerical methods were used. A new analytic dispersion relation was derived keeping toroidal corrections to Maxwell's equations. The new theory overcomes some intrinsic deficiencies of previous theories. We have compared growth rates for the negative mass instability obtained from the theory with 3-D numerical simulations using IVORY. Good agreement is obtained over a wide range of parameters. The growth rate of the negative mass instability is so large that it can seriously disrupt the beam in a microsecond. Addition of an energy spread and transverse emittance give reductions on the order of 30% in growth rate. Much larger reductions clearly are needed. Based on our work to date, we believe that this can be accomplished only by starting with a beam whose radius is comparable to the minor radius of the torus.

In addition to the negative mass instability we looked at resistive wall, beam breakup and image displacement instabilities. In general, these have growth rates substantially less than the negative mass instability. The resistive wall instability can probably be eliminated by using a copper lining for the torus and decreasing the acceleration time to hundreds of microseconds. The beam breakup and image displacement instabilities were considered for their relevance to recirculating devices which use acceleration gaps. We found that by using low quality-factor gaps the growth can be made negligible.

REFERENCES

1. D. W. Kerst, Phys. Rev. 58, 841 (1940).

2. C. A. Kapetanakos, P. Sprangle, and S. J. Marsh, Phys. Rev. Lett. 49, 741 (1982).

3. P. Sprangle, C. A. Kapetanakos, and S. J. Marsh, Proc. 4th International Conf. on High Power Electron and Ion Beams (Palaiseau, France, 1981).

4. M. M. Campbell B. B. Godfrey, D. J. Sullivan, AMRC-R-454 (Mission Research Corporation, Albuquerque, 1983).

5. P. Sprangle and J. L. Vomvoridis, NRL-4688 (Naval Research Laboratory, Washington, 1981).

6. H. S. Uhm and R. C. Davidson, Phys. Fluids 25, 2334 (1982).

7. J. M. Finn and W. M. Manheimer, Phys. Fluids 26, 3400 (1983).

8. J. M. Finn, private communication.

9. P. Sprangle and D. Chernin, "Beam Current Limitations in Modified and Conventional Betatrons," submitted to Particle Accelerators.

10. J. M. Grossmann, J. Finn, and W. Manheimer, Bull. Am. Phys. Soc. 28, 1155 (1983).

11. See e.g., "Theoretical Aspects of the Behavior of Beams in Accelerators and Storage Rings," CERN 77-13 (1977).

12. A. Faltens, G. R. Lambertson, J. M. Peterson and J. P. Rechen, in Proceeding of IXth International Conference of High Energy Accelerators (Stanford, 1974).

13. T. P. Hughes and B. B. Godfrey, AMRC-R-354 (Mission Research Corporation, Albuquerque, 1982).

14. C. W. Roberson, IEEE Nuc. Sci. NS-28, 3433 (1981).

15. V. K. Neil, L. S. Hall, and R. K. Cooper, Part. Accel. 9, 213 (1979).

16. R. J. Adler and B. B. Godfrey, AMRC-R-411 (Mission Research Corporation, Albuquerque, 1982).

APPENDIX A

APPENDIX A

UNCLASSIFIED

SECURITY CLASSIFICATION OF THIS PAGE (When Data Entered)

REPORT DOCUMENTATION PAGE		READ INSTRUCTIONS BEFORE COMPLETING FORM
1. REPORT NUMBER	2. GOVT ACCESSION NO.	3. RECIPIENT'S CATALOG NUMBER
4. TITLE (and Subtitle) IMPROVED LONG-WAVELENGTH DISPERSION RELATION FOR THE NEGATIVE MASS INSTABILITY IN HIGH CURRENT CONVENTIONAL AND MODIFIED BETATRONS		5. TYPE OF REPORT & PERIOD COVERED INTERIM 6. PERFORMING ORG. REPORT NUMBER AMRC-R-520
7. AUTHOR(s) B. B. Godfrey T. P. Hughes		8. CONTRACT OR GRANT NUMBER(s) N00014-84-C-0078
9. PERFORMING ORGANIZATION NAME AND ADDRESS MISSION RESEARCH CORPORATION 1720 Randolph Road, S.E. Albuquerque, New Mexico 87106		10. PROGRAM ELEMENT, PROJECT, TASK AREA & WORK UNIT NUMBERS
11. CONTROLLING OFFICE NAME AND ADDRESS Office of Naval Research 800 North Quincy Street Arlington, Virginia 22217		12. REPORT DATE November 1983 13. NUMBER OF PAGES 25
14. MONITORING AGENCY NAME & ADDRESS(if different from Controlling Office)		15. SECURITY CLASS (of this report) Unclassified 15a. DECLASSIFICATION DOWNGRADING SCHEDULE

16. DISTRIBUTION STATEMENT (of this Report)

Approved for Public Release - Distribution Unlimited.

17. DISTRIBUTION STATEMENT (of the abstract entered in Block 20, if different from Report)

18. SUPPLEMENTARY NOTES

19. KEY WORDS (Continue on reverse side if necessary and identify by block number)

High Current Betatron
Racetrack Induction Accelerator
Negative Mass Instability

20. ABSTRACT (Continue on reverse side if necessary and identify by block number)

A new linear dispersion relation, taking proper account of toroidal curvature effects on the electromagnetic fields, has been derived for the negative mass instability in high current betatrons. (The low frequency and paraxial approximations are employed.) The dispersion relation typically gives growth rates which are smaller than those from earlier analyses and are in better agreement with simulation code results. Applying these findings to the Office of Naval Research racetrack induction accelerator design suggests that it may be safe from severe negative mass instability development with only a modest

DD FORM 1 JAN 73 1473 EDITION OF 1 NOV 65 IS OBSOLETE

UNCLASSIFIED

SECURITY CLASSIFICATION OF THIS PAGE (When Data Entered)

beam energy spread.

TABLE OF CONTENTS

I. INTRODUCTION

An accurate cold beam linear dispersion relation for the negative mass instability in high current conventional or modified betatrons is critical for designing experiments, benchmarking computer simulations, and developing warm beam dispersion relations. In this report we derive a dispersion relation correct to first order in the toroidal aspect ratio of the betatron valid for small toroidal mode numbers. Limited comparisons with earlier work are provided for reference.

The two earlier treatments of negative mass instability growth in high current betatrons included toroidal curvature effects in the particle dynamics but not in the electromagnetic field equations.[1,2] In other words, the dispersion relations were derived for beam motion in a toroidal cavity but with fields computed for an off-center beam in a straight tube of circular crossection. The first analysis, that of Sprangle and Vomvoridis, used an equation of continuity appropriate to a straight cylinder, as well. In contrast, the second analysis, due to Hughes and Godfrey, incorporated an equation of continuity correct for a toroidal beam. Predicted growth rates from these two models often have been fc to disagree by factors of two for parameters corresponding to peak growth and by even more at higher beam energies. More disturbingly, both models systematically overestimate instability growth rates observed in three-dimensional computer simulations.[3,4] We attribute these discrepancies to incomplete treatment of toroidal curvature effects.

The dominant curvature correction to the field equations is easily identified. Radial motion of an electron ring (see Fig. 1) gives rise to azimuthal bunching. This constitutes the difference between charge continuity in cylindrical and toroidal geometry. Conversely, azimuthal bunching gives rise to a radial electric field, which constitutes the (main) difference between electromagnetic fields in cylindrical and toroidal geometry.

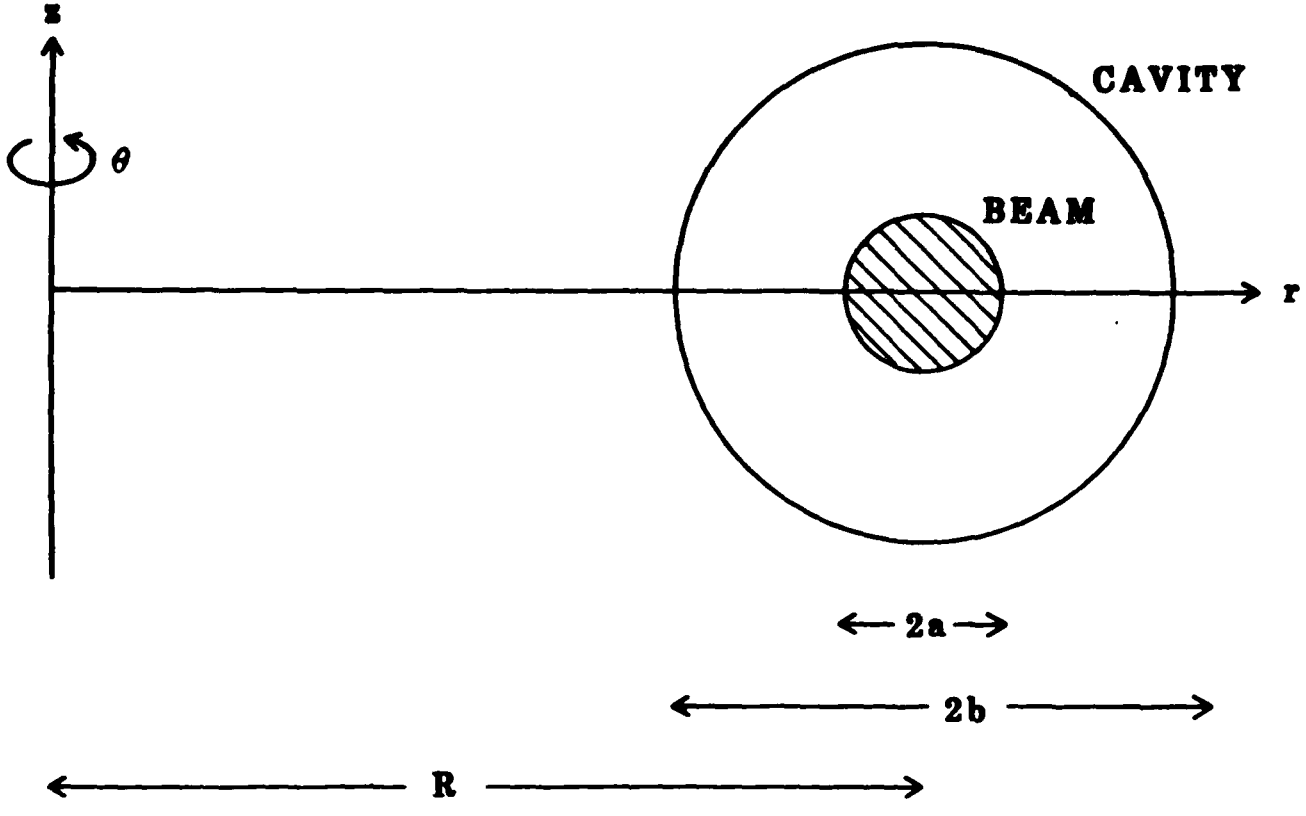

Figure 1. Schematic representation of betatron cavity with electron beam. Mirror and optional toroidal magnetic fields are applied.

The additional coupling between radial and azimuthal beam motion need not be small. Indeed, for sufficiently large energies this coupling through the fields must dominate coupling through the particle dynamics. The latter falls off with energy, while the former does not.

The present paper includes these and other (lesser) curvature effects to first order in the equilibrium and perturbed fields, producing what we believe to be a more accurate dispersion relation. Like its predecessors, this analysis ignores the internal dynamics of the beam, treating it as a string of rigid disks. The assumption of long azimuthal wavelengths also is implicit in our derivation. Relaxing the last constraint is conceptually straightforward but algebraically difficult.

In Section II we assemble the various particle and field equations into a 5×5 self-adjoint matrix operator acting on the perturbed beam centroid position and the electrostatic and electromagnetic potentials. The differential equations are solved to first order in the toroidal aspect ratio in Section III, and the remaining algebraic equations collapsed to the desired dispersion relation. When no toroidal magnetic field exists (i.e., for a conventional betatron), an analytic growth rate expression for the negative mass instability, valid over a wide parameter range, can be derived from the general dispersion relation, and this is done in Section IV. We have not yet attempted to obtain a corresponding simple growth rate expression for the modified betatron.

Finally, Section V presents a reevaluation of negative mass growth for the Office of Naval Research racetrack induction accelerator design,[5] based on the new dispersion relation. The average instability growth rate during acceleration from a few to 50 MeV is reduced by a factor of two relative to an earlier prediction.[6] With this improvement, the proposed accelerator may be able to "outrun" the instability with only a modest beam thermal energy spread.[7]

Comparisons with computer simulation results, as applied to the Naval Research Laboratory modified betatron design, are described elsewhere.[8]

II. FORMULATION OF THE PROBLEM

We consider an electron ring circulating in an azimuthally symmetric conducting cavity. Dimensions and coordinates are depicted in Figure 1. For the present we assume only that the beam and cavity crossections are symmetric about z=0. Otherwise, the crossections may assume any reasonable shape. The characteristic minor radius of the beam must be much less than that of the cavity so that the internal dynamics of the beam can be ignored. A mirror magnetic field maintains the beam in a circular orbit, and a toroidal field can be added to confine the beam against its self-fields, which need not be small.

Linearized equations for small transverse displacements of the beam centroid are easily obtained from the single particle equations of motion.

$$\gamma\, \delta\ddot{z} = \delta E_z - V_\theta\, \delta B_r + B_\theta\, \delta\dot{r} + \left(\frac{\partial E_z}{\partial z} - V_\theta\, \frac{\partial B_r}{\partial z}\right) \delta z \qquad (1)$$

$$\gamma\, \delta\ddot{r} = \delta E_r + V_\theta\, \delta B_z - B_\theta\, \delta\dot{z} + \left(\frac{\partial E_r}{\partial r} + V_\theta\, \frac{\partial B_z}{\partial r} - \frac{\gamma V_\theta^2}{R^2}\right) \delta r$$

$$+ \left(\left(\gamma^2 + 1\right)\, \frac{\gamma V_\theta}{R^2} + B_z\right) \delta V_\theta \qquad (2)$$

Perturbed quantities are preceded by a delta (e.g., δz), while unperturbed quantities are not. Total time derivatives of perturbed particle quantities are represented by dots above the quantities (e.g. $\delta\ddot{z}$). Note that the last term in Eq. (2) can be rearranged, if desired, by means of the equilibrium radial force balance equation,

$$E_r + V_\theta B_z + \gamma V_\theta^2/R = 0 \qquad (3)$$

Although the perturbed azimuthal velocity equation can be derived in many ways, using the single particle energy formula seems simplest.

$$\gamma^3 \delta\dot{V}_\theta = \delta E_\theta + \frac{E_r}{V_\theta} \delta r \tag{4}$$

The perturbed azimuthal angle $\delta\theta$ of a beam disk is related to δV_θ by

$$\delta V_\theta = R \, \delta\dot{\theta} + \frac{V_\theta}{R} \delta r \tag{5}$$

Perturbed beam currents resulting from the centroid displacements described by Eq. (1), (2), (4), and (5) are

$$\delta J_r = \rho \, \delta\dot{r}, \quad \delta J_z = \rho \, \delta\dot{z}$$

and

$$\delta J_\theta = \rho \, \delta V_\theta + V_\theta \, \delta\rho \tag{6}$$

Perturbed charge density is, in turn, derived by substituting the perturbed currents into the continuity equation and integrating the result in time.

$$\delta\rho + \frac{\partial}{\partial\theta} \rho\delta\theta + \frac{1}{r} \frac{\partial}{\partial r} r \rho\delta r + \frac{\partial}{\partial z} \rho\delta z = 0 \tag{7}$$

Alternatively, Eq. (7) can be obtained by considering how the density of a beam element changes as it is displaced infinitesimally in each direction.

As explained in the Introduction, we are limiting consideration to low frequencies and long azimuthal wavelengths. In this limit we need only determine the electrostatic and azimuthal electromagnetic potentials, which satisfy

$$\left(\frac{1}{r} \frac{\partial}{\partial r} r \frac{\partial}{\partial r} + \frac{\partial^2}{\partial z^2} \right) \delta\phi = - \delta\rho \tag{8}$$

$$\left(\frac{\partial}{\partial r} \frac{1}{r} \frac{\partial}{\partial r} r + \frac{\partial^2}{\partial z^2} \right) \delta A = - \delta J_\theta \tag{9}$$

The electric and magnetic field combinations appearing in Eq. (1), (2), and (4) are expressed in terms of these potentials as

$$\delta E_z - V_\theta \delta B_r = - \frac{\partial}{\partial z} \delta\phi + V_\theta \frac{\partial}{\partial z} \delta A \tag{10}$$

$$\delta E_r + V_\theta \delta B_z = - \frac{\partial}{\partial r} \delta\phi + V_\theta \frac{1}{r} \frac{\partial}{\partial r} r \delta A \tag{11}$$

$$\delta E_\theta = - \frac{1}{r} \frac{\partial}{\partial \theta} \delta\phi - \frac{\partial}{\partial t} \delta A \tag{12}$$

These equations complete our model.

Let us now cast the equations in matrix form for compactness and to emphasize their symmetry. In so doing we also Fourier transform the equations in time and azimuthal angle, i.e.,

$$\frac{\partial}{\partial t} \rightarrow -i\omega, \qquad \frac{\partial}{\partial \theta} \rightarrow i\ell$$

and eliminate δV_θ and the perturbed electric and magnetic fields.

$$
\begin{bmatrix}
\alpha_z & -i\Omega B_\theta & 0 & -\frac{\partial}{\partial z} & V_\theta \frac{\partial}{\partial z} \\
i\Omega B_\theta & \alpha_r & -i\Omega\beta & -\frac{\partial}{\partial r} & V_\theta \frac{1}{r} \frac{\partial}{\partial r} r \\
0 & i\Omega\beta & \Omega^2\gamma^3 & -i\frac{\ell}{r} & i\omega \\
\frac{\partial}{\partial z}\rho & \frac{1}{r}\frac{\partial}{\partial r} r\rho & \frac{i\ell}{r}\rho & -\left(\frac{1}{r}\frac{\partial}{\partial r} r \frac{\partial}{\partial r} + \frac{\partial^2}{\partial z^2}\right) & 0 \\
-V_\theta \frac{\partial}{\partial z}\rho & -V_\theta \frac{\partial}{\partial r}\rho & -i\omega\rho & 0 & \left(\frac{\partial}{\partial r}\frac{1}{r}\frac{\partial}{\partial r} r + \frac{\partial^2}{\partial z^2}\right)
\end{bmatrix}
\begin{bmatrix}
\delta z \\ \delta r \\ r\delta\theta \\ \delta\phi \\ \delta A
\end{bmatrix}
$$

$$
= 0 \qquad (13)
$$

Note that the matrix operator is self-adjoint, as one would hope. Certain symbols appearing in Eq. (13) are defined as

$$
\alpha_z \equiv \gamma\,\Omega^2 + \frac{\partial E_z}{\partial z} - V_\theta \frac{\partial B_r}{\partial z} \qquad (14)
$$

$$
\alpha_r \equiv \gamma\,\Omega^2 + \frac{\partial E_r}{\partial r} + V_\theta \frac{\partial B_z}{\partial r} + \frac{V_\theta}{R}\left(\gamma^3 \frac{V_\theta}{R} + B_z\right) \qquad (15)
$$

$$
\beta \equiv \gamma^3 \frac{V_\theta}{R} - \frac{E_r}{V_\theta} \qquad (16)
$$

$$
\Omega \equiv \omega - \ell \frac{V_\theta}{R} \qquad (17)
$$

Equation (13) can be solved numerically for beams and cavities of arbitrary cross section. (Before doing so, it probably would be desirable to perform a conformal transformation on r,z to map the beam and cavity boundaries onto coordinate surfaces.) In the next Section we instead assume the beam and cavity to be circular and concentric in cross section, as illustrated in Fig. 1, in order to obtain an analytical dispersion relation. We should bear in mind, however, that other configurations may exhibit improved stability.

III. DERIVATION OF THE DISPERSION RELATION

To develop a dispersion relation from Eq. (13), even for the simple geometry explicitly represented by Fig. 1, is a long and involved process. For the sake of brevity, we here restrict ourselves to outlining the procedure and citing pertinent results.

Converting the partial differential operators in Eq. (13) to a set of coupled ordinary differential operators is the first step. To do this we carry out the coordinate transformation

$$z = x\cos\psi, \quad r = R + x\sin\psi$$

and expand the potentials as Fourier series in poloidal angle ψ.

$$\delta\phi = \sum\delta\phi^m(x)\, e^{im\psi}, \qquad \delta A = \sum\delta A^m(x)\, e^{im\psi}$$

Next, we recast Eq. (13) as a variational integral, insert the $\delta\phi$ and δA expansions, explicitly integrate over ψ, and perform variations with respect to $\delta\phi^m$ and δA^m. This results in an infinite set of differential equations in $\underline{x}$ coupling all the poloidal modes of the potentials.

Expanding the differential equations in x with respect to the cavity aspect ratio, b/R, leads to a natural truncation of the infinite system. Basically, an expansion to order $|m|$ in b/R is consistent with dropping all higher poloidal mode numbers. Two orderings spring to mind. In the first ω, ℓ/R and the electron oscillation frequencies all are taken to be of order unity (or smaller), and the equations expanded to order b/R. In the second, ω and ℓ/R are taken to be of order b/R, and the equations expanded to b^2/R^2. The first alternative is much simpler, seems to capture the essential physics, and agrees reasonably well with simulation results, so we use it in the following calculations. We are, however, investigating the consequences of the second ordering and will publish our findings at a later date.

With the ordering selected, straightforward but tedious calculations yield for $x < a$:

$$\delta\phi = \frac{1}{4}\left(i\frac{\ell}{R}\rho R\delta\theta + \frac{1}{R}\rho\delta r\right)\left(x^2 - a^2\left(1 + 2\ell n\frac{b}{a}\right)\right)$$

$$+ \frac{1}{8R}\rho\delta r\left(-x^2\left(1 - \frac{a^2}{b^2}\right) + 2a^2\ell n\frac{b}{a}\right)$$

$$+ \frac{1}{2}\left(1 - \frac{a^2}{b^2}\right)\rho\delta r \times \sin\psi$$

$$+ \frac{1}{16R} i\frac{\ell}{R}\rho R\delta\theta\left(-x + a^2\left(\frac{a^2}{b^2} + 4\ell n\frac{b}{a}\right)\right) \times \sin\psi$$

$$+ \frac{1}{2}\left(1 - \frac{a^2}{b^2}\right)\rho\delta z \times \cos\psi \qquad (18)$$

$$\delta A = \frac{1}{4} i\omega\rho R\delta\theta\left(x^2 - a^2\left(1 + 2\ell n\frac{b}{a}\right)\right)$$

$$+ \frac{V_\theta}{8R}\rho\delta r\left(-x^2\left(1 - \frac{a^2}{b^2}\right) + 2a^2\ell n\frac{b}{a}\right)$$

$$+ \frac{V_\theta}{2}\left(1 - \frac{a^2}{b^2}\right)\rho\delta r \times \sin\psi$$

$$+ \frac{1}{16R} i\omega\rho R\delta\theta\left(x^2 + a^2\left(3\frac{a^2}{b^2} - 4 + 4\ell n\frac{b}{a}\right)\right) \times \sin\psi$$

$$+ \frac{V_\theta}{2}\left(1 - \frac{a^2}{b^2}\right)\rho\,\delta z \times \cos\psi \qquad (19)$$

The validity of these solutions to the truncated equations has been verified using the symbolic manipulation program MAXIMA.

Back substitution of the potentials into the variational integral allows the remaining integrations to be carried out explicitly. (For consistency, the results are truncated to first order in b/R.) Again, MAXIMA was used to check the manipulations. The resulting matrix equations for the perturbed centroid location appear as Eq. (20). Its determinant is the sought-for dispersion relation.

$$\begin{bmatrix} \alpha_z - \frac{\rho}{2\gamma^2}\left(1-\frac{a^2}{b^2}\right) & -i\Omega B_\theta^\circ & 0 \\ i\Omega B_\theta^\circ & \alpha_r - \frac{\rho}{2\gamma^2}\left(1-\frac{a^2}{b^2}\right) & -i\Omega\beta - i\frac{\rho a^2}{16R}\cdot\left[\omega V_\theta\left(3-3\frac{a^2}{b^2}+4\ell n\frac{b}{a}\right)+\frac{\ell}{R}\left(1+\frac{a^2}{b^2}+4\ell n\frac{b}{a}\right)\right] \\ 0 & i\Omega\beta + i\frac{\rho a^2}{16R}\cdot\left[\omega V_\theta\left(3-3\frac{a^2}{b^2}+4\ell n\frac{b}{a}\right)+\frac{\ell}{R}\left(1+\frac{a^2}{b^2}+4\ell n\frac{b}{a}\right)\right] & \Omega^2\gamma^3 + \frac{\rho a^2}{8}\left(\omega^2-\frac{\ell^2}{R^2}\right)\left(1+4\ell n\frac{b}{a}\right) \end{bmatrix} \begin{bmatrix} \delta z \\ \delta r \\ R\delta\theta \end{bmatrix} = 0 \qquad (20)$$

In evaluating the matrix elements, it is necessary to know the equilibrium fields. They are[9]

$$E_r = \frac{\rho}{2}(r-R) + \frac{\rho a^2}{16R}\left(\frac{a^2}{b^2} + 4\,\ell n\frac{b}{a}\right) \tag{21}$$

$$B_z = -V_\theta\,\frac{\rho}{2}\,(r-R) + V_\theta\,\frac{\rho a^2}{16R}\left(-\frac{a^2}{b^2} + 4 + 4\,\ell n\frac{b}{a}\right)$$

$$+\; B_z^\circ\left(1 - n\frac{r-R}{R}\right) \tag{22}$$

with similar expressions for E_z and B_r. Eq. (3) determines the magnitude of B_z°, and B_θ° is arbitrary.

The dispersion relation is

$$\left(\Omega^2 - \omega_z^2\right)\left(\Omega^2 - \omega_r^2 - \chi/\varepsilon\right) - \Omega^2\,B_\theta^{\circ 2}/\gamma^2 = 0 \tag{23}$$

It represents two longitudinal ($m = 0$) modes, described by the longitudinal dielectric constant,

$$\varepsilon \equiv \Omega^2 - \frac{\nu}{\gamma^3}\left(\frac{1}{2} + 2\,\ell n\frac{b}{a}\right)\left(\frac{\ell^2}{R^2} - \omega^2\right) \tag{24}$$

and four transverse ($m = \pm 1$) modes, described by Eq. (23) with $\chi = 0$. The transverse oscillation frequencies ω_z and ω_r are,

$$\omega_z^2 \equiv -n\,V_\theta\,\frac{B_z^\circ}{\gamma R} - \frac{2\nu}{\gamma^3 b^2} \tag{25}$$

$$\omega_r^2 \equiv -(1-n)\, V_\theta \frac{B_z^\circ}{\gamma R} - \frac{2\nu}{\gamma^3 b^2} - \frac{B_z}{\gamma R} - \frac{2E_r}{\gamma R} + \left(\frac{E_r}{\gamma^2 V_\theta}\right)^2 \quad (26)$$

E_r and B_z in Eq. (26) are given by Eq. (21) and (22) with r=R and B_z° omitted. The last term in Eq. (26) is very small. Typically, the external field index n is chosen such that $\omega_r^2 \approx \omega_z^2$. Note that ν is Budker's parameter, equal to $\rho a^2/4$.

The key result of our analysis is the coupling coefficient between longitudinal and transverse modes, which determines the negative mass instability growth rate.

$$\chi \equiv \left\{\left(\frac{\gamma V_\theta}{R} - \frac{E_r}{\gamma^2}\right)\Omega + \frac{\nu}{\gamma^2}\frac{1}{4R}\left[\omega V_\theta\left(3 - 3\frac{a^2}{b^2} + 4\,\ell n\,\frac{b}{a}\right) + \frac{\ell}{R}\left(1 + \frac{a^2}{b^2} + 4\,\ell n\,\frac{b}{a}\right)\right]\right\}^2 - \left(\frac{\gamma V_\theta}{R} - \frac{E_r}{\gamma^2}\right)^2 \varepsilon \quad (27)$$

For comparison, the dispersion relations from Ref. 1 and 2 also can be cast in the form of Eq. (23) but with coupling coefficients, respectively,

$$\chi \equiv \left(\frac{\gamma V_\theta}{R}\right)^2 (\Omega^2 - \varepsilon) \quad (28)$$

and

$$\chi \equiv \frac{\gamma V_\theta}{R}\,\Omega\left[\frac{\gamma V_\theta}{R}\,\Omega + \frac{\ell}{R^2}\,\frac{\nu}{\gamma^2}\left(1 + 2\,\ell n\,\frac{b}{a}\right)\right] - \left(\frac{\gamma V_\theta}{R}\right)^2 \varepsilon \qquad (29)$$

It should be noted that there is a degree of arbitrariness in the choice for the functional form of $\rho(r,z)$. In the preceding analysis we assumed ρ to be constant out to the beam minor radius a, where it drops abruptly to zero. One might instead have chosen $\rho r/R$ to be constant, for instance.[9] Fortunately, such changes lead only to insignificant modifications of χ, ω_z^2, and ω_r^2.

IV. $B_\theta^\circ = 0$ GROWTH RATE FORMULA

In the absence of a toroidal magnetic field, the negative mass instability dispersion relation reduces to

$$\Omega^2 - \omega_r^2 - \chi/\varepsilon = 0 \tag{30}$$

A simple analytical growth rate expression can be derived from Eq. (30) in a reasonably straightforward manner, if Ω^2 is much less than ω_r^2 and can be dropped from the equation. We address the validity of this assumption at the end of this Section.

Solely for the sake of algebraic simplicity, we invoke four approximations.

$$\frac{1}{\gamma^2} \ll 1$$

$$\frac{\nu}{\gamma^3}\left(1 + 2\ell n \frac{b}{a}\right) \ll 1$$

$$\frac{a^2}{b^2} \ll 1$$

$$\frac{E_r}{\gamma^2} \ll \gamma \frac{V_\theta}{R}$$

All four are well satisfied for typical cases of interest. Then,

$$\varepsilon = \Omega^2 + 2\Omega \frac{V_\theta}{R} \frac{\nu}{\gamma^3}\left(\frac{1}{2} + 2\ell n \frac{b}{a}\right)$$

$$- \frac{\ell^2}{R^2} \frac{\nu}{\gamma^5}\left(\frac{1}{2} + 2\ell n \frac{b}{a}\right) \tag{31}$$

$$\chi = \left[\gamma \frac{V_\theta}{R}\Omega + \frac{\ell}{R^2}\frac{\nu}{\gamma^2}\left(1 + 2\ell n \frac{b}{a}\right)\right]^2$$

$$- \left(\gamma \frac{V_\theta}{R}\right)^2 \varepsilon \qquad (32)$$

Significant cancellations occur when Eq. (32) is expanded.

$$\chi = \Omega \frac{V_\theta}{R}\frac{\ell}{R^2}\frac{\nu}{\gamma} + \frac{V_\theta^2}{R^2}\frac{\ell^2}{R^2}\frac{\nu}{\gamma^3}\left(\frac{1}{2} + 2\ell n \frac{b}{a}\right) \qquad (33)$$

The term linear in Ω, in fact, only survives due to the difference in the factors

$$1 + 2\ell n \frac{b}{a}, \quad \frac{1}{2} + 2\ell n \frac{b}{a}$$

which appear in the first and second terms, respectively, of the definition for χ. Modifications to the expression for χ discussed near the end of the preceding Section, due to changing the functional form of ρ, are of higher order than the terms in Eq. (33) and so drop out. Nonetheless, we should not be surprised if more accurate dispersion relation derivations, perhaps including high frequency electromagnetic effects, adjust the linear term somewhat.

Substitution of Eq. (31) and (33) into

$$\omega_r^2 \varepsilon + \chi = 0$$

leads immediately to the desired growth rate formula.

$$\Omega = \frac{1}{1-n}\frac{\ell}{R}\left\{-\frac{\nu}{2\gamma} \pm i\left[\left(1-n\right)\frac{\nu}{\gamma^3}\left(\frac{1}{2} + 2\ell n \frac{b}{a}\right) - \left(\frac{\nu}{2\gamma}\right)^2\right]^{1/2}\right\} \qquad (34)$$

In obtaining Eq. (34), we have taken

$$\omega_r^2 = (1-n)\ \frac{V_\theta^2}{R^2}\ ,$$

which is accurate for γ^2 not too small, an assumption we have already made. Equation (34) reproduces the exact numerical solutions of the dispersion relation presented in the next Section to an accuracy of 10%.

Equation (34) predicts an instability cutoff for

$$\nu\gamma > 4(1 - n)\ \left(\frac{1}{2} + 2\ell n\ \frac{b}{a}\right) \tag{35}$$

At smaller values of $\nu\gamma$, the negative mass instability reduces to the well known expression[10,11]

$$\Gamma = \frac{\ell}{R}\left[\frac{1}{1-n}\ \frac{\nu}{\gamma^3}\ \left(\frac{1}{2} + 2\ell n\ \frac{b}{a}\right)\right]^{1/2} \tag{36}$$

We remark for completeness that Eq. (28), from Ref. 1, and Eq. (29), from Ref. 2, also yield high $\nu\gamma$ cutoffs. In the case of Eq. (29) instability ceases for[2,12]

$$\nu\gamma > 4(1 - n)/(1 + 2\ell n\ \frac{b}{a}) \tag{37}$$

while Eq. (28) has the same limit without the factor of four. Both analyses lead to Eq. (36) for sufficiently small $\nu\gamma$.

Let us return to our initial assumption,

$$\Omega^2 \ll \omega_r^2$$

Based on Eq. (34), this inequality becomes

$$\left(\frac{\ell}{1-n}\right)^2 \frac{\nu}{\gamma^3}\left(\frac{1}{2} + 2\ell n \frac{b}{a}\right) \ll 1 \qquad (38)$$

or for typical parameters

$$\ell^{2/3} \ll \gamma$$

We see that Eq. (34) is quite generally accurate for $B_\theta^\circ = 0$.

V. THE ONR RACETRACK INDUCTION ACCELERATOR

The Office of Naval Research together with the Naval Research Laboratory have developed the design for a racetrack induction accelerator intended to accelerate a 1 kA ($\nu = 0.0588$) electron beam to 40 MeV ($\gamma = 80$) in fifty revolutions. In an earlier report,[6] we investigated the beam breakup and negative mass instabilities for this design, concluding that the beam breakup instability poses few problems for induction module O's of order six, a realistic value. The negative mass instability was found to be somewhat more threatening, although there was reason to hope that thermal effects would reduce the predicted growth rates, especially for large toroidal mode numebrs.[7] Our work was based on the dispersion relation of Ref. 2. Here, we repeat the analysis using Eqs. (23) - (27).

We treat the racetrack cavity as a torus of major radius R = 70 cm. (Straight sections of the racetrack are expected to have a favorable, but very small, effect on total negative mass instability growth.) Varying the assumed radius has little affect, because changes in the growth rate are approximately balanced by changes in the path length. In accordance with the accelerator design, the cavity and beam minor radii are taken to be b = 7 cm and a = 1 cm. A B_θ° = 2 kG ($\omega_c = 1.73$) guide field is applied.

The numerically determined growth rate for these parameters and ℓ = 13, a toroidal mode number near the upper end of the range for which the model is valid, is plotted as the solid curve in Fig. 2. The result from Ref. 6 is shown as a dashed line. The average growth rate is reduced by about a factor of two. Our more optimistic findings suggest a total negative mass instability amplification factor of fifteen e-foldings. This growth level probably can be reduced to an acceptable level (say, five e-foldings) by thermal effects or design changes.

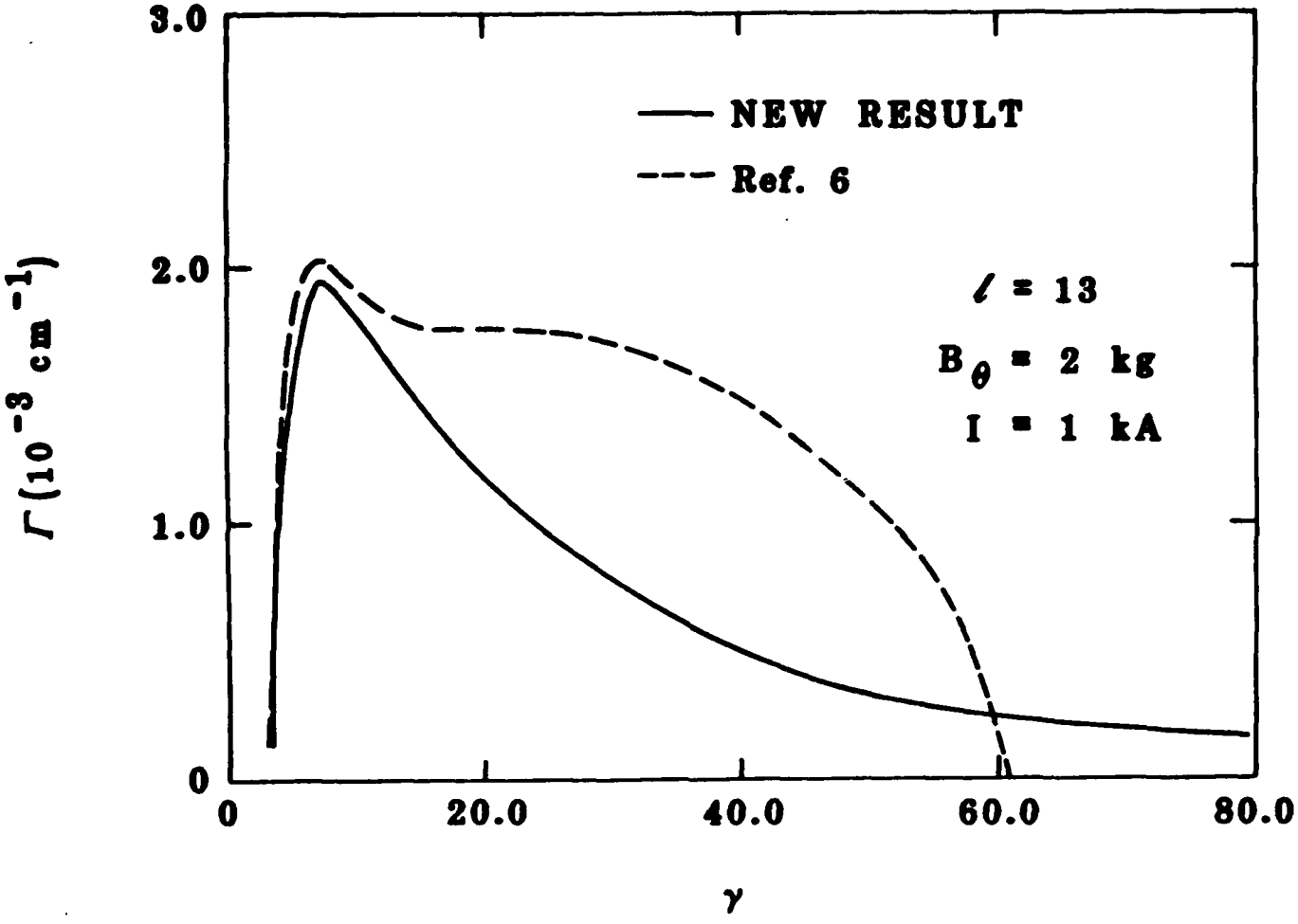

Figure 2. Predicted negative mass instability growth rate as a function of energy for the ONR racetrack induction accelerator design with a 2 kG guide field.

Figure 3 illustrates the corresponding $B_\theta^\circ = 0$ growth rates. Peak values are reduced somewhat relative to the earlier results, but the high energy cutoff is shifted up in energy by a factor of twenty. For $\gamma \gtrsim 20$, Eq. (34) reproduces the solid curve well.

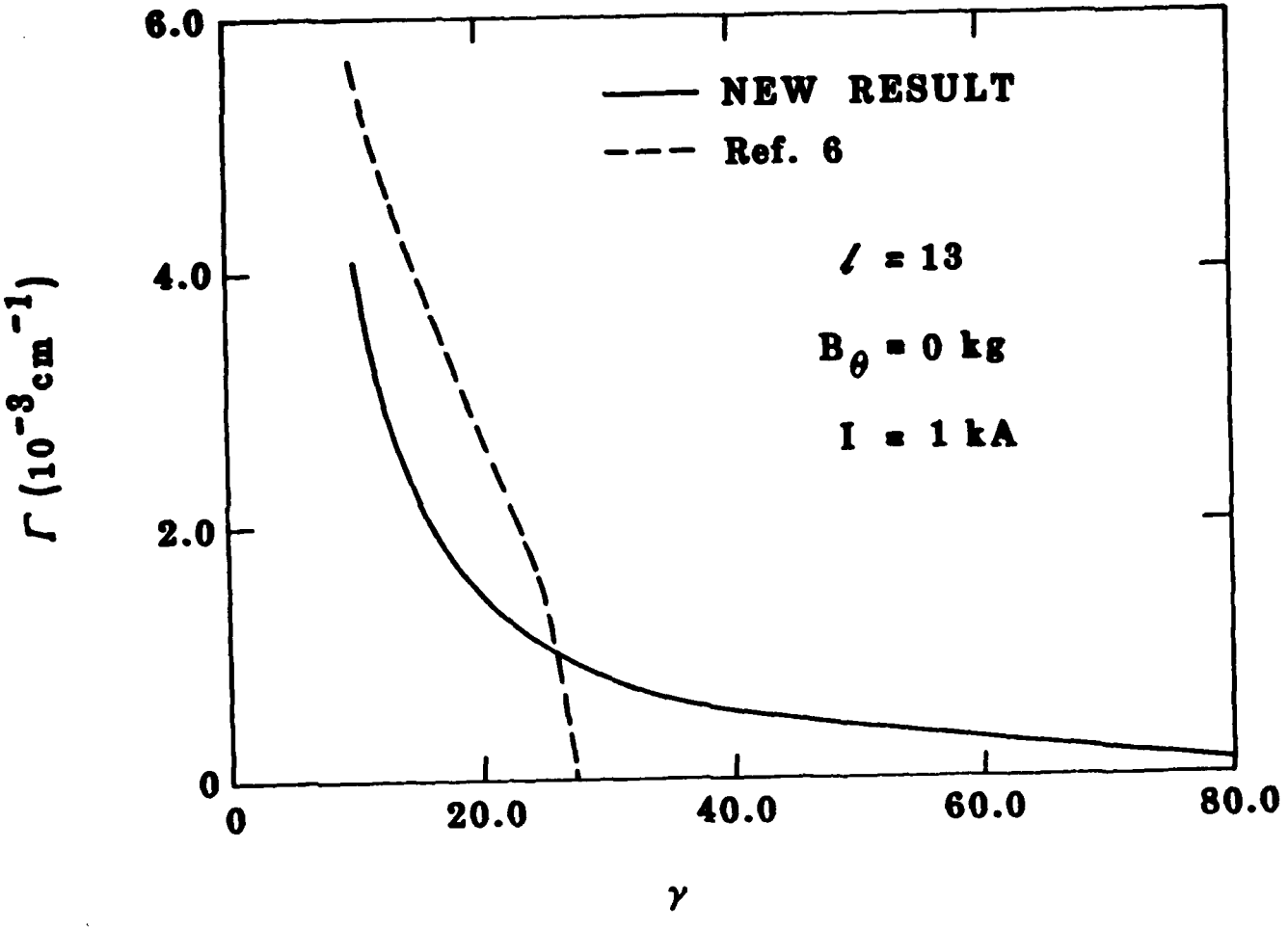

Figure 3. Predicted negative mass instability growth rate as a function of energy for the ONR racetrack induction accelerator design with no guide field.

REFERENCES

1. P. Sprangle and J. L. Vomvoridis, "Longitudinal and Transverse Instabilities in a High Current Modified Betatron Electron Accelerator," NRL-4688 (Naval Research Laboratory, Washington, 1981).

2. T. P. Hughes and B. B. Godfrey, "Linear Stability of the Modified Betatron," AMRC-R-354 (Mission Research Corporation, Albuquerque, 1982).

3. T. P. Hughes, M. M. Campbell, and B. B. Godfrey, "Analytical and Numerical Studies of the Modified Betatron," IEEE Nuc. Sci. NS-30, 2528 (1983).

4. T. P. Hughes, M. M. Campbell, and B. B. Godfrey, "Linear and Nonlinear Development of the Negative Mass Instability in a Modified Betatron Accelerator," Beams 83, to be published.

5. C. W. Roberson, "The Racetrack Induction Accelerator," IEEE Nuc. Sci. NS-28, 3433 (1981).

6. B. B. Godfrey and T. P. Hughes, "Beam Breakup Instabilities in High Current Electron Beam Racetrack Induction Accelerators," IEEE Nuc. Sci. NS-30, 2531 (1983).

7. P. Sprangle and D. Chernin, "Beam Current Limitations Due to Instabilities in Modified and Conventional Betatrons," NRL-5176 (Naval Research Laboratory, Washington, 1983).

8. T. P. Hughes, M. M. Campbell, and B. B. Godfrey, "Simulations and Theory of the Negative Mass Instability in a Modified Betatron," AMRC-N-247 (Mission Research Corporation, Albuquerque, 1983).

9. D. Chernin and P. Sprangle, "Transverse Beam Dynamics in the Modified Betatron," Part. Accel. 12, 85 (1982).

10. V. K. Neil and A. M. Sessler, Rev. Sci. Instr. 36, 429 (1965).

11. R. W. Landau and V. K. Neil, "Negative Mass Instability," Phys. Fluids 9, 2412 (1966).

12. B. B. Godfrey and T. P. Hughes, "Beam Breakup Instabilities in High Current Electron Beam Racetrack Induction Accelerators," AMRC-R-469 (Mission Research Corporation, Albuquerque, 1983).

APPENDIX B

APPENDIX B

UNCLASSIFIED

SECURITY CLASSIFICATION OF THIS PAGE (When Data Entered)

REPORT DOCUMENTATION PAGE		READ INSTRUCTIONS BEFORE COMPLETING FORM
1 REPORT NUMBER	2. GOVT ACCESSION NO.	3 RECIPIENT'S CATALOG NUMBER
4. TITLE (and Subtitle) LINEAR STABILITY OF THE MODIFIED BETATRON		5 TYPE OF REPORT & PERIOD COVERED INTERIM
		6 PERFORMING ORG. REPORT NUMBER AMRC-R-354
7. AUTHOR(s) T. P. Hughes B. B. Godfrey		8 CONTRACT OR GRANT NUMBER(s) N00014-81-C-0647
9 PERFORMING ORGANIZATION NAME AND ADDRESS MISSION RESEARCH CORPORATION 1400 San Mateo Boulevard, S.E. Suite Albuquerque, New Mexico 87108		10 PROGRAM ELEMENT PROJECT, TASK AREA & WORK UNIT NUMBERS
11 CONTROLLING OFFICE NAME AND ADDRESS Office of Naval Research 800 North Quincy Street Arlington, Virginia 22217		12. REPORT DATE April 1982 13. NUMBER OF PAGES 30
14 MONITORING AGENCY NAME & ADDRESS(if different from Controlling Office)		15. SECURITY CLASS (of this report) Unclassified 15a. DECLASSIFICATION DOWNGRADING SCHEDULE

16 DISTRIBUTION STATEMENT (of this Report)

Approved for Public Release - Distribution Unlimited

17. DISTRIBUTION STATEMENT (of the abstract entered in Block 20, if different from Report)

18 SUPPLEMENTARY NOTES

19 KEY WORDS (Continue on reverse side if necessary and identify by block number)

Modified betatron
Negative mass instability
Resistive wall instabilities

20 ABSTRACT (Continue on reverse side if necessary and identify by block number)

The linear stability of the modified betatron is investigated by deriving and numerically solving a dispersion relation. For nonresistive modes, growth rates significantly larger than those of previous calculations are obtained. The effects of a thermal spread in beam energy is estimated, and we conclude that there will be significant Landau damping of the most dangerous nonresistive and resistive modes.

DD FORM 1 JAN 73 1473 EDITION OF 1 NOV 65 IS OBSOLETE

UNCLASSIFIED

SECURITY CLASSIFICATION OF THIS PAGE (When Data Entered)

CONTENTS

LIST OF ILLUSTRATIONS

I. INTRODUCTION

The modified betatron concept,[1-3] illustrated in Fig. 1, may provide a compact means of accelerating intense electron beams to high energies. A dispersion relation for the linear stability of the electron ring in the device has been derived by Sprangle and Vomvoridis.[4] In this report, we show that some of the approximations in their derivation are not well justified, and we obtain more accurate expressions. In Sec. II, the approximation that the phase velocity of unstable waves is approximately the same as the beam velocity,[4] $V_\phi \approx V_b$, is discarded. This significantly alters the results obtained in two ways. Firstly, the growth rates obtained are typically two to ten times larger. Secondly, we find that the conventional negative mass instability does not exist in modified betatrons. Rather, the beam is subject to a predominantly transverse instability at high energies. We have made a rough estimate of the effect of a spread in beam energy on this mode. In Sec. III, we examine the effect of a moderate spread in beam energy on the transverse resistive wall instability. We find that in some cases, the effect is negligible because $V_b - V_\phi$ is too large. For the most dangerous nonresistive and resistive instabilities, however, significant damping is expected.

II. LINEAR DISPERSION RELATION

A. Derivation

Our analysis follows that of Ref. 4, except that we assume a monoenergetic beam. The details of the derivation are given in the Appendix, and here we give only the main points. The beam is modeled as a circulating ring of charge which can displace rigidly in the transverse direction and which can compress in the toroidal direction (see Fig. 1).

In equilibrium, the beam is positioned at the center of the minor cross-section of the torus, and executes a cyclotron orbit in the mirror B_z field. Toroidal corrections to the field equations are dropped, so that the $m = 0$ and $m = 1$ fields are not directly coupled. They are, however, coupled via the perturbed charge and current. Thus, the $m = 0$ component of the charge density ρ satisfies

$$\frac{\partial \rho}{\partial t} + \frac{\rho V_r}{r} + \frac{\partial}{\partial \theta}\left(\frac{\rho V_\theta}{r}\right) = 0 , \qquad (1)$$

where $r(\theta)$ is the radial location of the center of the beam, and V_r, V_θ are the beam velocity components. The second term in Eq. (1) shows that a rigid transverse ($m = 1$) displacement contributes to the perturbed net ($m = 0$) charge density. Contributions from perturbed $m = 0$ quantities to the $m = 1$ charge density are second order in the beam transverse displacement, and so do enter the linear dispersion relation. Consequently, the perturbed $m = 1$ fields can be computed directly in terms of the transverse displacements of the beam. The results are substituted into the $m = 0$ field equation for the perturbed toroidal electric field $E_\theta^{(1)}$, namely

$$\nabla_\perp^2 E_\theta^{(1)} = \left(\nabla \rho^{(1)} + \frac{\partial \underset{\sim}{J}^{(1)}}{\partial t}\right)_\theta$$

$$= i\ell/r_0 \, \rho^{(1)} - i\omega J_\theta^{(1)} ,$$

(see Appendix for definitions and normalizations.) Linearizing Eq. (1), we obtain

$$\nabla_\perp^2 E_\theta^{(1)} = \frac{i\ell}{r_o}\,\frac{\rho_o}{\Delta\omega}\left(\frac{\ell}{r_o}\,V_\theta^{(1)} - \frac{iV_r^{(1)}}{r_o}\right)\left(1 - \frac{\omega^2 r_o^2}{\ell^2}\right) + \frac{\rho_o \omega V_r^{(1)}}{\ell} \qquad (2)$$

Solving this equation with appropriate conducting wall boundary conditions yields the linear dispersion relation

$$1 = \frac{1}{4}\rho_o r_b^2 \left\{ \frac{\ell}{\gamma_o \Delta\omega^2 r_o^2}\left(1 - \frac{\omega^2 r_o^2}{\ell^2}\right)\left(\frac{\ell}{\gamma_o^2} - \frac{\omega\Omega_{zo}/\gamma_o}{D}\left(\omega_z^2 - \Delta\omega^2 - \bar{\xi}\right)\right)\right. \qquad (3)$$

$$\left. - \frac{\omega^2\,\Omega_{zo}/\gamma_o}{\ell D \gamma_o \Delta\omega}\left(\omega_z^2 - \Delta\omega^2 - \bar{\xi}\right)\right\}\left(1 + 2\ell n\, a/r_b\right)\left(1 - (1+i)\,\varepsilon_\parallel\right)$$

This equation differs from the results of all earlier work in that the approximation $\omega \approx \ell\Omega_{zo}/\gamma_o$ has not been made. Also, the first term on the second line is new.

B. Nonresistive Instabilities

Equation (3) has some unstable roots due to the coupling of longitudinal and transverse modes of oscillation. The instabilities persist when the wall conductivity is infinite. The instabilities are low frequency in the sense the transverse component of their motion is associated with the slow rotation frequency $\omega_B = \omega_r\omega_z/(\Omega_{\theta o}/\gamma_o)$. The beam can also oscillate transversely at the fast rotation frequency, $\Omega_{\theta o}/\gamma_o$, but there are no nonresistive instabilities associated with this resonance.

We can clarify the origin of the nonresistive instabilities by simplifying Eq. (3). We assume $\omega_z^2 \ll \Omega_{\theta o}^2/\gamma_o^2$, $\Delta\omega^2 \ll \omega_z^2$ and obtain

$$P \equiv \frac{1}{4}\,\rho_o r_b^2\,(1 + 2\ell n\, a/r_b)\left[\frac{\ell^2/r_o^2 - \omega^2}{\Delta\omega^2} - \frac{\omega\alpha\omega_B^2\,(\Delta\omega - \ell\, B_z/\gamma_o^3)}{\Delta\omega^2\,(\Delta\omega^2 - \omega_B^2)}\right] = 1 \qquad (3a)$$

where $\alpha = \gamma_o^2/(1 - n - n_s\, r_b^2/a^2)$. The function $P(\Delta\omega)$ has a different character depending on whether $|\omega_B| < \ell\Omega_{zo}/\gamma_o^3$ or $|\omega_B| > \ell\Omega_{zo}/\gamma_o^3$, as shown in Fig. 2. For typical betatron parameters, the point $|\omega_B| = \ell\Omega_{zo}/\gamma_o^3$ occurs approximately at $\gamma_o \equiv \gamma_{tran} = [4\nu\, r_o^2/a^2]^{1/3}$ where ν is Budker's parameter. When $\gamma_o < \gamma_{tran}$, the roots of the quartic $P(\Delta\omega) = 1$ consist of two complex conjugate pairs. For $\gamma_o > \gamma_{tran}$, we have two real roots and a complex conjugate pair. We note that the conventional negative mass instability[5] is not present in typical modified betatrons. The derivation of the dispersion relation for the latter instability involves the replacement of $\gamma_\phi^2 = (1 - \omega^2 r_o^2/\ell^2)^{-1}$ by $\gamma_b^2 = (1 - V_b^2)^{-1}$ in the field equation. This procedure is valid only if $2\nu\gamma_o\,(1 + 2\ell n\, a/r_b) < 1$ which is not the case for modified betatron parameters (cf. Table 1).

Frequencies and growth rates for the $\ell = 1$, 2, 3, and 4 nonresistive modes obtained by solving Eq. (3) numerically for the parameters in Table 1 are given in Figs. 3, 4, and 5. As we have seen, for $\gamma_o < \gamma_{tran}$ there are two unstable modes, one with $\omega > \ell\Omega_{zo}/\gamma_o$, the other with $\omega < \ell\Omega_{zo}/\gamma_o$, and we term these modes "fast" and "slow" accordingly. In Figs. 3 and 4, only the slow modes are depicted for clarity. The maximum growth rates are for $\gamma_o > \gamma_{tran}$, and since most of the acceleration period lies in this region, we shall examine the region more closely. For $\alpha \approx 2\gamma_o^2 \gg 1$, Eq. (3a) reduces to

$$\Delta\omega\,(\Delta\omega^2 - \omega_B^2) + \nu\,(1 + 2\ell n\, a/r_b)\,\omega\alpha\omega_B^2/\gamma_o^3 = 0 \qquad (3b)$$

The condition for this cubic in $\Delta\omega$ to have complex roots is $\nu(1 + 2\ell n a/r_b)\ \omega\alpha/\gamma_o^3 > 2\ \omega_B/(3\sqrt{3})$. This criterion yields the upper bound on the unstable range of γ_o, namely

$$\gamma_{max} = (6\sqrt{3}\nu r_o\ (1 + 2\ell n\ a/r_b)\ \ell\ B_{\theta o})^{1/2}$$

where we have assumed $\omega_B \ll \ell\Omega_{zo}/\gamma_o$. This expression gives $\gamma_{max} = 153$ for the parameters in Table 1(a). The exact numerical results give $\gamma_{max} = 156$.

For $\gamma_o^2 \ll \gamma_{max}^2$ the complex roots of Eq. (3b) are given approximately by

$$\Delta\omega = [\gamma_o \nu\ \ell(1 + 2\ \ell n\ a/r_b)/(2r_o^5 B_{\theta o}^2)]^{1/3}\ e^{i\phi}\ ,$$

where $\phi = 2\pi/3,\ 4\pi/3$. Thus, the growth rate scales as $\ell^{1/3}$, $B^{-2/3}$, etc. For the parameters in Table 1(a), this expression yields $\omega = 6.81\times10^{-3} + i\ 2.4\times10^{-4}$ for $\gamma_o = 50$, compared to the exact answer $\omega = 6.82\times10^{-3} + i\ 2.1\times10^{-4}$. Numerically we find that throughout most of the range of this instability we have $\Delta\omega \simeq \omega_B$, so that the mode is mostly transverse in character. The conventional negative mass instability is longitudinal in character, being associated with the $\Delta\omega = 0$ resonance.

A comparison between our dispersion relation, Eq. (3) and that in Ref. 4 is given in Fig. 6. The mathematical differences between the two dispersion relations were described in Sec. IIA. Equation (3) gives growth rates which are two to ten times larger than those from Ref. 4. We discuss the effect of a thermal spread in energy on these instabilities in subsection D below.

C. Resistive Wall Instabilities

The presence of resistive material in the walls of the betatron gives rise to additional instabilities,[4] and modifies the growth rates of nonresistive instabilities. To illustrate this effect, we have chosen a stainless steel wall, for which the conductivity σ is 5.2×10^6 in normalized

units (see Appendix). The results for the $\ell = 1$ mode are shown in Fig. 7. The resistive wall has little effect on the nonresistive instabilities. However, some modes whose growth rates are zero for $\sigma = \infty$ are driven unstable by the resistivity. They are, the fast mode in the region $\gamma_0 < \gamma_{tran}$ and a slow mode in the region $\gamma_0 > \gamma_{tran}$, denoted by A and B respectively in Fig. 7(a). (In Fig. 7(b), branch A' is unstable even for $\sigma = \infty$.) Branch B is due mainly to the term ϵ_{11} in Eq. (3). The growth rates of this branch are much smaller than those obtained by using the approximate ϵ_{11} in Ref. 4. Since the resistive modes are driven by the boundary condition at the wall, they are sensitive to the value of a, the minor radius of the torus.[6] This is why the resistive mode growth rate is smaller in Fig. 7 than in Fig. 6 (cf. Table 1). The growth rate is approximately independent of γ_0.

The slow mode associated with the toroidal magnetic field cyclotron resonance, $\omega = \ell\Omega_{z0}/\gamma_0 - \Omega_{\theta 0}/\gamma_0$, is also driven unstable by wall resistivity.[6] As indicated in subsection B, none of the modes associated with this resonance are unstable when $\sigma = \infty$. With finite wall conductivity the mode, which is primarily a transverse oscillation, becomes unstable when ω goes through zero and becomes positive. In a betatron, $\Omega_{z0} \propto \gamma_0$ during the acceleration, so that the instability turns on when $\Omega_{z0} = \Omega_{\theta 0}/\ell$ and continues for the remainder of the acceleration period. This behavior is shown in Fig. 8. Again, the difference in growth rates between the two parts of the figure is due mainly to the differences in the quantities a and $B_{\theta 0}$ in Table 1. For large γ_0, the growth rate is approximately independent of γ_0.

D. Practical Implications for Betatrons

For the sample parameters given in Table 1, it is clear that the nonresistive instability in the region $\gamma_0 > \gamma_{tran}$ is the most important instability. Thus, for the parameters in Table 1(a), the number of e-

foldings of the ℓ=1 component during a 1 millisecond acceleration time is about 4000. This result is for a monoenergetic beam, and gives an upper bound on the growth. We can estimate the effect of a spread in beam energy as follows. The thermal spread enters the model in the combination $\omega - \ell(\Omega_{z0}/\gamma_0 - k\Delta P_0)$, where ΔP_0 is the spread in canonical toroidal momentum (cf. Eq. (4)). The instability for $\gamma_0 > \gamma_{tran}$ is associated with the resonance $\Delta\omega = \omega_B$. Therefore, a small-thermal-expansion for this mode is an expansion in the parameter $\epsilon^2=(\ell k\Delta P_0)^2/(\Delta\omega - \omega_B)^2$. If $\epsilon^2 \ll 1$, Landau damping is negligible, whereas if $\epsilon^2 \gtrsim 1$, we expect significant damping. As an example, we use the numerical results shown in Fig. 3(a), and assume an initial spread in γ_0 of 5%. Then, for the ℓ=1 mode at γ_0 = 50, we obtain $\epsilon^2 \simeq 4$, so that we can expect a significant reduction in growth rate. A more rigorous treatment of thermal effects is needed to confirm this result.

III. THERMAL EFFECTS ON RESISTIVE INSTABILITIES

It has been suggested[4] that a moderate spread in beam particle energies may reduce instability growth rates to acceptably low values through Landau damping. Here we look at the effect of a thermal spread on the transverse cyclotron resistive wall instability. We choose this case because the dispersion relation, Eq. (4) is relatively simple and does not require numerical solution.

A. High Frequency Limit: $\delta/a \ll 1$

From Ref. 4 the approximate dispersion relation for the cyclotron mode including thermal effects is

$$1 + \Omega_s^2 \int \frac{g(\Delta P)\, d\Delta P}{\omega_r^2 - \Delta\omega^2 \pm \Delta\omega\Omega_{\theta o}/\gamma_o} = 0, \qquad (4)$$

where, in normalized units,

$$\Delta\omega = \omega - \ell(\Omega_{zo}/\gamma_o - k\Delta P) ,$$

$$k = \frac{1}{\gamma_o r_o^2}\left(\frac{1}{\gamma_o^2} - \frac{1}{1 - n - n_s}\right) ,$$

$$\Omega_s^2 = n_s (1 - r_b^2/a^2)\left[1 - \beta_o^2\gamma_o^2 (1 + i)\frac{r_b^2}{a^2}\frac{\delta}{a}\right]\frac{\Omega_{zo}^2}{\gamma_o^2}$$

$$\delta = \left(\frac{2}{\sigma\omega}\right)^{1/2} ,$$

$$\omega_r^2 = (\tfrac{1}{2} - n_s)\,\Omega_{zo}^2/\gamma_o^2 , \qquad (n = 1/2 \text{ is assumed})$$

$g(\Delta P)$ = distribution function of toroidal canonical momentum spread. See Appendix for additional definitions.

Write $\Delta\omega^2 - \omega_r^2 \mp \Delta\omega\Omega_{\theta o}/\gamma_o = (\Delta\omega + \ell k\Delta P - \alpha_1)\ (\Delta\omega + \ell k\Delta P - \alpha_2)$. Assuming $|\alpha_2| >> |\alpha_1|$, the instability comes from the following choice of roots,

$$\alpha_1 = \frac{\omega_r^2 \gamma_o}{\Omega_{\theta o}}, \qquad \alpha_2 = -\Omega_{\theta o}/\gamma_o \ . \tag{5}$$

For g, choose a flat-topped distribution function,

$$\begin{aligned} g(\Delta P) &= \frac{1}{2\Delta P_o} \quad \text{for } |\Delta P| < \Delta P_o \ , \\ g(\Delta P) &= 0 \qquad \text{for } |\Delta P| > \Delta P_o \ . \end{aligned} \tag{6}$$

Performing the integration in Eq. (4), we get

$$1 + \frac{\Omega_s^2}{2\ell k\Delta P_o(\alpha_1 - \alpha_2)} \ell n \frac{\Delta\omega_o - \ell k\Delta P_o - \alpha_2}{\Delta\omega_o + \ell k\Delta P_o - \alpha_2} \cdot \frac{\Delta\omega_o + \ell k\Delta P_o - \alpha_1}{\Delta\omega_o - \ell k\Delta P_o - \alpha_1} = 0, \tag{7}$$

where $\Delta\omega_o = \omega - \ell\Omega_{zo}/\gamma_o$. The mode we are concerned with has $\Delta\omega \approx \alpha_2$. To do a small-thermal-spread expansion, we assume $k\Delta P_o << \Delta\omega - \alpha_2$. In what follows, we shall in essence be checking the consistency of these two approximations. Expanding Eq. (7), we obtain

$$1 - \frac{\Omega_s^2}{\alpha_2}\left(\frac{1}{\Delta\omega_o - \alpha_2} + \frac{1}{3}\frac{(\ell k\Delta P_o)^2}{(\Delta\omega_o - \alpha_2)^3}\right) = 0 \ .$$

Assuming $\delta/a \ll 1$, the real part of the frequency, $\Delta\omega_r$, is

$$\Delta\omega_r \simeq -\Omega_{\theta o}/\gamma_o - \frac{\Omega_s^2}{\Omega_{\theta o}/\gamma_o}\left(1 + \frac{1}{3}\,\frac{(\ell k \Delta P_o)^2}{(\Delta\omega_r - \alpha_2)}\right) \qquad (8)$$

Our expansion parameter is thus

$$\epsilon \equiv \left|\frac{\ell k \Delta P_o}{\Delta\omega_r - \alpha_2}\right| \simeq \frac{\ell k \Delta P_o \Omega_{\theta o}/\gamma_o}{\Omega_s^2} \quad .$$

With $\Delta P_o \equiv \gamma_{th} r_o$, and γ_o large enough such that $n_s \ll 1$, we have

$$\epsilon \simeq \frac{4\ell\Omega_{\theta o}\gamma_o^2}{n_o r_o} \cdot \frac{\gamma_{th}}{\gamma_o}$$

If $\epsilon \ll 1$ for a given choice of parameters, then our small-thermal-spread expansion is valid. In this limit, there is no Landau damping from a flat-topped distribution. If $\epsilon \gg 1$, on the other hand, the phase velocity of the mode lies well within the distribution of particle velocities. The mode is then highly damped. Putting in numbers from Table 1(a)with $\gamma_o = 50$, we obtain $\epsilon = 3.3\times10^3(\gamma_{th}/\gamma_o)$. Assuming a 10% spread in γ_o at the beginning of the acceleration period, we have $\gamma_{th} \simeq 0.5$. Thus $\epsilon \simeq 33$ at $\gamma_o = 50$. Consequently, there will be significant Landau damping of this mode.

B. Low Frequency Limit: $\omega \simeq 0$

When $\omega \simeq 0$, the small-thermal-spread expansion of Eq. (7) leads to

$$\omega^{3/2} + \frac{\Omega_{so}^2}{\alpha_2}\,\eta\, e^{i\pi/4}\,(1 + \tfrac{1}{3}\,\epsilon) = 0 \qquad (9)$$

where $\Omega_{so}^2 = n_s(1 - r_b^2/a^2)\,\Omega_{zo}^2/\gamma_o^2$, and $\eta = \beta_o^2\gamma_o^2(r_b^2/a^3)(2/\sigma)^{1/2}$. The

unstable solutions to Eq. (9) are

$$\omega = \frac{\Omega_{so}^2 \eta}{\Omega_{\theta o}/\gamma_o}\left(1 + \frac{\varepsilon}{3}\right)^{2/3} e^{i\phi} \quad , \tag{10}$$

where $\phi = \pi/6, -7\pi/6$. In this case, we obtain

$$\varepsilon = \frac{\gamma_{th}}{\gamma_o}\ \frac{\ell a^2}{2r_o}\left(\frac{\Omega_{\theta o}}{2\nu}\right)^{2/3}\left(\frac{\sigma}{2}\right)^{1/3}$$

For the parameters in Table 1(a), we obtain $\varepsilon \simeq 27(\gamma_{th}/\gamma_o)$. Thus, for an initial 10% spread in γ_o, there will be substantially less Landau damping in this case than where $\delta/a \ll 1$. For the parameters in Table 1(b), $\varepsilon \simeq 4(\gamma_{th}/\gamma)_o$. In this case, Landau damping will be negligible, and Eq. (10) shows that there will be a slight increase in the growth rate due to thermal effects.

IV. SUMMARY

We have rederived the dispersion relation for linear instabilities in betatrons based on the simple model of Ref. 4. Our analysis shows that at high beam energies, the dispersion relation does not reduce to that of the conventional negative mass instability. Instead, we find a mode which is primarily transverse in nature. Furthermore, we obtain growth rates which are from two to ten times larger than those obtained in previous calculations. We have estimated the effects of a moderate spread in beam energy on nonresistive and resistive instabilities, and find that significant damping is expected. A more rigorous calculation is needed to prove this.

ACKNOWLEDGEMENTS

We would like to thank Dr. P. Sprangle for useful conversations. This research is supported by the Office of Naval Research contract N00014-81-C-0647, monitored by C. Roberson.

APPENDIX

DERIVATION OF DISPERSION RELATION

Figure 1 illustrates the physical parameters of the system. The beam is modeled as a line of charge. In equilibrium, it is situated at $r = r_o$ $z = 0$, and executes a cyclotron orbit in the mirror B_z field. As pointed out in Sec. IIA, only the transverse motion of the beam needs to be considered when computing the perturbed transverse fields. When the center of the beam is displaced rigidly to position $(r_o + \Delta r, \Delta z)$, it experiences the following fields:[4]

$$\text{Applied fields:} \quad B_z = B_{zo}\,(1 - n\Delta r/r_o) \ ,$$
$$B_r = -B_{zo}\, n\Delta r/r_o \ , \qquad \text{(A1)}$$
$$B_\theta = B_{\theta o}\,(1 - \Delta r/r_o) \ .$$

$$\text{Induced fields:} \quad E_r^{(1)} = \frac{n_o}{2}\,\frac{r_b^2}{a^2}\,\Delta r \ ,$$

$$E_z^{(1)} = \frac{n_o}{2}\,\frac{r_b^2}{a^2}\,\Delta z \ ,$$

$$B_r^{(1)} = \frac{n_o V_{\theta o}}{2}\left(\frac{r_b^2}{a^2} - (1 - r_b^2/a^2)\,\xi\right)\Delta z \ ,$$

$$B_z^{(1)} = -\frac{n_o V_{\theta o}}{2}\left(\frac{r_b^2}{a^2} - (1 - r_b^2/a^2)\,\xi\right)\Delta r, \qquad \text{(A2)}$$

where $$\xi = (1 + i)\,\frac{r_b^2}{a^2 - r_b^2}\left(\frac{2}{\sigma\omega a^2}\right)^{1/2} \ .$$

In our normalization scheme, frequencies are normalized to ω_0 which is defined by $c/\omega_0 = 1$ cm. Lengths are normalized to c/ω_0, velocities to c, fields to $mc\omega_0/e$, and densities to $\omega_0^2 m/4\pi e^2$, where m and e are the electronic mass and charge respectively. Thus, for example, B_{z0} and Ω_{z0} have the same normalized values. The conductivity is normalized to $\omega_0/4\pi$. In Eqs. (A1) and (A2) above n is the external field index, i.e., $r_0\, \partial/\partial r\, \ell n\, B_z(r_0)$, n_0 is the equilibrium beam density and $V_{\theta 0}$ is the equilibrium azimuthal beam velocity. A positive beam charge is assumed. The equations of motion of a beam particle are,

$$-\gamma \frac{V_\theta^2}{r} + \frac{dp_r}{dt} = E_r + V_\theta B_z - V_z B_\theta \quad ,$$

$$\frac{dp_z}{dt} = E_z + V_r B_\theta - V_\theta B_r \quad ,$$

$$\gamma \frac{V_\theta V_r}{r} + \frac{dp_\theta}{dt} = E_\theta + V_z B_r - V_r B_z \quad ,$$

where (V_r, V_θ, V_z) and (p_r, p_θ, p_z) are the velocity and momentum components of a beam particle. Linearizing these equations, we obtain

$$\Delta\ddot{r} + (\omega_r^2 - \bar{\xi})\Delta r + \Delta\dot{z}\, \frac{B_{\theta 0}}{\gamma_0} = -\gamma_0^2 \frac{B_{z0}}{\gamma_0} V_\theta^{(1)} \quad ,$$

$$\Delta\ddot{z} + (\omega_z^2 - \bar{\xi})\, \Delta z - \Delta\dot{r}\, \frac{B_{\theta 0}}{\gamma_0} = 0 \quad , \qquad \text{(A3)}$$

$$\frac{dV_\theta^{(1)}}{dt} = \frac{E_\theta^{(1)}}{\gamma_0^3} \quad ,$$

where the superscript $^{(1)}$ denotes perturbed quantities, $\omega_r^2 = (1 - n - n_s\, r_b^2/a^2)B_{zo}^2/\gamma_o^2$, $\omega_z^2 = (n - n_s\, r_b^2/a^2)B_{zo}^2/\gamma_o^2$, $n_s = n_o/(2\gamma_o B_{zo}^2)$ and $\bar{\xi} = n_s\gamma_o^2 V_{\theta o}^2(1 - r_b^2/a^2)\xi B_{zo}^2/\gamma_o^2$. Assuming Δr, $\Delta z \sim \exp(-i\omega t + i\ell\theta)$, we obtain the following solutions to Eqs. (A3),

$$\Delta r = \frac{V_\theta^{(1)}\gamma_o^2\ (\Delta\omega^2 - \omega_z^2 + \bar{\xi})\ B_{zo}/\gamma_o}{D} \quad ,$$

$$\Delta z = \frac{V_\theta^{(1)}\gamma_o^2\ (B_{zo}/\gamma_o)(B_{\theta o}/\gamma_o)}{D} \quad , \tag{A4}$$

where $\Delta\omega = \omega - \ell V_{\theta o}/r_o$ and $D = (\Delta\omega^2 - \omega_r^2 + \bar{\xi})(\Delta\omega^2 - \omega_z^2 + \bar{\xi}) - \Delta\omega^2\, B_{\theta o}^2/\gamma_o^2$. Using the third member of Eqs. (A3), $V_\theta^{(1)}$ can be expressed in terms of $E_\theta^{(1)}$, the only unknown. To close the system, we obtain a field equation for $E_\theta^{(1)}$. We assume that the beam excites only the $m = 0$ component of $E_\theta^{(1)}$. This is reasonable provided $r_b \ll a$, since higher m number components go to zero at the center of the minor cross section of the torus. Further, we assume that only the lowest radial mode is excited, so that the eigenfunction is approximately constant over the beam cross section. This is valid provided $|\ell/r_o| \sim |\omega| \ll 2\pi/a$. Then from Maxwell's equations we obtain

$$\nabla_\perp^2 E_\theta^{(1)} = i\ell\rho^{(1)}/r_o - i\omega J_\theta^{(1)} \quad , \tag{A5}$$

where "$\perp$" refers to the transverse direction, $\rho^{(1)}$ is the perturbed charge density, and $J_\theta^{(1)}$ is the perturbed azimuthal current. Since the eigenfunction is assumed to be flat in the center, the perturbed charge density $\rho^{(1)}$ is proportional to the perturbed line charge $\nu^{(1)}$. To obtain an expression for $\nu^{(1)}$ we use the continuity equation for ρ,

$$\partial\rho/\partial t + \underset{\sim}{\nabla} \cdot (\rho \underset{\sim}{V}) = 0. \qquad \text{(A6)}$$

Put $\rho = \nu\delta(R - R_0(\theta))\,\delta(\phi - \phi_0(\theta))/R$, where R, ϕ are local cylindrical coordinates ($r - r_0 = R\cos\phi$, $z = r\sin\phi$), and (R_0, ϕ_0) is the position of the displaced beam. Multiplying Eq. (A6) by $\int R dR d\phi$, we obtain

$$\frac{\partial \nu}{\partial t} + \frac{\nu V_r}{r} + \frac{\partial}{\partial \theta}\left(\frac{\nu V_\theta}{r}\right) = 0 \qquad \text{(A7)}$$

Linearizing, and replacing ν by ρ, we have

$$\rho^{(1)} = (\ell\rho_0 V_\theta^{(1)}/r_0 - \rho_0 \omega r^{(1)}/r_0)/\Delta\omega$$

$$J_\theta^{(1)} = \omega(r_0\rho^{(1)} + r^{(1)}\rho_0)/\ell$$

where ρ_0 is the unperturbed charge density . Equation (A5) becomes

$$\nabla_\perp^2 E_\theta^{(1)} = -\frac{\ell\rho_0 E_\theta^{(1)}}{\gamma\Delta\omega^2 r_0^2}\left\{\frac{\ell}{\gamma_0^2} + \frac{\omega B_{z0}/\gamma_0}{D}(\omega_z^2 - \Delta\omega^2 - \bar{\xi})\right\}\left(1 - \frac{\omega^2 r_0^2}{\ell^2}\right)$$

$$- \frac{\omega^2 \rho_0 B_{z0}/\gamma_0}{\ell D \gamma \Delta\omega}(\omega_z^2 - \Delta\omega^2 - \bar{\xi})E_\theta^{(1)}$$

$$\equiv A E_\theta^{(1)} \qquad \text{(A8)}$$

To obtain the dispersion relation, we need to solve

$$\nabla_\perp^2 E_\theta^{(1)} = A E_\theta^{(1)} \qquad r < r_b$$

$$\nabla_\perp^2 E_\theta^{(1)} = 0 \qquad r_b < r < a$$

$$\nabla_\perp^2 E_\theta^{(1)} = -i\sigma\omega E_\theta^{(1)} \qquad r > a,$$

together with the following boundary conditions,

$$E_\theta^{(1)} \ , \ \frac{\partial E_\theta^{(1)}}{\partial r} \quad \text{continuous at } r = r_b \ ,$$

$$E_\theta^{(1)} = - \frac{\omega(i+1)}{\omega^2 - \ell^2/r_o^2} \left(\frac{\omega}{2\sigma}\right)^{1/2} \frac{\partial E_\theta^{(1)}}{\partial r} \quad \text{at } r = a.$$

As a result, we obtain

$$1 = \frac{1}{4} \rho_o r_b^2 (1 + 2\ell n \, a/r_b) [1 - (i+1)\epsilon_{11}]$$

$$\times \left\{ \frac{\ell}{\gamma_o \Delta\omega^2 r_o^2} (1 - \frac{\omega^2 r_o^2}{\ell^2}) \left[\frac{\ell}{\gamma_o^2} + \frac{\omega B_{zo}/\gamma_o}{D} (\omega_z^2 \Delta\omega^2 - \bar{\xi}) \right] \right.$$

$$\left. + \frac{\omega^2}{\ell D \gamma_o \Delta\omega} (\omega_z^2 - \Delta\omega^2 - \bar{\xi}) \right\} \ , \qquad \text{(A9)}$$

where

$$\epsilon_{11} = \frac{\omega^2 r_o^2/\ell^2 \ (2/\sigma\omega a^2)^{1/2}}{(1 - \omega^2 r_o^2/\ell^2)(1 + 2\ell n \, a/r_b)} \ .$$

For a negatively charged beam, we let $B_{zo} \to - B_{zo}$.

REFERENCES

1. P. Sprangle and C. A. Kapetanakos, J. Appl. Phys. 49, 1 (1978).

2. P. Sprangle, C. A. Kapetanakos, and S. J. Marsh, NRL Memorandum Report 4666 (1981).

3. N. Rostoker, Bull. Am. Phys. Soc. 26, 161 (1980).

4. P. Sprangle and J. L. Vomvoridis, NRL Memorandum Report 4688 (1981).

5. R. W. Landau and V. K. Neil, Phys. Fluids 9, 2412 (1966).

6. B. B. Godfrey and T. P. Hughes, AMRC-R-332, Mission Research Corporation (1981).

TABLE 1. SAMPLE PARAMETERS FOR MODIFIED BETATRON

The values for $B_{\theta o}$ are approximate practical upper and lower bounds.

QUANTITY	SYMBOL	VALUES	
		(a)	(b)
Major Radius	r_o	150 cm	100 cm
Minor Radius	a	5 cm	10 cm
Beam Radius	r_b	1 cm	1 cm
Toroidal Magnetic Field	$B_{\theta o}$	6 (10 kG)	1.5 (2.5 kG)
Beam Current	ν	0.59	0.59 (10 kA)
Beam γ-factor	γ_o	5-100	
Transition Energy	γ_{tran}	12.9	6.2
Acceleration Time	τ_a	3×10^7 cm (1 millisec)	

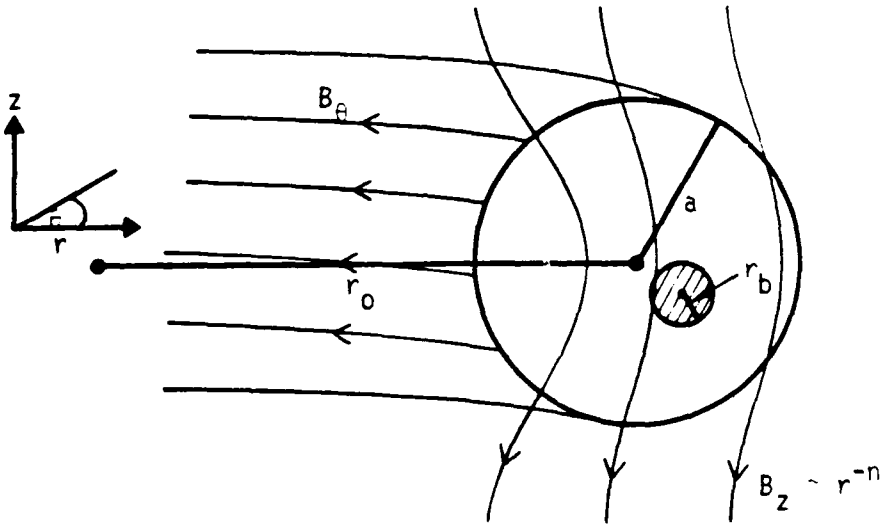

Figure 1. Illustration of modified betatron concept. The major radius of the torus is r_o, the minor radius is a and the beam radius is r_b. The external magnetic fields consist of a focusing mirror field B_z and a toroidal field B_θ.

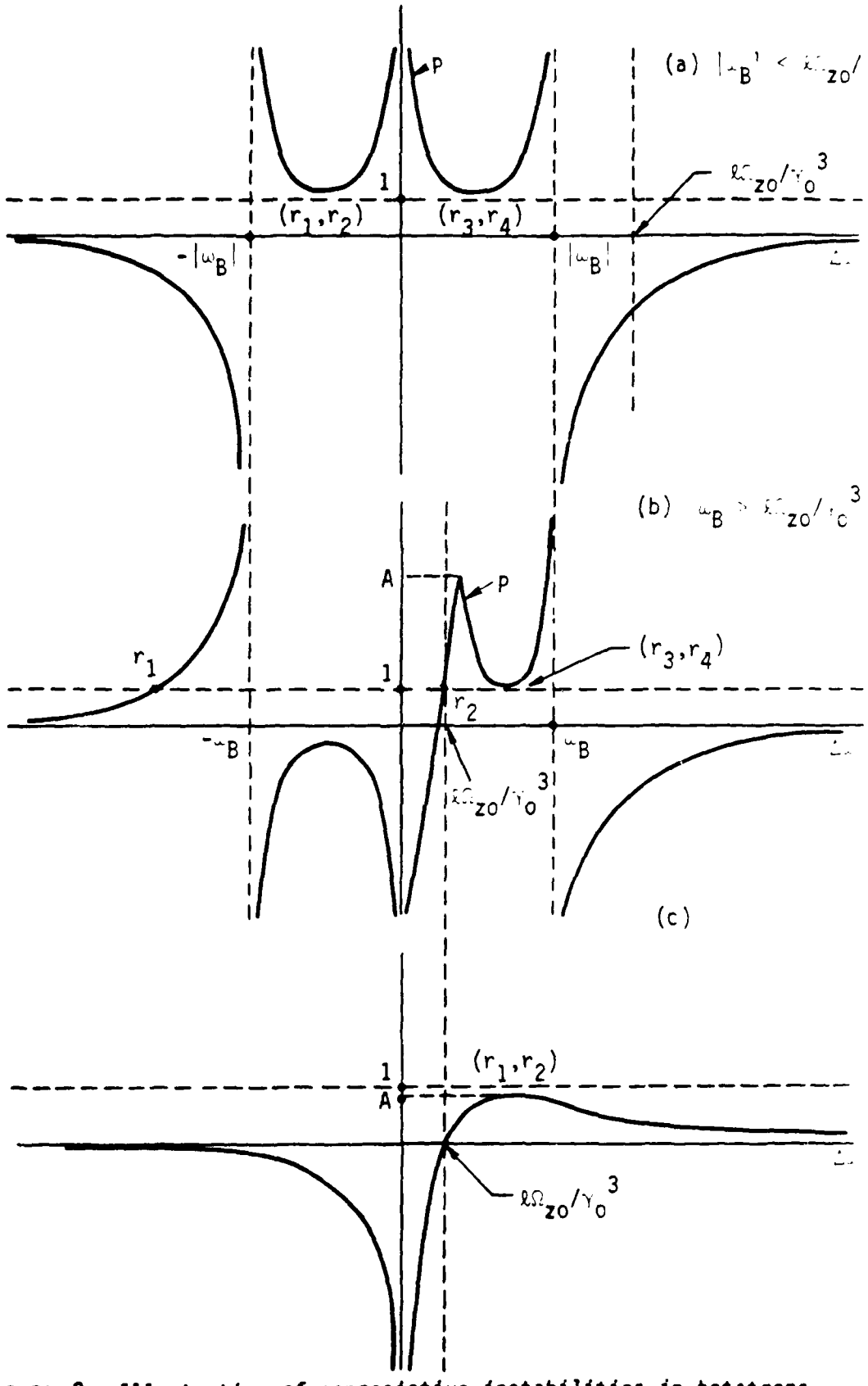

Figure 2. Illustration of nonresistive instabilities in betatrons. The dispersion relation is P=1. The roots are denoted by r_1, r_2, etc., and brackets (,) denote complex conjugate pairs. In (a) and (b), we depict two regimes of instability in the modified betatron. In (c), we show the origin of the longitudinal negative mass instability, which requires $A = 2\nu\gamma_o (1 + 2 \ell n\, a/r_b) < 1$.

AD-A137 508 MODIFIED BETATRON ACCELERATOR STUDIES(U) MISSION RESEARCH CORP ALBUQUERQUE NM T P HUGHES ET AL. DEC 83 AMRC-R-524 N00014-81-C-0647 2/2

UNCLASSIFIED F/G 20/7 NL

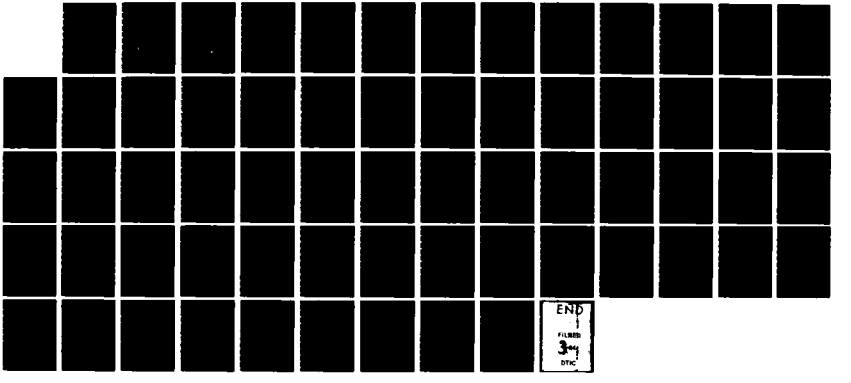

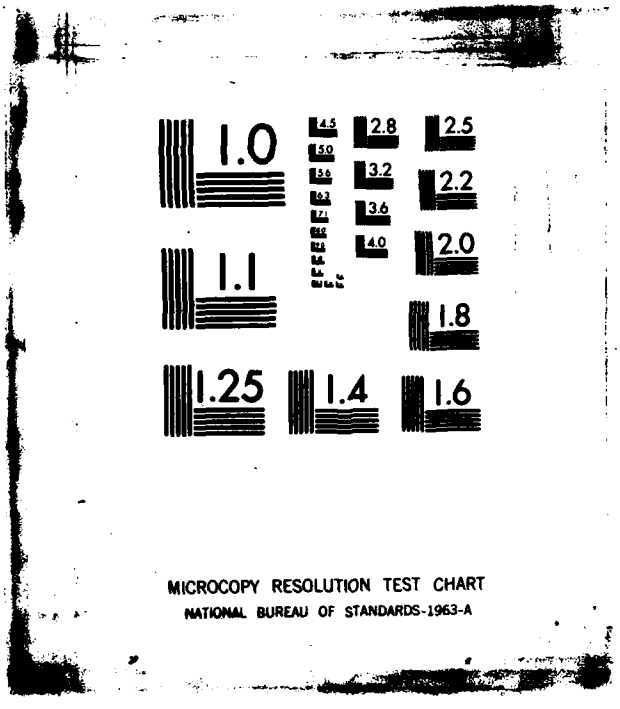
1.0
1.1
1.25
1.4
1.6
1.8
2.0
2.2
2.5
2.8
3.2
3.6
4.0
4.5
5.0
5.6
MICROCOPY RESOLUTION TEST CHART
NATIONAL BUREAU OF STANDARDS-1963-A

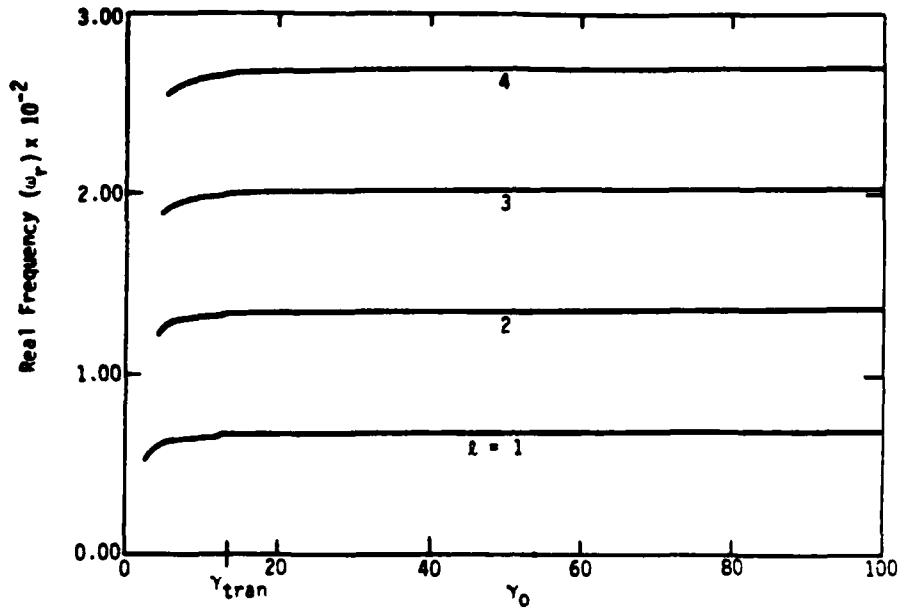

a)

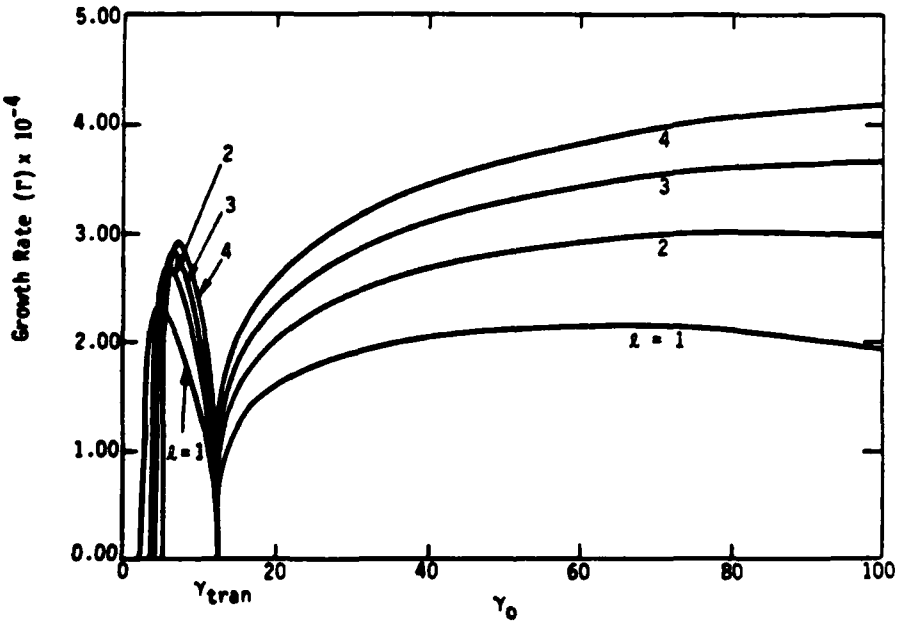

b)

Figure 3. Real and imaginary parts of the nonresistive ℓ = 1, 2, 3, 4 modes obtained by solving Eq. (3) numerically for the equilibrium parameters given in Table 1(a). The frequencies are in units of 3×10^{10} sec^{-1}. For $\gamma_o < \gamma_{tran}$, only the slow mode is included (cf. Fig. 2).

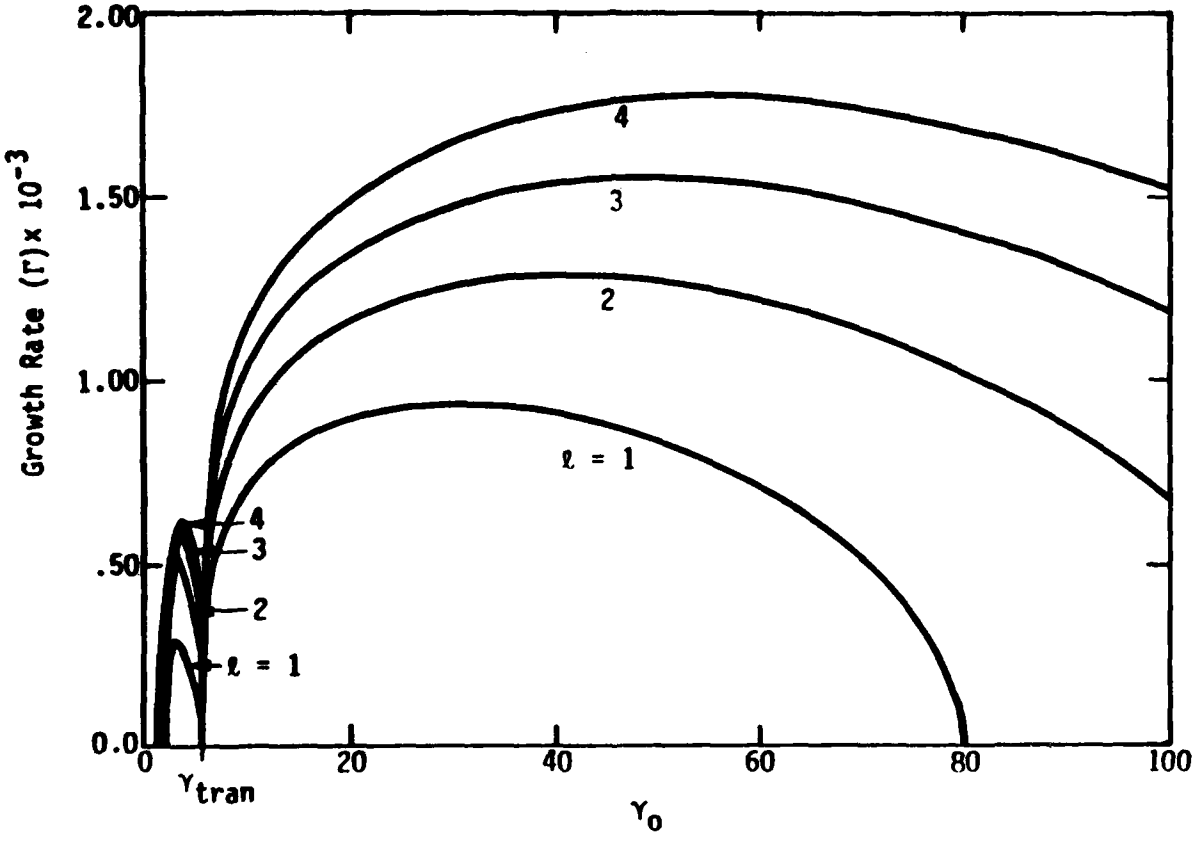

Figure 4. Growth rates of the nonresistive ℓ = 1, 2, 3, 4 instabilities for the parameters in Table I(b).

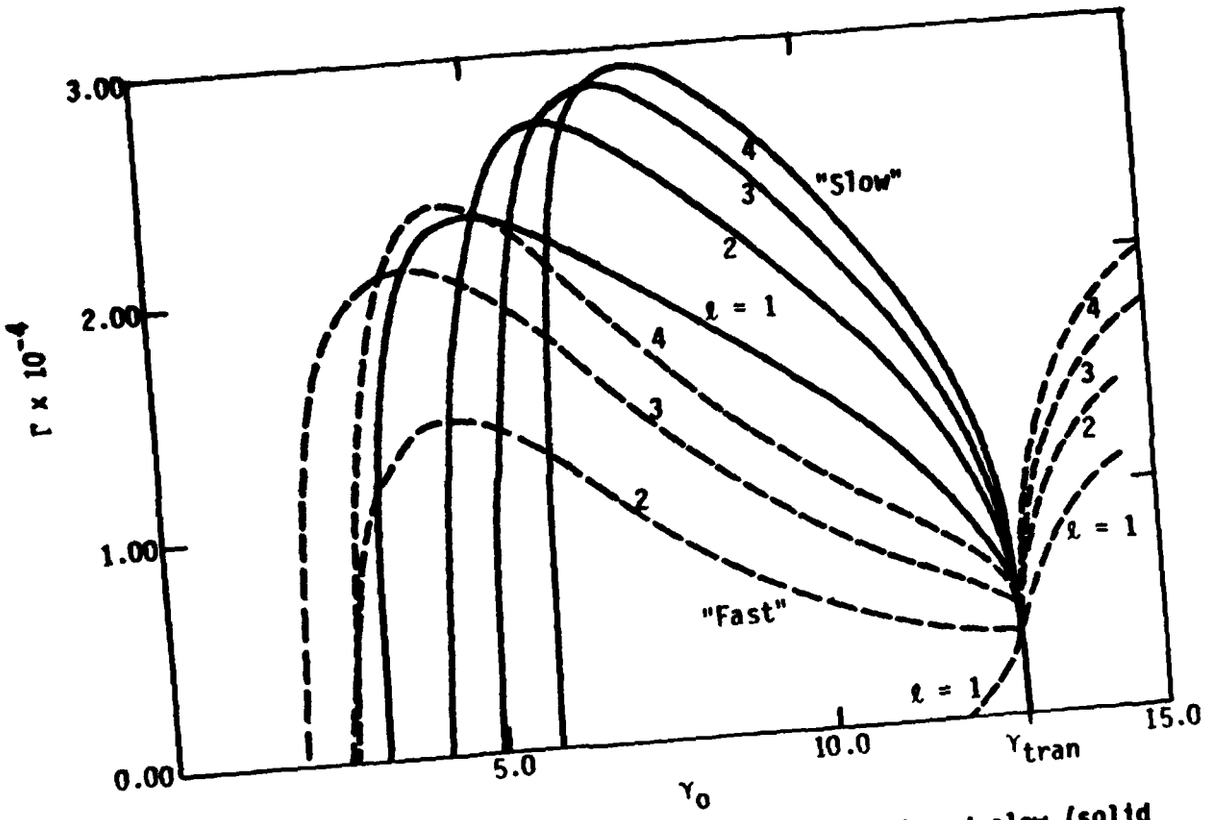

Figure 5. Growth rates of the fast (dashed lines) and slow (solid lines) branches of the nonresistive instabilities in the region $\gamma_0 < \gamma_{tran}$. In going through γ_{tran}, the fast modes join onto the instabilities in the region $\gamma_0 > \gamma_{tran}$, while the slow modes join onto modes with zero growth rate. The betatron parameters are those of Table 1(a).

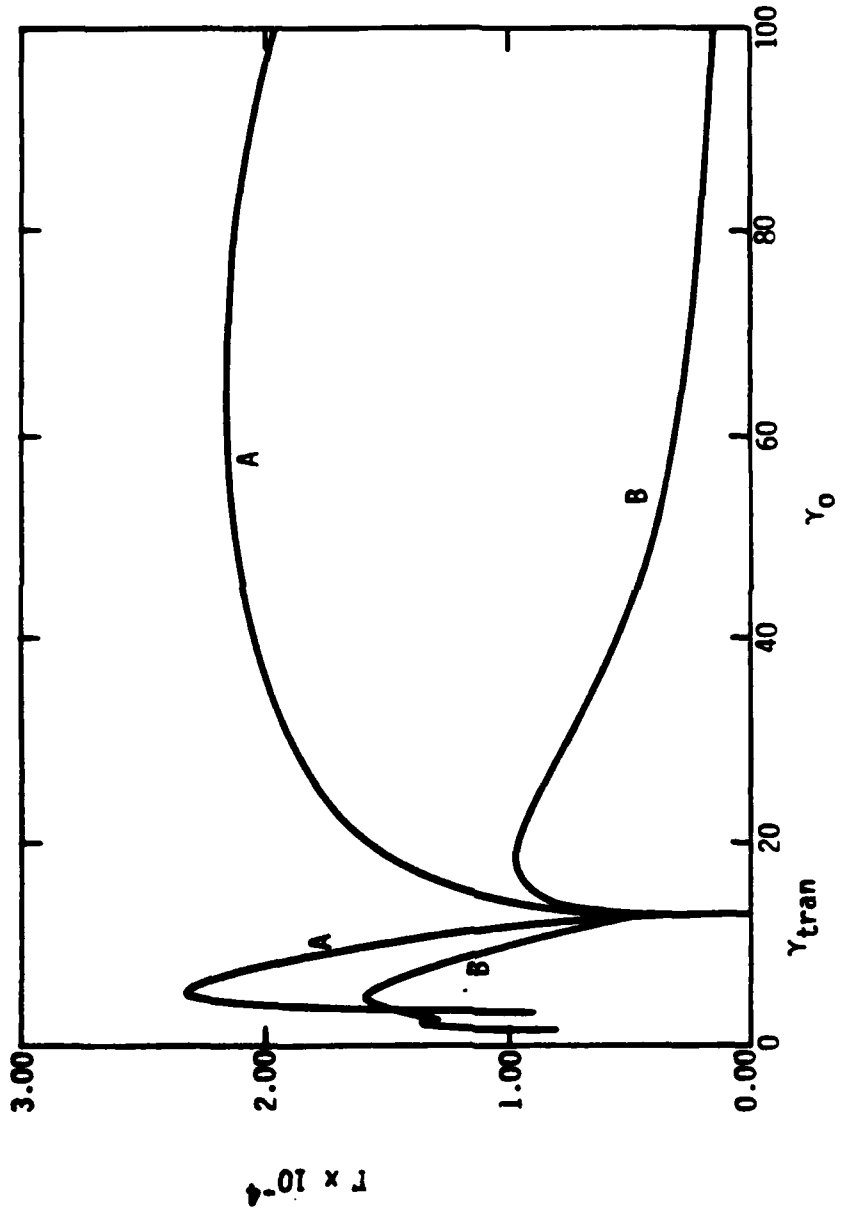

Figure 6. Comparison between growth rates obtained from Eq. (3) (Curve A) and those obtained from the dispersion relation in Ref. 4 (Curve B), for the nonresistive $\mu = 1$ instability. The betatron parameters are from Table 1(a).

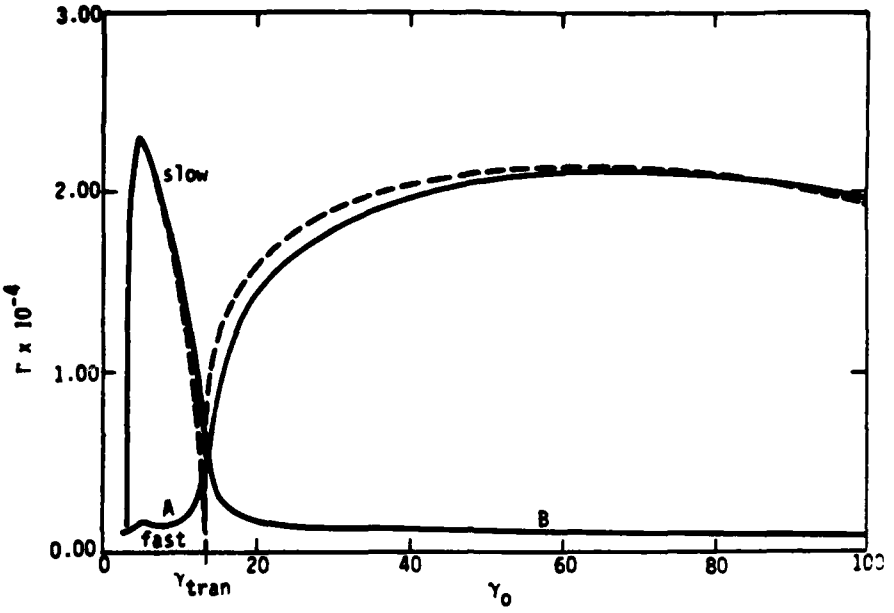

a)

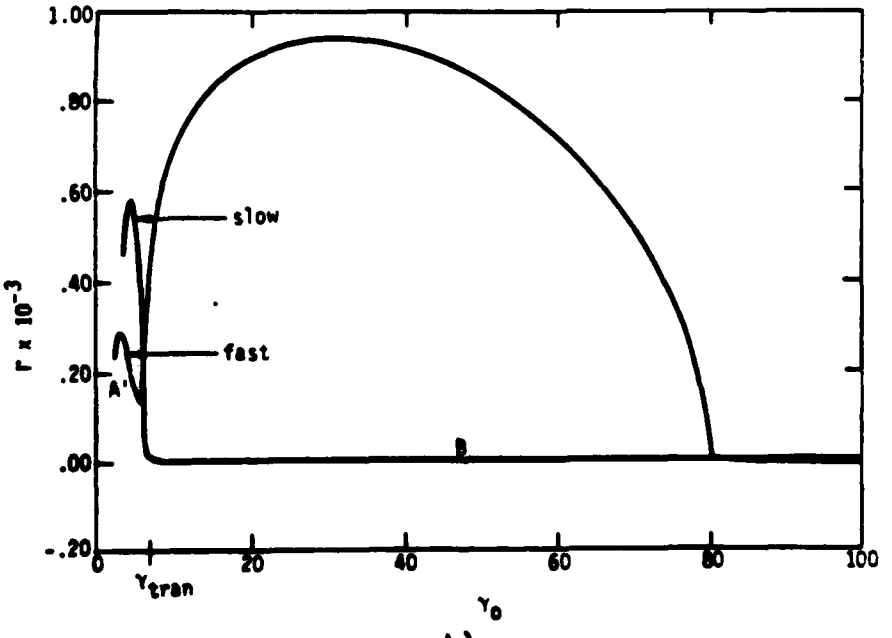

b)

Figure 7. Growth rates for the $\ell = 1$ instability with perfectly conducting walls (dashed lines) and stainless steel walls (solid lines). Part (a) is for the parameters in Table 1(a), and part (b) is for parameters in Table 1(b). Branches A and B are modes which have become unstable due to the wall resistivity alone. In part (b) the solid and dashed lines are indistinguishable (the growth rate of Branch B is approximately 4×10^{-6} cm^{-1}). Branch A' is unstable for even $\sigma = \infty$.

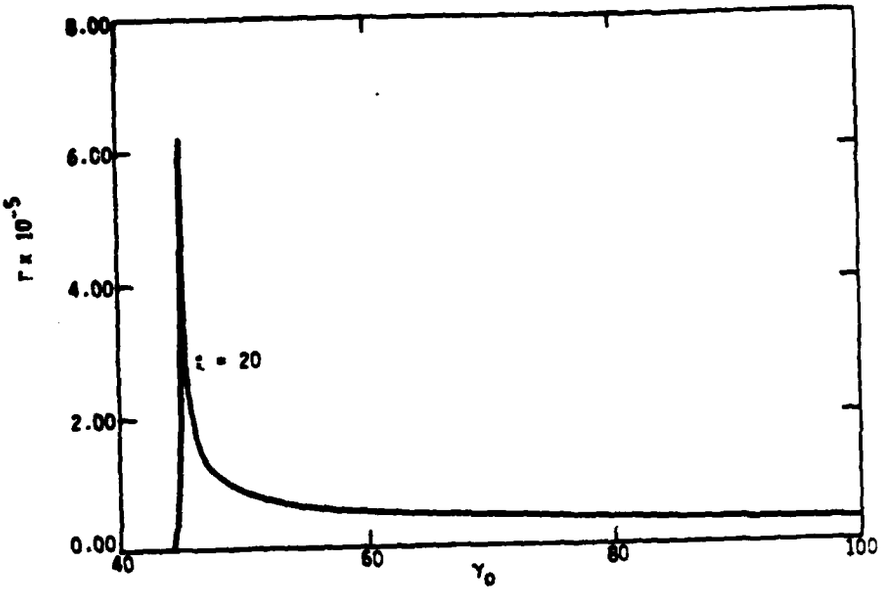

a)

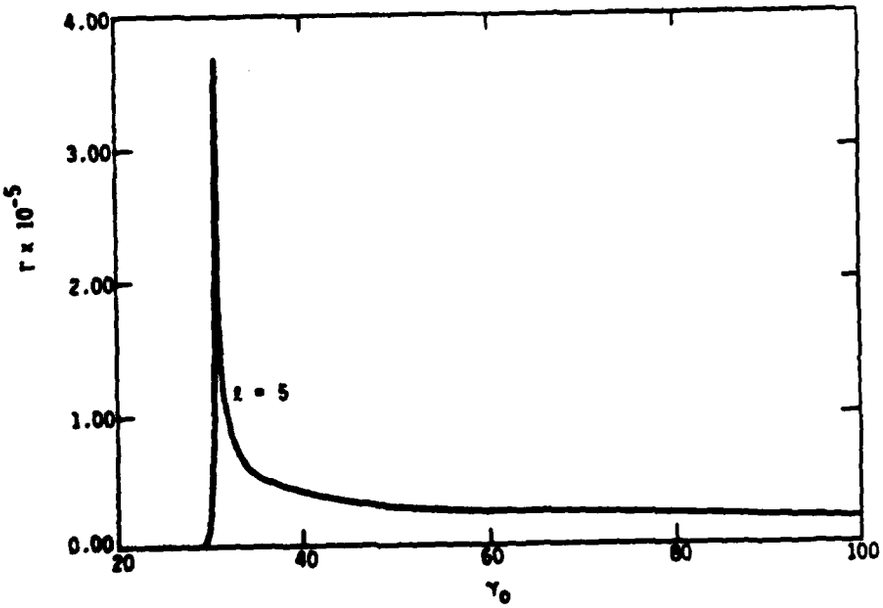

b)

Figure 8. Growth rates of the transverse resistive wall cyclotron mode. Part (a) is for the parameters in Table 1(a) and part (b) is for those in Table 1(b). For (a), $\ell = 20$ and for (b) $\ell = 5$. The instability turns on when $\Omega_{z0} = \Omega_{\theta 0}/\ell$ i.e., $\gamma_0 = B_{e0} r_0/\ell$ (= 45 for case (a)). The height of the initial peak is independent of ℓ and γ_0 (cf. Ref. 6).

APPENDIX C

UNCLASSIFIED

APPENDIX C

SECURITY CLASSIFICATION OF THIS PAGE (When Data Entered)

REPORT DOCUMENTATION PAGE		READ INSTRUCTIONS BEFORE COMPLETING FORM
1. REPORT NUMBER	2. GOVT ACCESSION NO.	3. RECIPIENT'S CATALOG NUMBER
4. TITLE (and Subtitle) Resistive Wall Instabilities in the Modified Betatron		5. TYPE OF REPORT & PERIOD COVERED Interim 6. PERFORMING ORG. REPORT NUMBER AMRC-R-332
7. AUTHOR(s) Brendan B. Godfrey Thomas P. Hughes		8. CONTRACT OR GRANT NUMBER(s) N00014-81-C-0647
9. PERFORMING ORGANIZATION NAME AND ADDRESS MISSION RESEARCH CORPORATION 1400 San Mateo Boulevard, S.E. Suite A Albuquerque, New Mexico 87108		10. PROGRAM ELEMENT PROJECT TASK AREA & WORK UNIT NUMBERS
11. CONTROLLING OFFICE NAME AND ADDRESS Office of Naval Research 800 North Quincy Street Arlington, Virginia 22217		12. REPORT DATE 30 November 1981 Revised April 1982 13. NUMBER OF PAGES 12
14. MONITORING AGENCY NAME & ADDRESS(if different from Controlling Office)		15. SECURITY CLASS. (of this report) Unclassified 15a. DECLASSIFICATION DOWNGRADING SCHEDULE

16. DISTRIBUTION STATEMENT (of this Report)

Approved for Public Release - Distribution Unlimited

17. DISTRIBUTION STATEMENT (of the abstract entered in Block 20, if different from Report)

18. SUPPLEMENTARY NOTES

19. KEY WORDS (Continue on reverse side if necessary and identify by block number)

Modified Betatron
Resistive Wall Instability

20. ABSTRACT (Continue on reverse side if necessary and identify by block number)

Resistive wall instabilities in modified betatrons are analyzed in several limits. The moderate frequency, negative energy, m=1 spacecharge and cyclotron waves are found to be most dangerous, potentially capable of disrupting acceleration for typical betatrons parameters. A moderate spread in electron energy can, however, stabilize these modes.

DD FORM 1 JAN 73 1473 EDITION OF 1 NOV 65 IS OBSOLETE

UNCLASSIFIED

SECURITY CLASSIFICATION OF THIS PAGE (When Data Entered)

RESISTIVE WALL INSTABILITIES IN THE MODIFIED BETATRON

Brendan B. Godfrey and Thomas P. Hughes

MISSION RESEARCH CORPORATION

ABSTRACT

Resistive wall instabilities in modified betatrons are analyzed in several limits. The moderate frequency, negative energy, m=1 spacecharge and cyclotron waves are found to be most dangerous, potentially capable of disrupting acceleration for typical betatron parameters. A moderate spread in electron energy can, however, stabilize these modes.

Spacecharge limits the circulating current in a conventional betatron to tens of amps, unless a very high initial electron energy is assumed. Adding a strong toroidal magnetic field, however, increases this limit by some two orders of magnitude.[1-3] The toroidal field also improves beam stability,[4] while a higher current has the opposite effect. This report discusses resistive wall instabilities[5] in a high current electron betatron with an applied toroidal magnetic field, referred to as a modified betatron.

Resistive-wall-driven instability occurs for both slow spacecharge and slow cyclotron beam modes, and over a wide range of frequencies.[6] Approximate analytical growth rate formulas are obtained in this report for the various branches of the resistive wall instability on a cold beam. The growth rate expressions are then evaluated for a typical set of modified betatron parameters. We find the spacecharge and cyclotron wave instabilities at frequencies comparable to the electron circulation frequency to be the most dangerous. Although slowly growing, they persist through a large fraction of the acceleration. If one can produce a spread of a few percent in electron energy, however, the modes can be stabilized. Alternatively, they can be avoided by limiting acceleration times to tens of microseconds.

The structure of the resistive wall instability dispersion relation is obtained for highly conducting cavity walls by a perturbation expansion (formally, a Rayleigh-Ritz approximation) about the beam modes in a perfectly conducting cavity. This procedure yields

$$2(\omega-\omega_0)U = P, \qquad (1)$$

where ω_0 is the unperturbed wave frequency, U is the wave energy, and P is the outward Poynting flux at the cavity wall due to finite conductivity. P is evaluated easily in the long wavelength limit to be[7]

$$P = R\omega\delta B^2 e^{i\pi/4} . \tag{2}$$

Here, R is the minor radius of the toroidal cavity, B is the wave magnetic field at the cavity wall, and δ is the skin depth,

$$\delta = \sqrt{2/\sigma\omega} . \tag{3}$$

Frequencies and conductivities are expressed in inverse cm; the speed of light is unity. Also, a factor of 4π is absorbed into the conductivity σ.

Solving Eq. (1)-(3) for the perturbed frequency yields

$$\omega^{1/2}(\omega - \omega_0) = 2(U/\omega)^{-1}(\omega^{1/2}\delta)RB^2 e^{i\pi/4} . \tag{4}$$

The right side of Eq. (4) is approximately independent of frequency, because $U \propto \omega$ for beam modes.[8] (This assertion is incorrect for m = 0 spacecharge waves. Nonetheless, the resulting dispersion relation has been found numerically to apply reasonably well even then.[7]) Evaluating the wave energy to complete the derivation is straightforward but tedious. Instead, we extract the needed term from the recent work of Sprangle and Vomvoridis.[9]

These authors determined the imaginary part of ω (the growth rate) to be

$$\Gamma = \frac{\Omega_2^2}{\Omega_0} \frac{n_s \gamma \delta a^2/R^3}{\Delta} \tag{5}$$

with

$$\Delta^2 = 1 + 2(1 - 2n_s a^2/R^2)\Omega_z^2/\Omega_\theta^2 \qquad (6)$$

for moderate frequency m=1 waves. The beam radius is a. Otherwise, symbols are defined as in Ref. 9. Recasting Eq. (5) as

$$\Gamma = \frac{\omega_p^2 \delta a^2/R^3}{2\Omega_\theta \Delta} \quad , \qquad (7)$$

we see that toroidal corrections to the cylindrical drift tube dispersion relation enter only through Δ. Comparison of Eqs. (4) and (7) yields

$$\omega^{1/2}(\omega - \omega_o) = \frac{\omega_p^2 a^2/R^3}{\sigma^{1/2}\Omega_\theta \Delta} \; f_\pm \; e^{i\pi/4} \qquad (8)$$

For increased generality we have included a geometrical factor f by analogy with cylindrical drift tube results.[7]

$$f_\pm = (m^2 + \ell^2 R^2/R_o^2) \left[\frac{I_{m \pm 1}(\ell a/R_o)}{I_{m+1}(\ell R/R_o) + I_{m-1}(\ell R/R_o)} \right] \qquad (9)$$

R_o is the major radius of the torus, I and K are modified Bessel functions, and ℓ amd m are the toroidal and poloidal wave numbers. With a/R and $\ell R/R_o$ both small, f is aproximately 1 for m = 1 and varies as $m^2(a/R)^{2(m-1)}$ for m > 1. The instability is weaker for m = 0 where f falls off as $(\ell a/R_o)^2$ and for m < 0 (wave poloidal helicity opposite that of the electrons), where f decreases as $m(a/R)^{2(m+1)}$

For slow cyclotron waves, characterized by

$$\omega = \ell \Omega_z/\gamma - \Omega_\theta/\gamma \; , \qquad (10)$$

the peak growth rate from Eq. (8) occurs at $\omega_0 \approx 0$.

$$\omega = \sigma^{-1/3}\left[\frac{\omega_p^2 a^2/R^3}{\Omega_\theta \Delta} f_\pm\right]^{2/3} e^{i\pi/6} . \tag{11}$$

The constraint $\omega_0 \approx 0$ implies $\ell \approx \Omega_\theta/\Omega_z$. During acceleration, the vertical magnetic field Ω_z (and the beam energy γ, which is proportional to Ω_z) increases adiabatically. Hence $\omega_0 \approx 0$ is satisfied for only a limited time period,

$$\Delta\omega \approx \frac{\Omega_\theta}{\gamma} \frac{d\gamma}{dt} \Delta t \tag{12}$$

Equating the instability band width $\Delta\omega$ to the growth rate Γ, replacing Ω_θ by $\ell\Omega_z$, and solving for Δt, we obtain the total growth occurring as the instability passes through resonance

$$\Gamma \Delta t \sim \frac{\Gamma^2}{\ell(\Omega_z/\gamma)} \frac{\gamma}{d\gamma/dt} . \tag{13}$$

Eq. (13) is maximized late in the acceleration cycle, when γ is large and the resonant ℓ value is small.

After passing through $\omega_0 \approx 0$, the cyclotron resistive wall instability for fixed ℓ does not, of course, cease but instead transitions smoothly to a lower growth rate regime.

$$\omega = \omega_0 + \sigma^{-1/2}\omega_0^{-1/2}\left[\frac{\omega_p^2 a^2/R^3}{\Omega_\theta \Delta} f_\pm\right] e^{i\pi/4} . \tag{14}$$

Setting $m = 1$ recovers Eq. (5). Although the growth rate of Eq. (14) is somewhat smaller than that of Eq. (11), the corresponding total growth of the former,

$$(\Gamma\Delta t)_{eff} \sim (2\sigma)^{-1/2}\left[\frac{\omega_p^2 a^2/R^3}{\Omega_\theta} f_\pm\right] \int \frac{dt}{(\omega_0\Delta)^{1/2}} , \tag{15}$$

may exceed Eq. (13). The integration in Eq. (15) extends from the time at which ω_0 is greater than a few times the ω in Eq. (11) until the end of the acceleration.

Parallel instabilities occur for slow spacecharge waves, characterized by

$$\omega_0 \approx \ell\Omega_z/\gamma - m\omega_B \ , \tag{16}$$

where ω_B is the beam poloidal rotation frequency, a small quantity.[9] For growth to occur at the rate in Eq. (11), we must have $m \approx \ell\Omega_z/\gamma\omega_B$. Even for ℓ as small as one (there is no $\ell = m = 0$ spacecharge wave), m must be quite large. Consequently, $f_\pm$ always is small near $\omega_0 = 0$ for spacecharge modes, and resistive wall growth is in this case negligible. On the other hand, for modest positive values of ω_0 instability of slow spacecharge waves is described by Eq. (14), with growth rates comparable to those of slow cyclotron waves.

Breizman and Ryutov have shown the existence of another, high frequency branch of the resistive wall instability for spacecharge modes.[10,11] To second order in R/R_0, the growth rate for this instability is identical to that in a straight tube. Peak growth for the $m = 0$ mode occurs at $\ell = \gamma R_0/R$, with γ the normalized electron energy.

$$\Gamma = \frac{1}{R(1 + 2\ell n(R/a))}\left(\frac{\nu}{2\sigma R}\right)^{1/2} \tag{17}$$

Note that this expression is independent of the magnetic guide-field strength. At long wavelengths the growth rate falls off as $\ell^{1/2}$, until it merges with the lower frequency branch. The growth rate decreases more gradually at shorter wavelengths. Interestingly, the instability persists for $m \neq 0$, although with reduced growth rates.[7]

Numerical studies with the laminar beam stability code GRADR[12,13] confirm the absence of a corresponding high frequency cyclotron wave resistive wall instability.[7]

We illustrate the relative importance of the various forms of the resistive wall instability for the typical modified betatron parameters listed in Table 1. A stainless steel tube wall, with normalized conductivity $\sigma = 5.24 \cdot 10^6$ cm^{-1}, is assumed. (The conductivity of copper is about forty times larger.) Inserting these values into Eq (11), we find $\Gamma = 4.0 \cdot 10^{-5}$ cm^{-1} for $m = 1$ cyclotron waves at $\omega_0 = 0$. The corresponding skin depth is $\delta = 0.07$ cm; the cavity wall must be at least this thick for Eq. (11) to be valid. The growth rate value just given assumes $\Delta = 1$. The increase of Δ near the end of the acceleration period reduces Γ by less than 25%. Equation (13) is maximized by $\gamma \sim 70$, where the ℓ value for the $\omega_0 = 0$ resonance drops to one. Total growth is $\Gamma\Delta t = 3.6$ in this case. After passing through the $\omega_0 = 0$ resonance, the $\ell = m = 1$ slow cyclotron mode continues to grow, at the rate in Eq. (14). Evaluating this expression for the typical frequency $\omega_0 = \Omega_z/\gamma$ yields $\Gamma = 5.1 \cdot 10^{-6}$ cm^{-1}. Growth occurs over about 1/3 the acceleration period, or $\Gamma\Delta t = 55$ when the $\omega_0 = 0$ contribution is included.

As already discussed, growth of slow spacecharge waves near $\omega_0 = 0$ is negligible. At higher frequencies. the growth rate of the $\ell = m = 1$ spacecharge wave is comparable to that of the corresponding cyclotron mode. Since growth occurs throughout the acceleration period, $\Gamma\Delta t = 150$. At still higher frequencies $m = 0$ spacecharge waves grow at a maximum rate of $\Gamma = 1.3 \cdot 10^{-6}$, or about 25% of the intermediate frequency growth rate. It is important to bear in mind that these growth estimates probably are uncertain by a factor of two, due to approximations made.

TABLE 1

Typical Modified Betatron Parameters Used in Evaluating Resistive Wall Instability Growth Rates.

Toroidal Magnetic Field	B_θ	2.5 kg
Vertical Magnetic Field (Initial)	B_z	115 g
Toroid Major Radius	R_o	100 cm
Toroid Minor Radius	R	10 cm
Beam Radius	a	1 cm
Beam Current	ν	0.59
Beam Energy	γ	7-100
Acceleration Time	τ	$3 \cdot 10^7$ cm

The preceding analysis ignores thermal spread in the beam electron velocities. As a result of the toroidal geometry, a spread in electron toroidal velocity can smear out the transverse resonances associated with the resistive instabilities. In a companion paper we find that the required spreads in toroidal and transverse velocities are achievable from a few percent spread in initial electron kinetic energy.[14] A similar conclusion was drawn in Ref. 9, based on a Lorentzian distribution of energies. Of course, this damping of spacecharge and cyclotron wave instabilities by a spread in electron velocities is ineffective for low frequency modes. As we have already seen, however, these latter modes are not a serious problem.

In summary, we find that the $m = 1$, low ℓ spacecharge and cyclotron wave instabilities are the most dangerous of the various resistive wall phenomena identified for modified betatrons. Amplification factors of $e^{150} \sim 10^{65}$ and $e^{55} \sim 10^{24}$, respectively, are predicted for the parameters in Table 1. Successful operation of a modified betatron requires cutting the growth exponent $\Gamma\Delta t$ to about unity. (Computer simulations suggest that initial perturbations may be quite large.[15]) Employing more highly conducting cavity walls provides a factor of six. Reducing the acceleration time by an order of magnitude would then effectively eliminate these instabilities. Alternatively, an initial spread of a few percent in the electron energy should be sufficient to damp out the modes.

We are indebted to M. Campbell, M. Jones, D. Sullivan, and particularly P. Sprangle for helpful discussions. This research is supported by Office of Naval Research contract N00014-81-C-0647, monitored by C. Roberson.

REFERENCES

1. P. Sprangle and C. A. Kapetanakos, "Constant Radius Magnetic Acceleration of a Strong Nonneutral Proton Ring," J. Appl. Phys. 49, 1 (1978).

2. P. Sprangle, C. A. Kapetanakos, and S. J. Marsh, "Dynamics of an Intense Electron Ring in a Modified Betatron Field," NRL-4666, (Naval Research Laboratory, Washington, 1981).

3. D. P. Chernin and P. Sprangle, "Transverse Beam Dynamics in the Modified Betatron," NRL-4687, (Naval Research Laboratory, Washington, 1981).

4. R. W. Landau, "Negative Mass Instability with B_θ Field," Phys. Fluids 11, 205 (1968).

5. L. J. Laslett, V. K. Neil, and A. M. Sessler, "Transverse Resistive Instabilities of Intense Coasting Beams in Particle Accelerators," Rev. Sci. Inst. 36, 436 (1965).

6. B. B. Godfrey, "Resistive Wall Instabilities in Radial Line Accelerators," AMRC-N-170, (Mission Research Corporation, Albuquerque, 1981).

7. B. B. Godfrey, "Resistive Wall Instabilities in Radial Pulseline Accelerators," AMRC-R-345, (Mission Research Corporation, Albuquerque, 1982).

8. B. B. Godfrey and B. S. Newberger, "Wave Amplitude Variation and Energy Flow in Autoresonant Collective Ion Acceleration," J. Appl. Phys. 50, 38 (1979).

9. P. Sprangle and J. L. Vomvoridis, "Longitudinal and Transverse Instabilities in a High Current Modified Betatron Electron Accelerator," NRL-4688, (Naval Research Laboratory, Washington, 1981).

10. B. N. Breizman and D. D. Ryutov, "Powerful Relativistic Electron Beams in a Plasma and in a Vacuum (Theory)," Nuc. Fus. 14, 873 (1974).

11. E. P. Lee, "Resistive Driven Bunching Mode of an Accelerator Ion Pulse," UCRL-86452, (Lawrence Livermore National Laboratory, Livermore, 1981).

12. B. B. Godfrey, "Linear Theory of Radially Inhomogeneous Unneutralized, Relativistic Electron Beams," IEEE Plas. Sci. PS-7, 32 (1979).

13. D. J. Sullivan and B. B. Godfrey, "GRADR: Interactive User's Manual," AMRC-R-309, (Mission Research Corporation, Albuquerque, 1981).

REFERENCES (Continued)

14. T. P. Hughes and B. B. Godfrey, "Linear Stability of the Modified Betatron," AMRC-R-354, (Mission Research Corporation, Albuquerque, 1982).

15. D. J. Sullivan, M. M. Campbell, and B. B. Godfrey, unpublished.

APPENDIX D

UNCLASSIFIED

SECURITY CLASSIFICATION OF THIS PAGE (When Data Entered)

REPORT DOCUMENTATION PAGE		READ INSTRUCTIONS BEFORE COMPLETING FORM
1. REPORT NUMBER	2. GOVT ACCESSION NO.	3. RECIPIENT'S CATALOG NUMBER
4. TITLE (and Subtitle) BEAM BREAKUP AND IMAGE DISPLACEMENT INSTABILITIES IN HIGH CURRENT ELECTRON BEAM RACETRACK INDUCTION ACCELERATORS		5. TYPE OF REPORT & PERIOD COVERED INTERIM 6. PERFORMING ORG. REPORT NUMBER AMRC-R-410
7. AUTHOR(s) B. B. Godfrey and T. P. Hughes		8. CONTRACT OR GRANT NUMBER(s) N00014-81-C-0647
9. PERFORMING ORGANIZATION NAME AND ADDRESS MISSION RESEARCH CORPORATION 1720 Randolph Road, S.E. Albuquerque, New Mexico 87106		10. PROGRAM ELEMENT, PROJECT, TASK AREA & WORK UNIT NUMBERS
11. CONTROLLING OFFICE NAME AND ADDRESS OFFICE OF NAVAL RESEARCH 800 North Quincy Street Arlington, Virginia 22217		12. REPORT DATE September 1982 13. NUMBER OF PAGES 21
14. MONITORING AGENCY NAME & ADDRESS (if different from Controlling Office)		15. SECURITY CLASS (of this report) UNCLASSIFIED 15a. DECLASSIFICATION DOWNGRADING SCHEDULE

16. DISTRIBUTION STATEMENT (of this Report)

Approved for Public Release - Distribution Unlimited

17. DISTRIBUTION STATEMENT (of the abstract entered in Block 20, if different from Report)

18. SUPPLEMENTARY NOTES

Earlier reports in this series are AMRC-R-332, AMRC-R-354, and AMRC-N-207.

19. KEY WORDS (Continue on reverse side if necessary and identify by block number)

Racetrack Electron Accelerator
Beam Breakup Instability
Image Displacement Instability

20. ABSTRACT (Continue on reverse side if necessary and identify by block number)

Beam breakup and image displacement instability growth rates for a 1 kA, 40 MeV electron beam racetrack induction accelerator are computed. The hypothetical device is taken to have four acceleration gaps, each with 0.2 MeV applied voltage and 15 ohm transverse impedance; the guide field is 2 kg. We find that the total amplification of the beam breakup mode is limited to 3.6 provided the cavity mode quality factor Q is 6. Image displacement mode growth is negligible. Thus, the negative mass instability, which grows about three

DD FORM 1 JAN 73 1473 EDITION OF 1 NOV 65 IS OBSOLETE

UNCLASSIFIED

SECURITY CLASSIFICATION OF THIS PAGE (When Data Entered)

times faster than the beam breakup instability for these parameters, is the dominant stability consideration. Probably, the negative mass instability can be controlled by sufficient spread in the electron energy.

CONTENTS

LIST OF ILLUSTRATIONS

LIST OF TABLES

I. INTRODUCTION

High current racetrack beam induction accelerators and modified betatrons are a subject of increasing interest as sources of high power electron beams for free electron lasers, flash radiography, and other applications. The racetrack induction accelerator geometry is illustrated in Figure 1. The beam is injected from a conventional pulsed diode beam generator into the drifttube, is progressively accelerated as it repetitively passes one or more induction modules, and then is extracted from the accelerator for its intended use. Beam extraction may even be unnecessary for microwave applications, because a slow-wave or rippled-magnetic-field cavity can be inserted in a straight section of the drifttube.[1]

Most beam stability studies for high current recirculating devices have dealt with negative mass and resistive wall instabilities.[2-5] However, experience with linear induction accelerators suggests that beam breakup and image displacement instabilities due to beam interaction with the induction modules and other discontinuities in the drifttube may be significant.[6,7] The beam breakup instability arises from a resonant coupling between beam transverse oscillations and m=1 electromagnetic cavity modes localized to the acceleration gaps,[8] while the image displacement instability is caused by interrupting the m=1 beam image current in the drifttube wall.[9] Clearly, the two are interrelated; in some contexts the image displacement instability can be viewed as the low frequency limit of the beam breakup instability.

This paper extends instability results developed for high current linear induction accelerators to cyclic devices. The primary differences are (1) that the beam passes the same few gaps again and again, and (2) that the curved beam trajectory couples longitudinal to transverse motion, perhaps leading to a hybridization of the negative mass and beam breakup modes. Experience with interaction among instabilities in other situations suggests that the latter item is the less important of the two.[10]

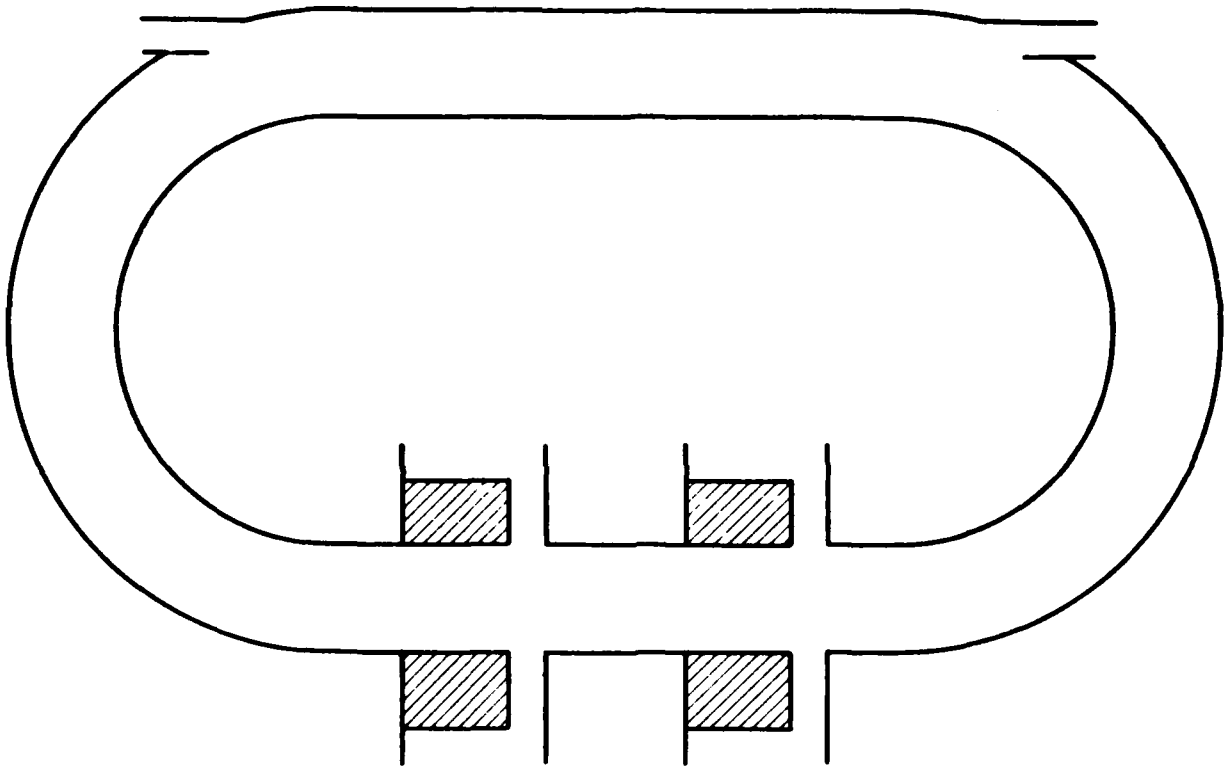

Figure 1. Simplified representation of cyclic induction accelerator with racetrack drift tube, acceleration gaps, and injection and extraction ports.

Therefore, we consider only the former aspect, periodicity of the interaction, and omit curvature effects. As in earlier calculations, we assume that the beam propagates at the speed of light, that lateral displacements of the beam are small and rigid, and that the gaps are narrow compared to the beam oscillation wavelength. The consequences of relaxing these approximations for the image displacement instability under different circumstances is discussed elsewhere.[9] We expect the three approximations to be adequate for present purposes.

A general dispersion relation for a multiple gap racetrack induction accelerator is derived in Section II. Because the resulting expression, a determinant, is cumbersome, we then specialize to the case of identical, uniformly spaced gaps, obtaining approximate analytical growth rate formulas for the beam breakup and image displacement instabilities. Section III illustrates instability growth for a 1 kA electron beam accelerated to 40 MeV through fifty cycles of a four gap device. (These parameters are based on an induction linac developed by the National Bureau of Standards and now being modified at the Naval Research Laboratory.[11]) First, growth rates are estimated based on the formulas of the preceding Section. Then, more precise numerical values are obtained with the beam transport code BALTIC, including the effects of acceleration and initial transients. Our findings, summarized in Section IV, are encouraging: The image displacement instability is negligible, and the beam breakup instability is manageable provided that the mode quality factor Q is kept low. A comparison with the negative mass and resistive wall instability growth rates also is provided.

II. DERIVATION OF GROWTH RATE EXPRESSIONS

In the long wavelength, paraxial approximation the linearized equation of transverse motion for the beam centroid is given by[9,10]

$$\left(\frac{d}{dt} + \frac{d}{dz}\right) \left[\gamma \left(\frac{d}{dt} + \frac{d}{dz}\right) - i\omega_c\right] \xi$$

$$- \frac{1}{2} \frac{\rho a^2}{\gamma^2 R^2} \xi = \sum F_j \delta(z - z_j) \xi \qquad (1)$$

Here, $\xi = x + iy$ is the (complex) transverse displacement of the beam centroid, ρ is the beam density, γ is the beam relativistic energy, a is the beam radius, R is the drifttube radius, and ω_c is the cyclotron frequency for the magnetic guide field. Time is normalized to the beam axial velocity, which is in turn assumed to be equal to the speed of light. The last term on the left side of Eq. (1) represents the combined transverse forces on the beam from its image charge and current in the smooth drifttube wall. Discontinuities in the wall are treated as impulsive forces appearing on the right side of Eq. (1).

We begin the derivation of the dispersion matrix by assuming the beam parameters to be constant in time and Fourier transforming Eq. (1).

$$\left(i\omega - \frac{d}{dz}\right) \left(i\omega - \frac{d}{dz} + i \frac{\omega_c}{\gamma}\right) \xi$$

$$- \frac{1}{2} \frac{\rho a^2}{\gamma^3 R^2} \xi = \frac{1}{\gamma} \sum F_j \delta(z - z_j) \xi \qquad (2)$$

As mentioned in the Introduction, we shall take account of time-varying γ in Sec. III by direct numerical integration of Eq. (1).

Next, Eq. (2) is solved for ξ, treating the right side of the equation as a source term. This can be done using a Green's function or, equivalently, by twice integrating the equation and imposing periodicity at $z = L$, the accelerator path length. The result is

$$\gamma(k_+ - k_-)\ \xi(z) =$$

$$(2\sin k_+ L/2)^{-1} \sum_{j=1}^{N} F_j\ \xi(z_j)\ \exp[ik_+(\mathrm{sign}[z_j - z]L/2 - (z_j - z))] \tag{3}$$

$$- (2\sin k_- L/2)^{-1} \sum_{j=1}^{N} F_j\ \xi(z_j)\ \exp[ik_-(\mathrm{sign}[z_j - z]L/2 - (z_j - z))]$$

where N is the number of acceleration gaps and Sign(x) is the sign of x. The wavenumbers $k_\pm$ characterize the beam cyclotron and spacecharge waves, respectively, as determined by the left side of Eq. (2), i.e., between gaps.

$$k_\pm = \omega + (\omega_c \pm [\omega_c^2 - 2\rho a^2/\gamma R^2]^{1/2})/2\gamma \tag{4}$$

For typical induction linac parameters, $k_+ \approx \omega + \omega_c/\gamma$ and $k_- \approx \omega$. Although it may not be immediately apparent, $\xi(z)$ as expressed in Eq. (3) is everywhere continuous; its first derivative is discontinuous at z_j.

Evaluating Eq. (3) at each of the gaps yields the system of equations

$$\gamma(k_+ - k_-)\ \xi\ (z_\ell) =$$

$$(2\sin k_+ L/2)^{-1} \sum_{j=1}^{N} F_j\ \xi(z_j)\ \exp[ik_+(L/2 - \mathrm{Mod}[z_j - z_\ell, L])] \tag{5}$$

$$- (2\sin k_- L/2)^{-1} \sum_{j=1}^{N} F_j\ \xi(z_j)\ \exp[ik_-(L/2 - \mathrm{Mod}[z_j - z_\ell, L])]$$

Here, Mod (x,L) is x modulo L, defined to lie between 0 and L. The determinant of the coefficient matrix of Eq. (5) is the desired dispersion relation. In general, it must be solved numerically to obtain ω. Additional analytical progress can, however, be made when the gaps are spaced uniformly and all have the same response function F.

$$\gamma(k_+ - k_-)\,\xi(\ell L/N) =$$

$$(2\sin k_+ L/2)^{-1}\ F\sum_{j=0}^{N-1}\xi(jL/N)\exp[ik_+(L/2 - \mathrm{Mod}[j-\ell,N]L/N)]$$

$$-(2\sin k_- L/2)^{-1}\ F\sum_{j=0}^{N-1}\xi(jL/N)\exp[ik_-(L/2 - \mathrm{Mod}[j-\ell,N]L/N)] \qquad (6)$$

Since its right side is a discrete convolution, Eq. (6) is readily solved by performing a finite Fourier transform. We find

$$\gamma(k_+ - k_-) = iF\ \{\ (1 - \exp[2\pi im/N - ik_+ L/N])^{-1} - (1 - \exp[2\pi im/N - ik_- L/N])^{-1}\ \} \qquad (7)$$

or, more simply,

$$1 = \frac{F}{2\gamma(k_+ - k_-)}\ \left\{\ \mathrm{ctn}\left[\frac{k_+ L/2 - \pi m}{N}\right] - \mathrm{ctn}\left[\frac{k_- L/2 - \pi m}{N}\right]\ \right\}. \qquad (8)$$

The transform index m ranges between 0 and N-1. Still another useful representation, reminiscent of results for nonrecirculating devices, is[8,9]

$$\cos[(k_+ + k_-)L/2N - \pi m/N] =$$

$$\cos[(k_+ - k_-)L/2N] + \frac{F}{\gamma(k_+ - k_-)}\ \sin[(k_+ - k_-)L/2N]\,. \qquad (9)$$

For F/ω_c small these equation are approximately satisfied by $k_+ \approx k_n$ or $k_- \approx k_n$, with $k_n \equiv 2\pi n/L$. Correspondingly,

$$\omega \approx \omega_n \equiv k_n - (\omega_c \pm [\omega_c^2 - 2\rho a^2/\gamma R^2]^{1/2})/2\gamma \ . \qquad (10)$$

Instability may occur when ω matches a resonant frequency of F or when the right side of Eq. (9) exceeds unity away from a resonance. These two possibilities are realized in the beam breakup and image displacement instabilities, respectively.

The beam breakup instability is caused by TM_{1n0} oscillatory electromagnetic fields localized to the acceleration gaps and adjacent drift-tube regions. These cavity modes are conveniently represented by damped harmonic oscillator equations for their normalized vector potentials.

$$\left(\frac{d^2}{dt^2} + \frac{\omega_o}{Q}\frac{d}{dt} + \omega_o^2\right) A_i = \frac{\omega_o Z_\perp}{2Q}\ \frac{\omega_o^2 \rho a^2}{2}\ \xi(z_i) \qquad (11)$$

Q is the cavity mode quality factor, while ω_o is its frequency. Coupling between the beam and a cavity mode is given by its transverse impedance $Z_\perp/Q$. The transverse impedance is basically a geometrical factor, which tends to scale linearly with the gap width.

Fourier transforming Eq. (11) in time, we obtain for $F = A/\xi$

$$F = -\frac{\omega_o^2}{\omega^2 + i\omega\omega_o/Q - \omega_o^2}\ \frac{\omega_o Z_\perp}{2Q}\ \frac{\rho a^2}{2} \ . \qquad (12)$$

The beam breakup instability growth rate now can be approximated in the usual manner by expanding Eq. (8) and (12) about ω_n, defined in Eq. (10). The resulting quadratic in $\omega - \omega_n$ shows instability only for $k_n = k_-$, with growth rate

$$\omega - \omega_n = i\frac{\omega_o}{2}\left\{\left[\frac{NZ_\perp}{2Q}\frac{\rho a^2}{\omega_c L} + \left(\frac{1}{2Q} - i\frac{\omega_n - \omega_o}{\omega_o}\right)^2\right]^{1/2} - \left(\frac{1}{2Q} - i\frac{\omega_n - \omega_o}{\omega_o}\right)\right\} \tag{13}$$

Note that this derivation fails for $\sin[(k_+ - k_-)L/2]$ too small; see Eq. (9). More precisely, the instability growth rate is reduced whenever $|Nk_n - \omega_c/\gamma|$ is less than the absolute value of the right side of Eq. (13) and finally vanishes when $Nk_n = \omega_c/\gamma$.

The image displacement instability arises due to interruption of the beam image current at a discontinuity in the drifttube wall, such as occurs at an acceleration gap. The analysis in Ref. 9 and 12 gives a force coefficient

$$F = \frac{\ell}{R^2}\frac{\rho a^2}{2} \tag{14}$$

The effective gap width ℓ is given by the physical width when the latter is small compared to the drifttube radius R. In the opposite limit, $\ell < R$. As already noted, growth occurs whenever the right side of Eq. (9) exceeds unity. For F/ω_c small this happens only in a narrow parameter region centered on $\tan[(k_+ - k_-)L/2] = F/\gamma(k_+ - k_-)$, for which the growth rate is

$$\Gamma = NF/\omega_c L. \qquad (15)$$

In the next section we evaluate these two growth rates for possible recirculating induction accelerator parameters and then generalize our numerical results to include irregular gap spacing and beam acceleration by computer solution of Eq. (1).

III. NUMERICAL EVALUATION OF GROWTH RATES

The four gap linear induction accelerator at the Naval Research Laboratory is an attractive candidate for a recirculating device. The acceleration gaps are in pairs with the members separated by about 30 cm. The distance between the two pairs is arbitrary within reasonable limits. Here we take the distance to be 200 cm, giving a total round-trip path length of L = 460 cm. (The specific value chosen does not strongly influence our conclusions.) The principle m=1 gap normal mode is at 880 MHz with a transverse impedance of 15 ohms and a Q of 60. Each gap provides an acceleration of 0.2 MeV, resulting in an energy gain for the electron beam of 40 MeV after 50 passes. A beam current of 1 kA and guide field of 2 kg are assumed. These parameters are summarized in Table 1. Note that γ in the table has been corrected for the spacecharge depression in the drifttube and also that $Z_\perp/Q$ has been expressed in dimensionless form by dividing the transverse impedance by 30 ohms.

Although the four gaps are not spaced uniformly, a reasonable upper bound on beam breakup instability growth can nonetheless be obtained from Eq. (13). We find $\Gamma = 12.9 \cdot 10^{-4}$ cm^{-1}, corresponding to about 30 e-foldings during the course of acceleration. (We assume $\omega_0 = \omega_n$.) The most obvious way of cutting this amplification to an acceptable level is by reducing Q. Recent work at Lawrence Livermore National Laboratory on short pulse induction accelerators suggests that a quality factor as low as

TABLE 1. NOMINAL RACETRACK INDUCTION ACCELERATOR PARAMETERS

Path Lengths	L = 460 cm	
Drifttube Radius	R = 7 cm	
Beam Radius	a = 1 cm	
Guide Field	B_z = 2 kg	(ω_c = 1.173 cm^{-1})
Beam Current	I = 1 kA	(ν = 0.0588)
Beam Energy	U = 0.4 - 40 MeV	(γ = 1.5 - 80)
Number of Revolutions	50	
Number of Gaps	N = 4	
Acceleration per Gap	ΔU = 0.2 MeV	($\Delta\gamma$ = 0.4)
Gap Resonant Frequency	880 MHz	
Mode Quality Factor	Q = 60	
Gap Transverse Impedance	15 ohms	($Z_\perp/Q$ = 0.5)
Gap Width	ℓ = 5 cm	

six is achievable.[13] For Q=6, $\Gamma = 2.4 \cdot 10^{-4}$ cm^{-1}, or 5.5 e-foldings. As many as eight e-foldings may be tolerable provided the gaps are not excited appreciably at their resonant frequency prior to beam injection.

More precise growth rates can be obtained by numerically solving Eq. (5) plus Eq. (12), and this is not difficult to do. Instead, we choose to integrate Eq. (1) plus Eq. (11) directly using the computer program BALTIC. The code was exercised extensively in support of the RADLAC radial pulseline accelerator program and so is well tested.[10] BALTIC has the advantage over a dispersion relation solver that it takes account of beam acceleration and of transients. It is, of course, much slower.

Table 2 summarizes thirteen runs of the BALTIC code. The quantities N, Q, ω_0, and γ were varied, but with $NZ_\perp/Q$ held fixed. Some calculations involved an accelerating beam. Cases 1-4 illustrate the effect of changing $\omega_0 - \omega_n$. Because $k_n = 0.014 \cdot n$ cm^{-1}, the pattern of growth rate variation with ω_0 in these four cases repeats itself with the same 0.014 cm^{-1} periodicity in ω_0. It so happens that $\sin[(k_+ - k_-)L/2]$ is small for $\gamma = 80$, the value chosen in cases 1-4, which reduces the growth rate some. Setting $\gamma = 60$ avoids this situation, increasing Γ by 25%, as illustrated in cases 5 and 6. The growth rate change caused by dropping Q from 60 to 10, as in case 7, is consistent with Eq. (13).

The seven cases just discussed were for a single gap. Cases 8 and 9 treat two gaps evenly spaced. Growth rates are comparable to the single gap runs, as expected. The enhancement of Γ for case 9 relative to case 8 again arises from adjusting $\sin[(k_+ - k_-)L/2]$.

Finally, cases 10-13 treat four gaps spaced as described at the beginning of this Section. Also, the beam is accelerating in these last four runs. It is clear from the resulting growth rates that the gradual acceleration which occurred has little effect on stability except to average

TABLE 2. SUMMARY OF BEAM BREAKUP INSTABILITY CALCULATIONS WITH BALTIC

Case	N	Q	ω_0 (cm^{-1})	γ	Γ (10^{-4} cm^{-1})
1	1	60	0.18	80	8.3
2	1	60	0.1732	80	3.3
3	1	60	0.17757	80	8.9
4	1	60	0.1787	80	8.8
5	1	60	0.18	60	10.0
6	1	60	0.17757	60	12.3
7	1	10	0.18	80	3.4
8	2	60	0.18	80	9.6
9	2	60	0.18	1.5	12.0
10	4	60	0.18	1.5-80	9.8
11	4	10	0.18	1.5-80	2.6
12	4	6	0.18	1.5-80	1.2
13	4	6	0.17757	1.5-80	1.6

over $\omega_0 - \omega_n$ and $\sin[(k_+ - k_-)L/2]$. In case 13, ω_0 was decreased slightly to maximize growth at large γ. Indeed, Γ increased by one-third relative to case 12.

Figure 2 depicts the maximum transverse displacement of the beam as a function of time for case 13. It and the other runs were initiated with a uniform transverse offset of unit magnitude for the beam. The cavity modes were initially excited at an amplitude consistent with injection of the offset beam with zero risetime, a worst case assumption. The displacement is seen to grow by a factor of about 3.6.

The image displacement instability turns out to be insignificant. From Eq. (15) its peak growth rate is $0.9 \cdot 10^{-4}$ cm^{-1}. Since this occurs only over a narrow range of parameters, however, we should expect a much slower average growth during acceleration. Indeed, a four gap BALTIC run gave no coherent growth whatsoever, and transient fluctuations amounted to less than 15% of the initial displacement.

IV. CONCLUSIONS

In this report we have developed a simple theory of beam breakup and image displacement instabilities in cyclic induction accelerators and applied it to obtain growth rate estimates for a possible device. The theoretical model takes recirculation into account primarily by enforcing periodicity on the unstable transverse models. Drifttube curvature effects were not considered. We find for the 1 kA, 40 MeV accelerator that neither the beam breakup nor the image displacement instability should be serious. Specifically, with $Q=6$ and parameters otherwise as in Table 1 the beam breakup growth rate is $\Gamma = 1.6 \cdot 10^{-4}$ cm^{-1}; the image displacement growth is negligible.

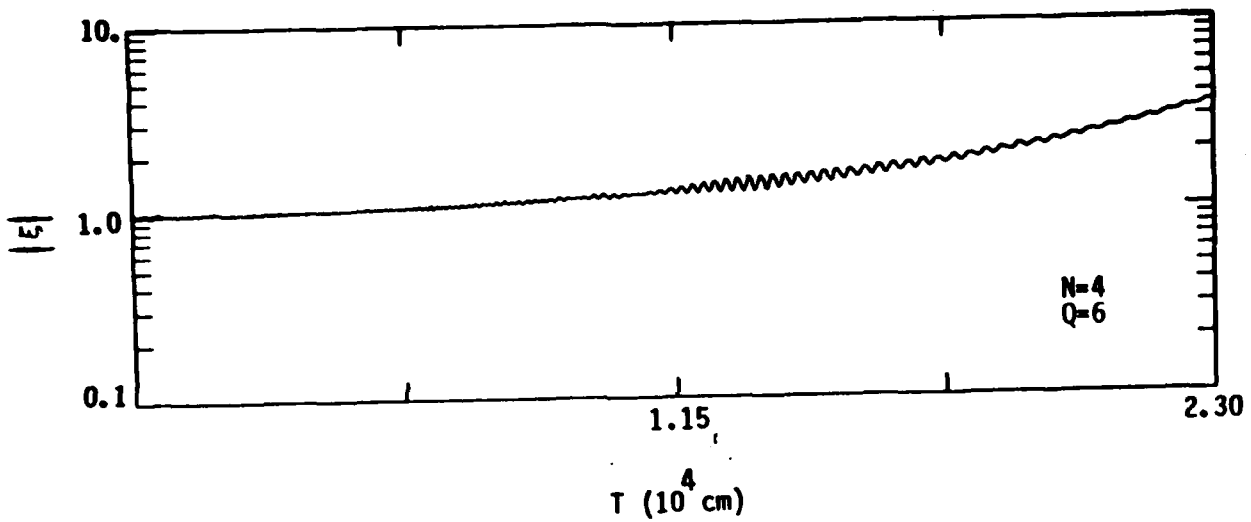

Figure 2. Time history of maximum beam transverse displacement for case 13 of Table 2.

For comparison, growth rates of the negative mass and resistive wall (for stainless steel) instabilities for comparable parameters are of order $5 \cdot 10^{-4}$ cm^{-1} and $0.2 \cdot 10^{-4}$ cm^{-1}, respectively.[3-5] Thus, the negative mass instability is somewhat more serious than the gap-induced instabilities in this instance.

The accelerator path length L = 460 cm chosen for the numerical calculations is perhaps small for practical devices. Increasing L by lengthening the straight sections of the racetrack geometry would have little impact on any but the resistive wall instability integrated growth: Growth rates of the gap-induced instabilities decrease roughly as L^{-1}, so that growth per pass remains fixed, while the negative mass instability grows only in the curved sections of the drift tube. In fact, the negative mass mode may decay in straight sections. Growth per cycle of the resistive wall instability, of course, increases linearly with L. Its growth rate is so slow, however, that the path length could be increased by an order of magnitude or more before the resistive wall instability became competitive with the other modes.

The important stabilizing influences of electron energy spread and transverse oscillations have been omitted from our calculations. Recent estimates for betatrons with comparable parameters suggest that a 10% spread in the injected beam electron energies is sufficient to suppress the negative mass instability provided that the mean injection energy is greater than about 3 MeV.[2-5] Additionally, research in support of the ATA accelerator program predicts that employing occasional nonlinear focusing elements to spread the electron transverse oscillation frequencies can limit beam breakup instability growth.[14] We remark also that varying the resonant frequencies ω_0 from gap to gap can cut the beam breakup growth rate by N^{-1}, provided the relative shifts are greater than Q^{-1}.[15]

Extensions to the present research naturally fall into two categories, adding drifttube curvature and adding beam temperature. The former is relatively easily accomplished by inserting the transport equations of Ref. 4 or 16 into BALTIC. This also would allow us to determine the influence of straight drifttube sections on the negative mass instability. Treating beam temperature beyond what has already been done probably requires numerical simulation.

REFERENCES

1. C. W. Roberson, "The Racetrack Induction Accelerator," IEEE Nuc. Sci. NS-28, 3433 (1981).

2. P. Sprangle and J. L. Vomvoridis, "Longitudinal and Transverse Instabilities in a High Current Modified Betatron Electron Accelerator," NRL-4688 (Naval Research Laboratory, Washington, 1981).

3. B. B. Godfrey and T. P. Hughes, "Resistive Wall Instabilities in the Modified Betatron," AMRC-R-332 (Mission Research Corporation, Albuquerque, 1981).

4. T. P. Hughes and B. B. Godfrey, "Linear Stability of the Modified Betatron," AMRC-R-354 (Mission Research Corporation, Albuquerque, 1982).

5. B. B. Godfrey and T. P. Hughes, "Modified Betatron Stability Calculations," AMRC-N-207 (Mission Research Corporation, Albuquerque, 1982).

6. T. J. Fessenden, W. A. Atchison, D. L. Birx, R. J. Briggs, J. C. Clark, R. E. Hester, V. K. Neil, A. C. Paul, D. Rogers, and K. W. Struve, "Physics of a Repetitively Pulsed 10 kAmp Electron Beam," Proc. 4th Conf. Electron and Ion Beam Research and Technology (Palaiseu, 1981), p. 813.

7. R. B. Miller, J. W. Poukey, B. G. Epstein, S. L. Shope, T. C. Genoni, M. Franz, B. B. Godfrey, R. J. Adler, and A. Mondelli, "Beam Transport in High Current Linear Accelerators," IEEE Nuc. Sci. NS-28, 3343 (1981).

8. V. K. Neil, L. S. Hall, and R. K. Cooper, "Further Theoretical Studies of the Beam Breakup Instability," Part. Accel. 9, 213 (1979).

9. R. J. Adler, B. B. Godfrey, M. M. Campbell, and D. J. Sullivan, "The Image Displacement Effect in Intense Electron Beams," AMRC-R-333 (Mission Research Corporation, Albuquerque, 1982).

10. R. J. Adler and B. B. Godfrey, "Study of High Current Induction Linac Phenomena: Experiment and Theory," AMRC-R-411 (Mission Research Corporation, Albuquerque, 1982); and references therein.

11. J. E. Leiss, N. J. Norris, and M. A. Wilson, "The Design and Performance of a Long-Pulse High-Current Linear Induction Accelerator at the National Bureau of Standards," Part. Accel. 10, 223 (1980).

12. V. K. Neil, "The Image Displacement Effect in Linear Induction Accelerators," UCID-17976 (Lawrence Livermore National Laboratory, Livermore, 1978).

REFERENCES (Continued)

13. D. L. Birx, "Reduction of the Beam Breakup Mode Q Values in the ETA/ATA Accelerating Cells," UCID-18630 (Lawrence Livermore National Laboratory, Livermore, 1980).

14. E. P. Lee and others, private communication.

15. B. B. Godfrey and R. J. Adler, unpublished.

16. D. P. Chernin and P. Sprangle, "Transverse Beam Dynamics in the Modified Betatron," NRL-4687 (Naval Research Laboratory, Washington, 1981).

APPENDIX E

APPENDIX E

AMRC-R-469

BEAM BREAKUP INSTABILITIES IN HIGH CURRENT ELECTRON BEAM RACETRACK INDUCTION ACCELERATORS

B. B. Godfrey
T. P. Hughes

March 1983

Prepared for:

Office of Naval Research
Physical Sciences Division
800 North Quincy Street
Arlington, Virginia 22217

Under Contract:

N00014-81-C-0647

Prepared by:

MISSION RESEARCH CORPORATION
1720 Randolph Road, S.E.
Albuquerque, New Mexico 87106

SUMMARY

Beam breakup and negative mass instability growth rates for a 1 kA, 40 MeV electron beam racetrack induction accelerator are computed. The device is taken to have four acceleration gaps, each with 0.2 MeV applied voltage and 15 ohm transverse impedence; the guide field is 2 kg. We find that the total amplification of the beam breakup mode is limited to five e-foldings provided that the cavity mode quality factor Q is 6. Thus, the negative mass instability, which grows several times faster, is the dominant consideration. However, we also find that the energy range over which the negative mass instability occurs can be narrowed substantially by reducing the guide field strength after the beam has been accelerated to about 12 MeV. This approach, coupled with beam thermal effects, not considered here, probably is sufficient to limit negative mass growth to acceptable levels in the racetrack accelerator.

INTRODUCTION

High current racetrack induction accelerators and modified betatrons are a subject of increasing interest as sources of high power electron beams for free electron lasers, flash radiography, and other applications. The racetrack induction accelerator geometry is illustrated schematically in Figure 1. The beam is injected from a conventional pulsed diode beam generator into the drifttube, is progressively accelerated as it repetitively passes one or more induction modules, and then is extracted from the accelerator for its intended use. Extraction may even be unnecessary for microwave applications, because a slow-wave or rippled-magnetic-field cavity can be inserted in a straight section of the drifttube.[1]

Most beam stability studies for high current recirculating devices have dealt with the negative mass and resistive wall instabilities.[2-5] However, experience with linear induction accelerators suggests that beam

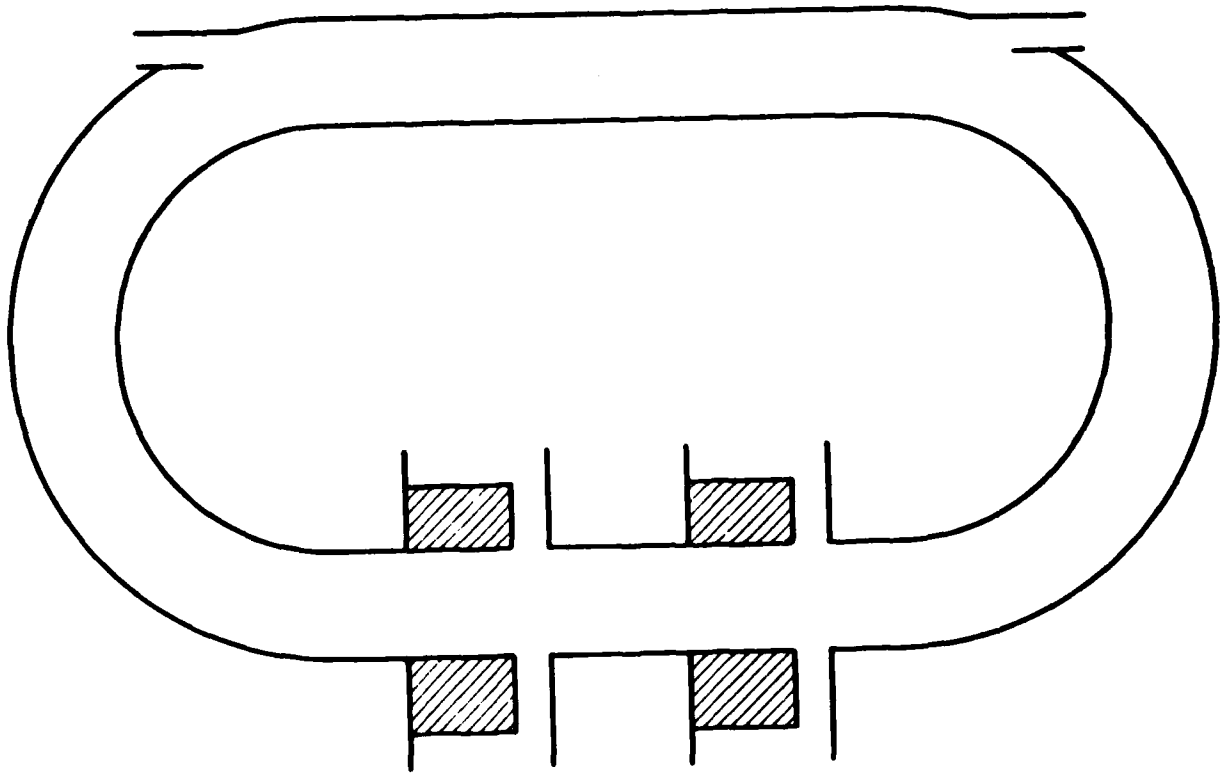

Figure 1. Simplified representation of cyclic induction accelerator with racetrack drift tube, acceleration gaps, and injection and extraction ports.

breakup due to interaction with the induction modules and other discontinuities in the drifttube may be significant.[6,7] The beam breakup instability arises from a resonant coupling between beam transverse oscillations and m=1 electromagnetic cavity modes localized to the acceleration gaps, resulting in large lateral displacements of the beam.[8,9] In this paper we present a linear dispersion relation describing both beam breakup and negative mass instabilities, including their possible interaction, and evaluate it for parameters of the proposed racetrack induction accelerator designed by the Naval Research Laboratory.[1]

The NRL device is based on the four module linear induction accelerator developed by the National Bureau of Standards.[10] It is expected to accelerate a 1 kA electron beam from 1 to 40 MeV in fifty cycles. The beam and drifttube radii are 1 and 7 cm, respectively. The principle m=1 resonance of the gaps has a frequency of 880 MHz, an impedence of 15 ohms, and a quality factor (Q) of 60. Experience with the ETA linear induction accelerator at Lawrence Livermore National Laboratory indicates that Q can be greatly reduced, however, and we shall take Q=6 in our numerical work.[11] The NRL design includes a 2 kg axial magnetic field to maintain the beam equilibrium and improve beam stability at low energies. Reducing or eliminating this guide field at higher energies is nonetheless an interesting possibility. The stability analyses below consider both options.

DISPERSION RELATION

For simplicity we represent the racetrack accelerator as a torus with a single gap. These two approximations are conservative in that omitting the straight sections of the racetrack and lumping the several gaps into one overestimate negative mass and beam breakup growth, respectively. The desired dispersion relation is

$$(\Omega^2-\omega_r^2 + F_r/\gamma L + \omega_\theta^2\gamma^2\chi)\ (\Omega^2-\omega_z^2 + F_z/\gamma L) \tag{1}$$

$$- (B_\theta/\gamma)^2\ \Omega^2 = 0$$

with

$$x = \bar{\nu}\ \frac{\omega}{v_\theta}\ (\omega v_\theta - \frac{\ell}{R})/[\Omega^2 + \bar{\nu}\ (\omega^2 - \frac{\ell^2}{R^2})] \tag{2}$$

$$\bar{\nu} = (1 + 2\ell n\ a/r_b)\ \nu/\gamma^3 \tag{3}$$

Here, $\Omega = \omega - \ell\omega_\theta$ is the Doppler-shifted wave frequency, ℓ is the toroidal mode number, and $\omega_\theta = v_\theta/R$ is the toroidal rotation frequency of the beam. (The poloidal rotation frequency is assumed negligible.) The radial and vertical betatron frequencies are

$$\omega_r^2 = (1 - n - n_s\ r_b^2/a^2)\ \omega_\theta^2$$

$$\omega_z^2 = (n - n_s\ r_b^2/a^2)\ \omega_\theta^2$$

$$n_s \equiv n_b/(2\omega_\theta^2\gamma^3) \tag{4}$$

with n the betatron index, n_b the beam density, $\nu = n_b r_b^2/2$ Budker's parameter, and γ the beam energy. The drifttube major radius is R, the drifttube minor radius is a, and the beam minor radius is r_b. $L=2\pi R$. The toroidal guide field strength is B_θ; the betatron field strength enters as $B_z = -\omega_\theta\gamma$.

In a high current betatron ω_r^2 and ω_z^2 can be of either sign. The beam is unstable, however, whenever

$$\omega_B^2 = \omega_z^2 \omega_r^2/(B_\theta/\gamma)^2 \tag{5}$$

is negative. To avoid this situation, as well as for simplicity, we take n=1/2. The energy at which $\omega_B^2 = 0$ typically is labeled the transition energy,

$$\gamma_{tr} = (4 \nu R^2/a^2)^{1/3} \tag{6}$$

The gap response function F is defined as[9]

$$\frac{F}{\gamma} = - \frac{Z_\perp}{Q} \frac{\omega_o^3}{\omega^2 + i\omega_o\omega/Q - \omega_o^2} \frac{\nu}{\gamma} \tag{7}$$

where ω_o is the resonant frequency, $Z_\perp/Q$ is the transverse impedence, and Q is the quality factor. Setting F=0 in (1) recovers the high current beam negative mass dispersion relation. The negative mass instability occurs for all ℓ over a broad range of energies when $\gamma > \gamma_{tr}$. For low ℓ only, one or two instability bands (often overlapping) also may exist when $\gamma < \gamma_{tr}$. Three of the six beam modes (m=0 spacecharge, m=1 spacecharge, and m=1 cyclotron; m is the poloidal mode number) have negative energy and so can couple unstably to the gap fields. Note that coupling in the m=0 spacecharge mode occurs only due to toroidal curvature. Choosing R=70 cm, we find maximum coupling at ℓ=13.

LARGE B ANALYSIS

For the parameters considered here and toroidal mode numbers in the vicinity of 13, the negative mass instability exists only beyond the transition energy $\gamma_{tr} = 2.9$. Just above the transition energy the instability is due solely to the interaction between the positive and negative energy m=1 spacecharge modes, while at still higher energies the m=0 spacecharge modes also are involved. This change is readily visible in the negative mass instability growth rate, the dashed curve in Figure 2. Which portion grows faster depends on circumstances.

Although the peak growth rate at lower energy is not readily determined analytically, the higher energy peak is easily shown to be

$$\Gamma = \frac{\sqrt{3}}{2} \left[2 \ell \omega_\theta \omega_B^2 \tilde{\nu} \gamma^2\right]^{1/3} \tag{8}$$

Instability ceases for

$$\gamma > \left[6\sqrt{3}\, \ell R B_\theta \nu (1 + 2 \ell n\, a/r_b)\right]^{1/2} \tag{9}$$

here about 62.

In the absense of curvature, the beam breakup growth rate also is easily estimated. For Q not too large,[9]

$$\Gamma = \omega_o Q \frac{\nu Z_\perp/Q}{B_\theta L} \tag{10}$$

Both m=1 negative energy modes grow at this rate when their frequencies roughly match ω_o.

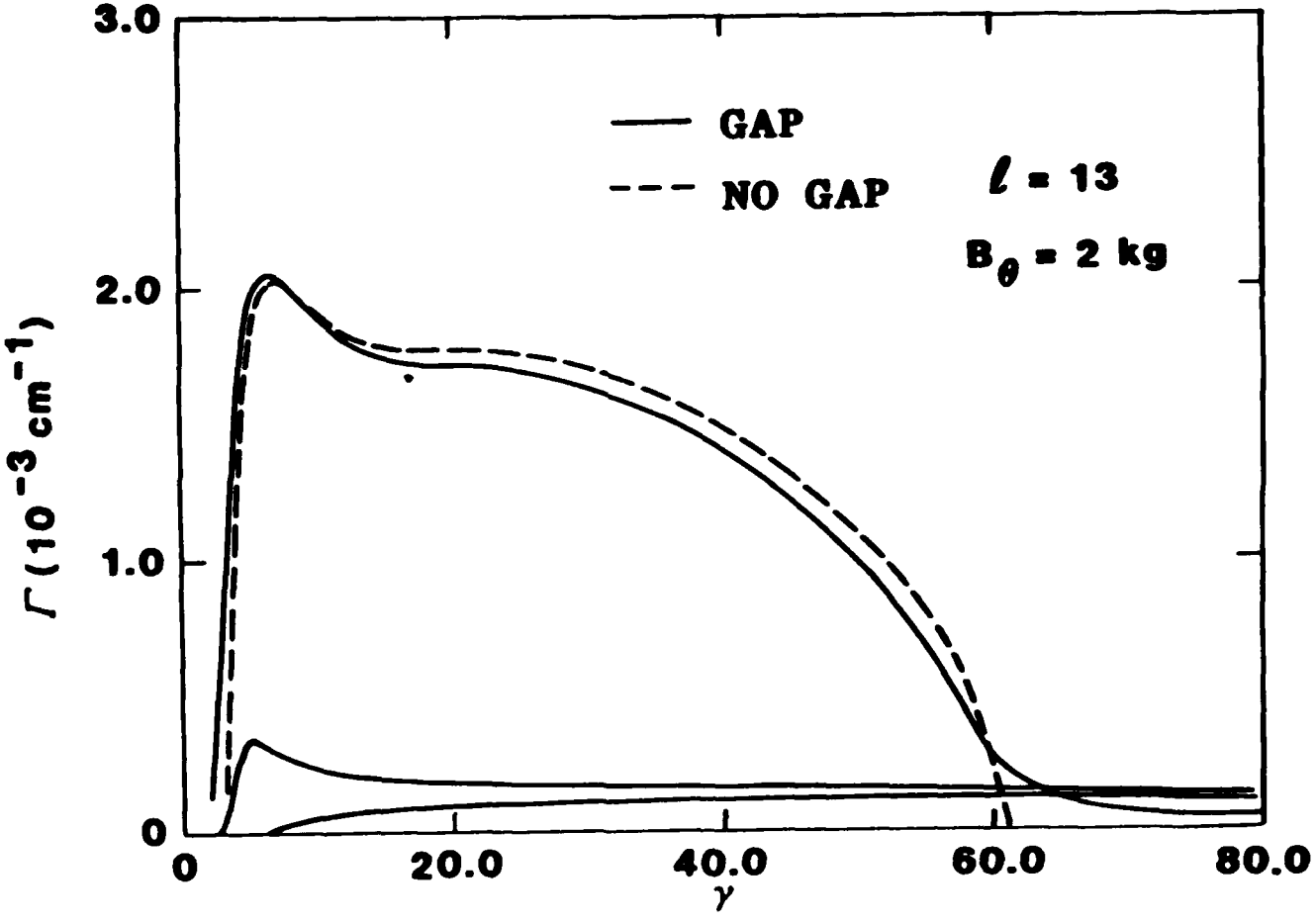

Figure 2. Combined negative mass and beam breakup instability growth rates (solid curves) for ℓ=13 and B_{θ}=2 kg. Growth of the negative mass instability alone (dashed curve) is included for comparison.

The solid curves in Figure 2 show growth rates of the negative mass and beam breakup instabilities combined. The negative mass results are seen to be only weakly affected by the gap resonance. The m=1 cyclotron and hybrid m=0/1 spacecharge modes have become unstable, however, with a growth rate agreeing with (10) to within a factor of 1.5. These findings are insensitive to small changes in the resonant frequency.

SMALL B ANALYSIS

Although modified betatron and racetrack induction accelerator studies usually assume a large toroidal guide field, large B_θ is in fact needed to provide a beam equilibrium only for γ small. Reducing or perhaps eliminating B_θ after the beam has been accelerated sufficiently has certain advantages for stability, as we see below.

For $B_\theta=0$, the negative mass growth rate is approximately

$$\Gamma = \frac{\sqrt{3}}{2} [\ell \omega_\theta{}^3 \tilde{\nu} \gamma^2]^{1/3} \qquad (11)$$

This expression exceeds (8) whenever $B_\theta/\gamma > \omega_\theta$. However, the corresponding high energy cutoff,

$$\gamma > 3\sqrt{6}\, \ell\nu\, (1+ 2\, \ell n\, a/r_b) \qquad (12)$$

here 27.5, typically is much lower than (9). See the dashed curve in Figure 3.

The beam breakup instability maximum growth rate is again readily estimated, this time giving

$$\Gamma = \omega_o Q \frac{\nu Z_\perp/Q}{2\omega_z L \gamma} \qquad (13)$$

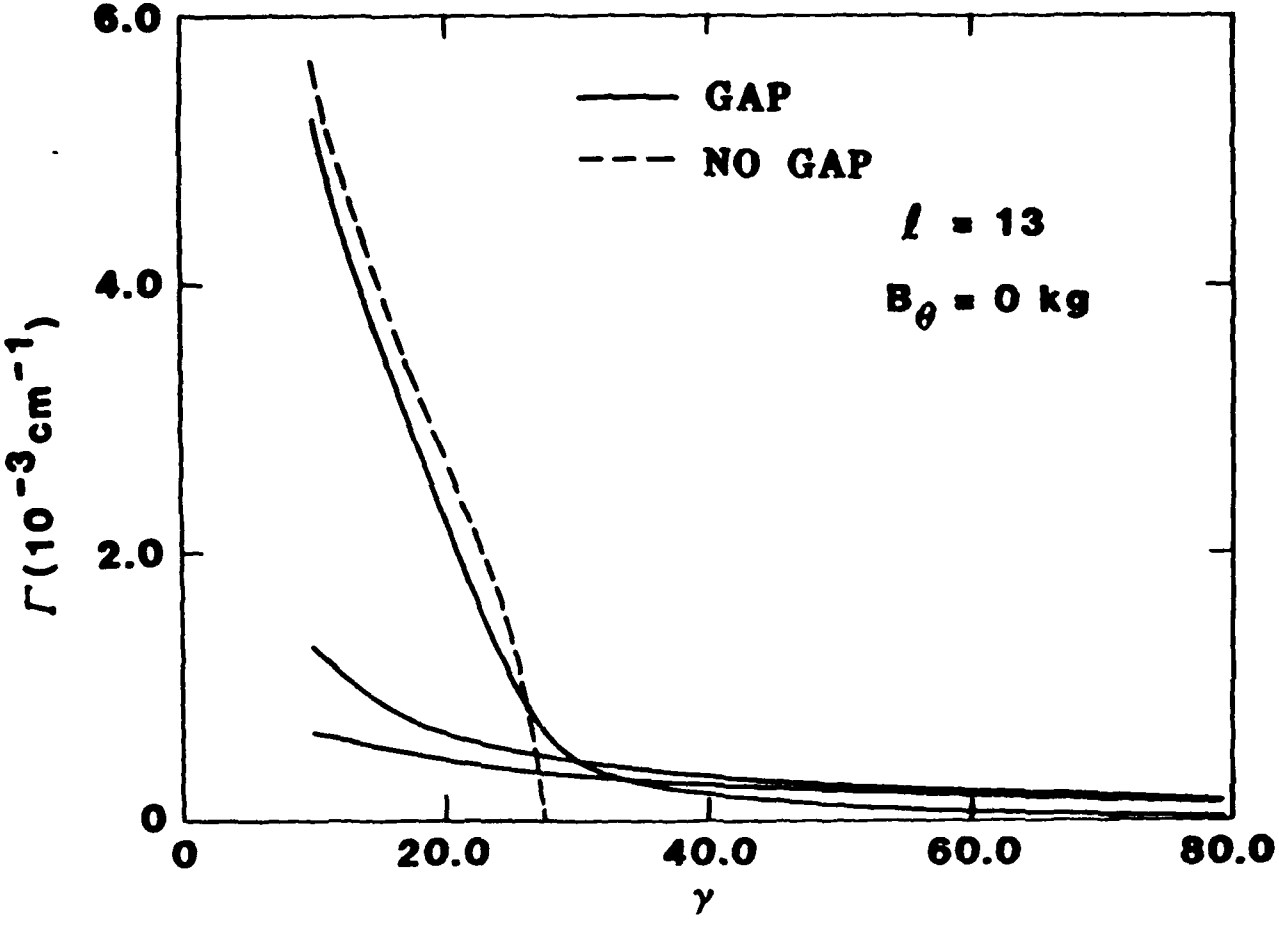

Figure 3. Combined negative mass and beam breakup instability growth rates (solid curves) for ℓ=13 and B_θ=0 kg. Growth of the negative mass instability alone (dashed curve) is included for comparison.

Equation (13) exceeds (10) for $B_\theta/\gamma > 2\omega_z$. The solid curves in Figure 3 show the effects of $F \neq 0$. As in Figure 2, the negative mass instability is only slightly modified by the gap; the beam breakup instability is described reasonably well by (13).

A comparison of the two figures suggests that some reduction in total instability growth during acceleration can be achieved by rapidly decreasing the guide field as the beam energy exceeds about 12 MeV.

RECOVERING "CONVENTIONAL" NEGATIVE MASS INSTABILITY BEHAVIOR FROM THE HIGH-CURRENT-BETATRON DISPERSION RELATION

The preceding small B_θ analysis predicts a high energy cutoff for the negative mass instability in a high current betatron, while standard derivations of negative mass growth, performed for a low current betatron, lead to no such cutoff.[12,13] The source of this apparent discrepancy, namely the failure of the usual approximation

$$1 - \omega^2 R^2/\ell^2 \approx \gamma^{-2} \tag{14}$$

when $\tilde{\nu}\gamma^4$ becomes large, has been noted previously.[4] To emphasize this point, we here recover the accepted low current growth rate and show that it too exhibits a high energy cutoff, where (14) breaks down. Interestingly, a comparison of the new cutoff with (12), the high current limit, indicates that practical betatron parameters exist for which the negative mass instability does not occur at all at moderate toroidal mode numbers.

We begin by setting B_θ (and F) to zero in (1).

$$\Omega^2 - \omega_r^2 + \omega_o^2 \gamma^2 \chi = 0 \tag{15}$$

Next, we drop Ω^2 as small compared to ω_r^2, valid for m=0 spacecharge waves in low current beams, and rearrange terms in the expression for χ.

$$1 = \left(\frac{\omega_\theta}{\omega_r}\right)^2 \gamma^2 \tilde{\nu} \frac{\ell}{R} \left(\Omega v_\theta - \frac{1}{\gamma^2} \frac{\ell}{R}\right) /$$

$$\left[\Omega^2 (1 + \tilde{\nu}) + 2\Omega \tilde{\nu} \frac{\ell}{R} v_\theta - \tilde{\nu} \frac{1}{\gamma^2} \frac{\ell^2}{R^2}\right] \qquad (16)$$

The conventional negative mass growth rate is obtained immediately by omitting terms linear in Ω from (16), an approximation equivalent to invoking (14).

Alternatively, (16) can be solved exactly.

$$2 (1 + \tilde{\nu}) \Omega = - \tilde{\nu} \frac{\ell}{R} v_\theta \left(2 - \frac{\omega_\theta^2}{\omega_r^2} \gamma^2\right) \pm$$

$$\left[\tilde{\nu} \frac{\ell}{R} v_\theta \left(2 - \frac{\omega_\theta^2}{\omega_r^2} \gamma^2\right)^2 + 4 (1 + \tilde{\nu}) \tilde{\nu} \frac{1}{\gamma^2} \frac{\ell^2}{R^2} \left(1 - \frac{\omega_\theta^2}{\omega_r^2} \gamma^2\right)\right]^{1/2} \qquad (17)$$

Instability occurs whenever the argument of the square root is negative, approximately

$$\frac{\tilde{\nu} \gamma^4}{4} \left(\frac{\omega_\theta}{\omega_r}\right)^2 < 1 \qquad (18)$$

Whe (18) is well satisfied, the criterion for (14) to be valid, the desired growth rate is recovered.

$$\Gamma = \tilde{\nu}^{1/2} \frac{\ell}{R} \frac{\omega_\theta}{\omega_r} \qquad (19)$$

This derivation shows clearly the the negative mass instability at low currents is associated only with the m=0 spacecharge waves. At higher currents, for which Ω and ω_r become comparable, the m=1 spacecharge waves also are involved, and the complete quartic equation must be solved to give (11).

For the parameters of Table 1, the low current negative mass instability has a cutoff at $\gamma = 7.0$. Since the equilibrium fails below $\gamma = 10.5$, we see that the low current instability does not arise. Figure 4, a numerical solution of (1) for 350 A, illustrates growth in the low current limit. The analytical result from (19) at $\gamma = 10.5$ exceeds the numerical by about 30%.

Rewriting inequality (18) as

$$\gamma > \frac{1}{\nu} \quad \frac{4(1 - n)}{1 + 2\ell n\ a/r_b} \tag{20}$$

simplifies comparison with (12). Note that (20) predicts a narrow energy bandwidth at high current, while (12) gives the opposite. A window, therefore, exists at moderate currents,

$$\nu\ (1 + 2\ell n\ a/r_b) \sim 0.5\text{-}1.0 \tag{21}$$

for which the energy range of the negative mass instability is minimal. For instance, a 750 A, 4.5 MeV electron beam injected into a betatron or racetrack accelerator with dimensions as in Table 1 exhibits no negative mass instability whatsoever for $\ell < 6$. Higher toroidal modes are likely to be stabilized by energy spread[2,4] or nonlinear effects.[14]

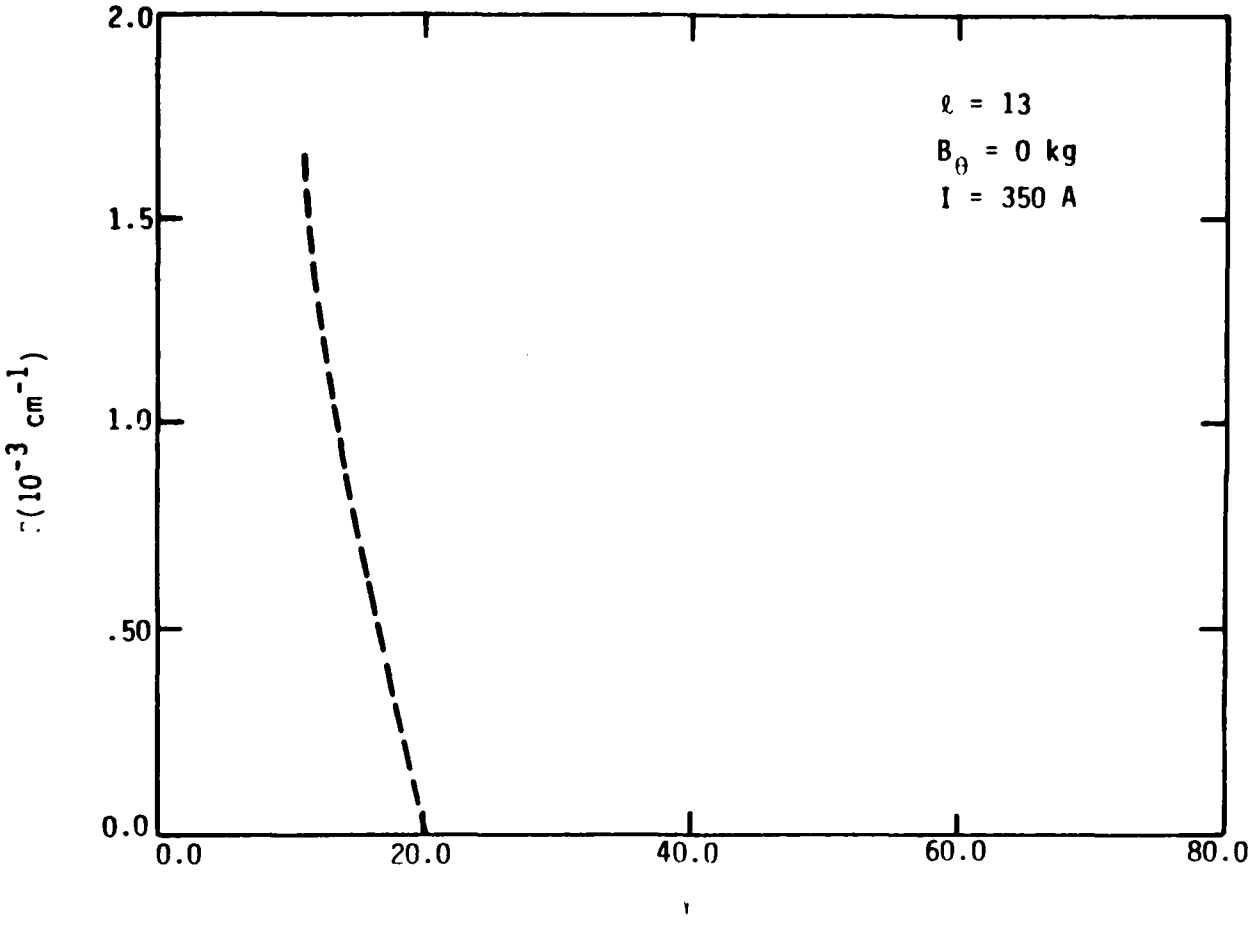

Figure 4. Growth rate of the low current negative mass instability for ℓ=13 and B_θ=0 kg at I=350 A.

TABLE 1. NOMINAL RACETRACK INDUCTION ACCELERATOR PARAMETERS

Path Lengths	$L = 460$ cm	
Drifttube Radius	$R = 7$ cm	
Beam Radius	$a = 1$ cm	
Guide Field	$B_\theta = 2$ kg	($\omega_c = 1.173\ cm^{-1}$)
Beam Current	$I = 1$ kA	($\nu = 0.0588$)
Beam Energy	$U = 0.4 - 40$ MeV	($\gamma = 1.5 - 80$)
Number of Revolutions	50	
Number of Gaps	$N = 4$	
Acceleration per Gap	$\Delta U = 0.2$ MeV	($\Delta\gamma = 0.4$)
Gap Resonant Frequency	880 MHz	
Mode Quality Factor	$Q = 60, 6$	
Gap Transverse Impedance	15 ohms	($Z_\perp/Q = 0.5$)
Gap Width	$\ell = 5$ cm	

REFERENCES

1. C. W. Roberson, IEEE Nuc. Sci. NS-28, 3433 (1981).

2. P. Sprangle and J. L. Vomvoridis, NRL-4688 (Naval Research Laboratory, Washington, 1981).

3. B. B. Godfrey and T. P. Hughes, AMRC-R-332 (Mission Research Corporation, Albuquerque, 1981).

4. T. P. Hughes and B. B. Godfrey, AMRC-R-354 (Mission Research Corporation, Albuquerque, 1982).

5. B. B. Godfrey and T. P. Hughes, AMRC-N-207 (Mission Research Corporation, Albuquerque, 1982).

6. T. J. Fessenden, W. A. Atchison, D. L. Birx, R. J. Briggs, J. C. Clark, R. E. Hester, V. K. Neil, A. C. Paul, D. Rogers, and K. W. Struve, Proc. 4th Conf. Electron and Ion Beam Research Technology (Palaiseu, 1981), p. 813.

7. R. B. Miller, J. W. Poukey, B. G. Epstein, S. L. Shope, T. C. Genoni, M. Franz, B. B. Godfrey, R. J. Adler, and A. Mondelli, IEEE Nuc. Sci. NS-28, 3343 (1981).

8. V. K. Neil, L. S. Hall, and R. K. Cooper, Part. Accel. 9, 213 (1979).

9. B. B. Godfrey and T. P. Hughes, AMRC-R-410 (Mission Research Corporation, Albuquerque, 1982).

10. J. E. Leiss, N. J. Norris, and M. A. Wilson, Part. Accel. 10, 223 (1980).

11. D. L. Brix, UCID-18630 (Lawrence Livermore National Laboratory, Livermore, 1980).

12. V. K. Neil and A. M. Sessler, Rev. Sci. Instr. 36, 429 (1965).

13. R. W. Landau and V. K. Neil, Phys. Fluids 9, 2412 (1966).

14. T. P. Hughes, M. M. Campbell, and B. B. Godfrey, IEEE Trans. Nuc. Sci., to be published.

APPENDIX F

APPENDIX F

REPORTS AND PRESENTATIONS

Reports and Publications

"Resistive Wall Instabilities in the Modified Betatron," B. B. Godfrey and T. P. Hughes (AMRC-R-332, November 1981).

"Linear Stability of the Modified Betatron," T. P. Hughes and B. B. Godfrey (AMRC-R-354, April 1982).

"Modified Betatron Stability Calculations," B. B. Godfrey and T. P. Hughes (AMRC-N-207, August 1982).

"Beam Breakup and Image Displacement Instabilities in High Current Electron Beam Recirculating Induction Accelerators," B. B. Godfrey and T. P. Hughes (AMRC-R-410, September 1982).

"Beam Breakup Instabilities in High Current Electron Beam Racetrack Induction Accelerators," B. B. Godfrey and T. P. Hughes, IEEE Trans. Nuc. Sci. NS-30, (1983).

"Analytic and Numerical Studies of the Modified Betatron," T. P. Hughes, M. M. Campbell, and B. B. Godfrey, IEEE Trans. Nuc. Sci. NS-30, 2528 (1983).

"Linear and Nonlinear Development of the Negative Mass Instability in a Modified Betatron Accelerator," T. P. Hughes, M. M. Campbell and B. B. Godfrey, to be published in Proceedings of the Fifth International Conference on High Power Particle Beams.

"Improved Long-Wavelength Dispersion Relation for the Negative Mass Instability in High Current Conventional and Modified Betatrons," B. B. Godfrey, T. P. Hughes and M. M. Campbell (AMRC-R-520, December 1983).

Presentations

"Beam Stability in the Modified Betatron Accelerator," B. B. Godfrey, M. M. Campbell, and T. P. Hughes, APS Plasma Physics Meeting, New Orleans, November 1982.

"Beam Breakup Instabilities in High Current Electron Beam Racetrack Induction Accelerators," B. B. Godfrey and T. P. Hughes, Particle Accelerator Conference, Santa Fe, March 1983.

"Analytic and Numerical Studies of the Modified Betatron," T. P. Hughes, M. M. Campbell, and B. B. Godfrey, Particle Accelerator Conference, Santa Fe, March 1983.

"High Current Betatrons (Theory and Computations)," B. B. Godfrey, University of New Mexico Nuclear Engineering Seminar, April 1983.

Presentations (Cont'd)

"Linear and Nonlinear Development of the Negative Mass Instability in a Modified Toroidal Betatron Accelerator," T. P. Hughes, M. M. Campbell, and B. B. Godfrey, Beams '83, San Francisco, September 1983.

"Toroidal Self-Field Corrections to the Linear Dispersion Relation for the Negative Mass Instability in a Modified Betatron," B. B. Godfrey, T. P. Hughes, and M. M. Campbell, APS Plasma Physics Meeting, Los Angeles, November 1983.

"Simulations and Theory of Negative Mass Instability in a Modified Betatron," T. P. Hughes, M. M. Campbell, and B. B. Godfrey, APS Plasma Physics Meeting, Los Angeles, November 1983.

END

FILMED

3-84

DTIC